



UNIVERSIDADE FEDERAL DE ALAGOAS



INSTITUTO DE QUÍMICA E BIOTECNOLOGIA

PROGRAMA DE PÓS-GRADUAÇÃO EM QUÍMICA E BIOTECNOLOGIA

KATHERINE LOZANO UNTIVEROS

**ELECTROCHEMICAL APPROACH AND DEVELOPMENT OF
AN ELECTROCHEMICAL BIOSENSOR BASED ON HAIRPIN-DNA MODIFIED
GOLD ELECTRODE FOR DETECTION OF DNA DAMAGE FOR A NEW
ACRIDINE-THIOPHENE CANCER DRUG**

Maceio-AL

2017

KATHERINE LOZANO UNTIVEROS

**ELECTROCHEMICAL APPROACH AND DEVELOPMENT OF
AN ELECTROCHEMICAL BIOSENSOR BASED ON HAIRPIN-DNA MODIFIED
GOLD ELECTRODE FOR DETECTION OF DNA DAMAGE FOR A NEW
ACRIDINE-THIOPHENE CANCER DRUG**

Defesa de tese de Doutorado ao programa em Química e Biotecnología da Universidade Federal de Alagoas, como parte dos requisitos para a obtenção do título de Doutor em Ciencias, com área de concentração em Bioquímica e Biotecnología.

Orientador: Prof.^a Dr.^a Fabiane Caxico de Abreu Galdino

Co-orientador : Prof.^a Dr.^a Karin Chumbimuni Torres

Maceio-AL

2017

Catálogo na fonte
Universidade Federal de Alagoas
Biblioteca Central

Bibliotecária Responsável: Helena Cristina Pimentel do Vale

- L925e Lozano Untiveros, Katherine.
Electrochemical approach and development of an electrochemical biosensor based on Hairpin-DNA modified gold electrode for detection of DNA damage for a new acridine-thiophene cancer drug / Katherine Lozano Untiveros. – 2017. 102 f.: il.
- Orientadora: Fabiane Caxisto de Abreu.
Coorientador: Karin Chumbimuni Torres.
Tese (doutorado em Química e Biotecnologia) – Universidade Federal de Alagoas. Instituto de Química e Biotecnologia. Maceió, 2017.
- Bibliografia: f. 98-102.
1. Biosensor. 2. Acridine-thiophene. 3. Cancer drug. 4. Hairain-DNA. 5. DNA damage. 6. Gold electrose. I. Título.

CDU: 544.6.018.2:544.6.076.326



UNIVERSIDADE FEDERAL DE ALAGOAS
INSTITUTO DE QUÍMICA E BIOTECNOLOGIA
PROGRAMA DE PÓS-GRADUAÇÃO EM QUÍMICA E
BIOTECNOLOGIA




BR 104 Km14, Campus A. C. Simões
Cidade Universitária, Tabuleiro dos Martins
57072-970, Maceió-AL, Brasil
Fone: (82) 3214-1144
Email: ppgqb.ufal@gmail.com

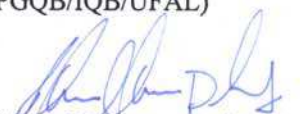
FOLHA DE APROVAÇÃO


Membros da Comissão Julgadora da Defesa de Tese da Doutoranda **Katherine Lozano Untiveros** intitulada: **"ELECTROCHEMICAL APPROACH AND DEVELOPMENT OF AN ELECTROCHEMICAL BIOSENSOR BASED ON HARPIN-DNA MODIFIED GOLD ELECTRODE FOR DETECTION OF DNA DAMAGE FOR A NEW ACRIDINE-THIOPHENE CANCER DRUG"**, apresentada ao Programa de Pós-Graduação em Química e Biotecnologia da Universidade Federal de Alagoas no dia 31 de março de 2017, às 09h30, na sala de reuniões do IQB/UFAL.


COMISSÃO JULGADORA


Prof.^a Dr.^a Fabiane Caxico de Abreu Galdino
Orientadora (PPGQB/IQB/UFAL)


Prof.^a Dr.^a Adriana Santos Ribeiro
(PPGQB/IQB/UFAL)


Prof. Dr. Thiago Mendonça de Aquino
(PPGQB/IQB/UFAL)


Prof. Dr. Eduardo Jorge da Silva Fonseca
(IF/UFAL)


Prof. Dr. Phabyanno Rodrigues Lima
(PPGQB/UFAL (IFAL))

ABSTRACT

The interaction of drugs with DNA is a significant feature in pharmacology and plays a vital role in the designing of more efficient and specifically targeted drugs. The concept of hybridization of two bioactive molecules often leads to increased activity due to synergistic effects of anticancer drugs have been studied. Two important pharmacophores: Acridine and thiophene were widely studied as antitumor, antiparasitic and antibacterial agents. We hypothesize that a conjugate comprised two pharmacophores with different mechanisms of antiproliferative action can result in enhanced DNA damage.

Electrochemical Studies in aprotic and protic media, electrochemical DNA biosensor at Glassy carbon electrode, electrochemical New Hairpin DNA biosensor at the Gold electrode (SL-DNA/GE), Molecular Modeling and Spectroscopic UV-Vis, were used to determine the damage caused to DNA by six Acridine-thiophene conjugates.

In this work, we report the synthesis of six synthetic DNA intercalators based on the acridine linked with thiophene conjugates (7CNAC01, 6CNAC01, 7ESTAC01, 6ESTAC01, ACS6CN, and ASC5CN). We identified the electrochemical behavior of these active redox drugs is strongly influenced by the nature of solvent (DMF and pH=7.2 phosphate buffer media). We recorded redox properties of 7CNAC01, 6CNAC01, 7ESTAC01, and 6ESTAC01 involve adsorption controlled quasi-reversible process and were investigated using differential pulse voltammetry (DPV) at a glassy carbon and Gold electrode. An effective and new electrochemical biosensor based on hairpin DNA (SL-DNA/GE) immobilized and functionalized on the surface of the gold electrode (GE) to detect oxidative Guanine damage was developed. As a result, two kinds of biosensor were tested with reduced acridine-thiophene conjugates showing better sensitivity the SL-DNA/GE sensor for the detection of DNA damage using the electrochemical signal of Oxidation of Guanine bases. Also, Molecular docking results showed predominantly hydrophobic interaction, and either high binding constant was recorded for Molecular docking and UV-Vis absorption spectroscopy showing an isosbestic point presence with dsDNA, for 7ESTAC01, 6ESTAC01, ACS6CN, ACS5CN.

Our findings indicate that three reduced acridine-thiophene compounds (7CNAC01, 6CNAC01, and ACS5CN) cause direct dsDNA damage and all our six reduced hybrid compounds are causing damage to single stranded ssDNA. Finally, we proposed for the first time a direct correlation between binding constant (K_b) and half-wave potential ($E_{1/2}$) for four acridine-thiophene derivatives (7ESTAC01, 6ESTAC01, ACS6CN, and ASC5CN).

Our results showed a promise sensitive electrochemical SL-DNA/GE sensor for the detection of DNA damage using the electrochemical signal of Oxidation of Guanine bases, to detect DNA-cancer drug interaction.

Keywords: DNA damage; Acridine-Thiophene derivatives; DNA-electrochemical biosensor; Stem-Loop DNA Biosensor; Differential Pulse Voltammetry.

RESUMO

A interação de drogas com DNA é uma característica significativa na farmacologia e desempenha um papel vital na concepção de drogas mais eficientes e especificamente direcionadas. O conceito de hibridização de duas moléculas bioativas leva ao aumento da atividade devido aos efeitos sinérgicos de drogas híbridas anticâncer com o uso dos farmacóforos importantes: Acridina e Tiofeno. Estes dois sítios ativos foram amplamente estudados como agentes antitumorais, antiparasitários e antibacterianos. Suspeitamos que um conjugado, composto por dois farmacóforos com diferentes mecanismos de ação antiproliferativa, pode resultar em danos ao DNA.

Estudos eletroquímicos em meios prótico e aprótico, biossensor de DNA eletroquímico em eletrodo de carbono vítreo, Hairpin DNA em eletrodo de ouro (SL-DNA/GE), modelagem molecular e Espectroscopia UV-Vis foram usados para determinar os danos causados ao DNA por seis conjugados de Acridina-Tiofeno.

Neste trabalho, relatamos o estudo de seis intercaladores de DNA com base na acridina ligada a conjugados de tiofeno (7CNAC01, 6CNAC01, 7ESTAC01, 6ESTAC01, ACS6CN e ACS5CN). As propriedades redox da 7CNAC01, 6CNAC01, 7ESTAC01 e 6ESTAC01 envolvem processo quase-reversível com corrente controlada por difusão. As propriedades redox desses compostos foram investigadas usando voltametrias cíclica e de pulso diferencial (VPD) em eletrodo de carbono vítreo e eletrodo de ouro. Foi desenvolvido um novo e eficiente biossensor eletroquímico baseado no Hairpin DNA (SL-DNA/GE) imobilizado e funcionalizado na superfície do eletrodo de ouro para detectar danos oxidativos da guanina através da interação com 7ESTAC01. Os biossensores SL-DNA e dsDNA foram testados com conjugados de acridina-tiofeno reduzidos, apresentando melhor sensibilidade o sensor SL-DNA na detecção de danos ao DNA. Além disso, os resultados de modelagem molecular mostraram predominantemente interação hidrofóbica e uma alta constante de ligação. Já os resultados de espectroscopia de absorção no UV-Vis mostraram a presença de ponto isobéstico com dsDNA, para os conjugados 7ESTAC01, 6ESTAC01, ACS6CN, ACS5CN.

Nossos resultados indicaram que três compostos de acridina-tiofeno reduzidos (7CNAC01, 6CNAC01 e ACS5CN) causaram danos direto ao dsDNA, e os seis compostos híbridos reduzidos, causaram danos ao DNA de cadeia simples. Finalmente, propusemos pela primeira vez uma correlação direta entre constante de ligação (K_b) e potencial de meia onda ($E_{1/2}$) para quatro derivados de acridina-tiofeno (7ESTAC01, 6ESTAC01, ACS6CN e ACS5CN). Além disso, o biossensor eletroquímico de SL-DNA/GE mostrou-se bastante sensível para a detecção dos danos causados ao DNA, através da interação entre o DNA e os compostos estudados.

Palavras-chave: Danos ao DNA; Biossensor de DNA Hairpin; Derivados Acridina - Tiofeno; drogas anticâncer-DNA; Biossensor eletroquímico de dsDNA; Voltametria de pulso diferencial.

LIST OF TABLES

Table 1 List of compounds based on the linked of acridine and thiophene derivates.....	21
Table 2 Mean parameter of Cyclic voltammetry in aprotic media, DMF/TBAP solution $v=0.1$ V/s. Experimental conditions as for Fig. 1 (Cathodic (E_c) and anodic (E_a) potentials	30
Table 3 Mean parameter of Cyclic voltammetry electrochemical studies in aqueous solution, pH 7.2 Phosphate buffer, and 20%DMF. $v=0.1$ V/s. Experimental conditions as for Fig. 2	36
Table 4 Electrochemical parameters obtained for 7CNAC01 in aprotic media. Study on function of scan rate.....	42
Table5 Electrochemical parameters obtained for 6CNAC01 in aprotic media. Study on the function of scan rate.....	42
Table 6 Electrochemical parameters obtained for 7ESTAC01 in aprotic media. Study on function of scan rate.....	43
Table 7 Electrochemical parameters obtained for 7ESTAC01 in aprotic media. Study on the function of scan rate.	43
Table 8 Detection of DNA damage at the ssDNA/7CNAC01 caused by three concentrations level of 7CNAC01 ($1.0 \times 10^{-6}M$, $1.0 \times 10^{-5}M$, $1.0 \times 10^{-4}M$) and short-lived radicals generated by electrochemical reduction of 7CNAC01 ($c=1.0 \times 10^{-4}M$) during DPV between 0 and +1.4 V (scan rate 5 mV s^{-1}). Experimental conditions as for Fig. 10 (IG, IA, represent anodic peak currents of guanine and adenine.....	51
Table 9 The shift potential of oxidation signal for guanine and adenine in ssDNA solution.....	51
Table 10 Detection of DNA damage at the ssDNA/6CNAC01 caused by three concentrations level of 6CNAC01 ($1.0 \times 10^{-6}M$, $1.0 \times 10^{-5}M$, $1.0 \times 10^{-4}M$) and short-lived radicals generated by electrochemical reduction of 6CNAC01 ($c=1.0 \times 10^{-4}M$) during DPV between 0 and +1.4 V (scan rate 5 mV s^{-1}). Experimental conditions as for Fig. 11 (IG, IA, represent anodic peak currents of guanine and adenine.	52
Table 11 Detection of DNA damage at the ssDNA/7ESTAC01 caused by three concentrations level of 7ESTAC01 ($1.0 \times 10^{-6}M$, $1.0 \times 10^{-5}M$, $1.0 \times 10^{-4}M$) and short-lived radicals generated by electrochemical reduction of 7ESTAC01 ($c=1.0 \times 10^{-4}M$) during DPV between 0 and +1.4 V (scan rate 5 mV s^{-1}). Experimental conditions as for Fig. 12 (IG, IA, represent anodic peak currents of guanine and adenine.....	53
Table 12 Detection of DNA damage at the ssDNA/6ESTAC01 caused by three concentrations level of 6ESTAC01 ($1.0 \times 10^{-6}M$, $1.0 \times 10^{-5}M$, $1.0 \times 10^{-4}M$) and short-lived radicals generated by electrochemical reduction of 6ESTAC01 ($c=1.0 \times 10^{-4}M$) during DPV between 0 and +1.4 V (scan rate 5 mV s^{-1}). Experimental conditions as for Fig. 13 (IG, IA, represent anodic peak currents of guanine and adenine.....	54
Table 13 Detection of DNA damage at the ssDNA/ACS6CN caused by three concentrations level of ACS6CN ($1.0 \times 10^{-6}M$, $1.0 \times 10^{-5}M$, $1.0 \times 10^{-4}M$) and short-lived radicals generated by electrochemical reduction of ACS6CN ($c=1.0 \times 10^{-4}M$) during DPV between 0 and +1.4 V (scan rate 5 mV s^{-1}). Experimental conditions as for Fig. 14 (IG, IA, represent anodic peak currents of guanine and adenine	55
Table 14 Detection of DNA damage at the ssDNA/ACS5CN caused by three concentrations level of ACS5CN ($1.0 \times 10^{-6}M$, $1.0 \times 10^{-5}M$, $1.0 \times 10^{-4}M$) and short-lived radicals generated by electrochemical reduction of ACS5CN ($c=1.0 \times 10^{-4}M$) during DPV between 0 and +1.4 V (scan rate 5 mV s^{-1}). Experimental conditions as for Fig. 15(IG, IA, represent anodic peak currents of guanine and adenine.	56

Table 15 Correlation values between binding constant (K_b) from UV-Vis and half-wave potential ($E_{1/2}$) from cyclic voltammetry in protic media (pH=7.2 phosphate buffer)	57
Table 16 Binding energy for acridine derivatives with ctDNA.....	66
Table 17 Electrochemical parameters obtained from a CV of 0.1 μ M SL-DNA and dsDNA immobilized for different Scan rates.	82
Table 18 Electrochemical parameters obtained from a CV of 1 μ M SL-DNA and dsDNA immobilized for different Scan rates.	87

LIST DE FIGURES

Figure1 Cyclic voltammetry of 1 mM of each compound in dimethylformamide (DMF) plus 0.1 M Tetrabutyl ammonium perchlorate (TBAP), with a Ag/AgCl reference electrode (RE), and the scan rate 0.1 V/s, E = electrochemical potential, V = volt, A = ampere.Using Glass carbon electrode (GCE)	31
Figure2 Cyclic voltammogram of 10 mmol L ⁻¹ hybrid drugs in mixture of pH 7.2 , aqueous phosphate buffer and 20%DMF at a GCE electrode , with a Ag/AgCl reference electrode (RE), and the scan rate 0.1 V/s, E = potential, V = volt, A = ampere	32
Figure3 Studies in aprotic media. (a) Scan speeds in aprotic media of 7CNAC01.(b) Graph of I_{pc} vs $v^{1/2}$; (c) Graph of E_{pc} vs. $\log v$. [7CNAC01] = 1,0 mmol L ⁻¹ in DMF/TBAP (0,1mol L ⁻¹);glassy carbon electrode. N ₂ atmosphere.	34
Figure4 Studies in aprotic media . (a) Scan speeds in aprotic media of 6CNAC01.(b) Graph of I_{pc} vs $v^{1/2}$; (c) Graph of E_{pc} vs $\log v$. [6CNAC01] = 1,0 mmol L in DMF/TBAP (0,1 molL ⁻¹);glassy carbon electrode	35
Figure5 Studies in aprotic media . (a) Scan speeds in aprotic media of 7ESTAC01.(b) Graph of I_{pc} vs $v^{1/2}$; (c) Graph of E_{pc} vs $\log v$. [7ESTAC01] = 1,0 mmol L ⁻¹ in DMF/TBAP (0,1 mol L ⁻¹);glassy carbon electrode	37
Figure6 Studies in aprotic media. (a) Scan speeds in aprotic media of 6ESTAC01.(b) Graph of I_{pc} vs $v^{1/2}$; (c) Graph E_{pc} vs $\log v$. [6ESTAC01] = 1,0 mmol L ⁻¹ in DMF/TBAP (0,1 molL ⁻¹);glassy carbon electrode.	38
Figure 7 Studies in aprotic media. (a) Scan speeds in aprotic media of ACS6CN. (b) Graph of I_{pc1} vs $v^{1/2}$; (c) Graph E_{pc} vs $\log v$. [ACS6CN] = 1, 0 mmol L ⁻¹ in DMF/TBAP (0,1 mol L ⁻¹);glassy carbon electrode.	39
Figure8 Studies in aprotic media. (a) Scan speeds in aprotic media of ACS5CN. (b) Graph of I_{pc1} vs $v^{1/2}$; (c) Graph E_{pc} vs $\log v$. [ACS5CN] = 1,0 mmol L ⁻¹ in DMF/TBAP (0,1 mol L ⁻¹);glassy carbon electrode	40
Figure 9 Reactivity with oxygen .Cyclic voltammetry of 1 mM Acridine-thiophene in dimethylformamide (DMF) plus 0.1 M Tetrabutyl ammonium perchlorate (TBAP), with a Ag/AgCl reference electrode (RE), and the scan rate 50 m V.s ⁻¹	46
Figure 10 a) DPV), at pH 4.5 in acetate buffer with 30% ethanol, of the dsDNA biosensor in the absence and in the presence of	50
Figure 11 (a) Differential pulse voltammogram(DPV), at pH 4.5 in acetate buffer with 30% ethanol, of the dsDNA biosensor	52
Figure 12 (b) Differential pulse voltammogram (DPV) at pH 4.5 in acetate buffer with 30% ethanol for the oxidation of 7ESTAC01 attached to the surface of glassy carbon electrode (GCE) in the presence of ssDNA solution. (a) Differential pulse voltammogram, at pH 4.5 in acetate buffer with 30% ethanol, of the dsDNA biosensor in the absence and in the presence of 7ESTAC01 in solution (1.0 x 10 ⁻⁵ M).	53
Figure 13 (a) Differential pulse voltammogram, at pH 4.5 in acetate buffer with 30% ethanol, of the dsDNA biosensor in the absence and in the presence of 6ESTAC01 in solution (1.0 x 10 ⁻⁵ M) (b) Differential pulse voltammogram (DPV) at pH 4.5 in acetate buffer with 30% ethanol for the oxidation of 6ESTAC01 attached to the surface of glassy carbon electrode (GCE) in the presence of a ssDNA solution.	54

Figure 14 (a) Differential pulse voltammogram, at pH 4.5 in acetate buffer with 30% ethanol, of the dsDNA biosensor in the absence and in the presence of ACS6CN in solution (1.0×10^{-5} M) (b) Differential pulse voltammogram (DPV) at pH 4.5 in acetate buffer with 30% ethanol for the oxidation of ACS6CN attached to the surface of glassy carbon electrode (GCE) in the presence of a ssDNA solution.....	55
Figure 15 (a) Differential pulse voltammogram(DPV), at pH 4.5 in acetate buffer with 30% ethanol, of the dsDNA biosensor	56
Figure 17 (a) Absorption spectrum of 6ESTAC01 (b)UV–Visible absorption spectra of 20 μ M 6ESTAC01 in presence of different concentrations of DNA:(μ M): (a)0.0 ;(b) 4; (c)6; (d)8;(e)10;(f)12 ;(g)14;(h) 16	58
Figure 16. (a) Absorption spectrum of 7ESTAC01 (b)UV–Visible absorption spectra of 20 μ M 7ESTAC01 in presence of different concentrations of DNA:(μ M): (a)0.0 ;(b) 2; (c)10; (d)12;(e)14;(f)16 ;(g)18;(h) 20	58
Figure 18 (a) Absorption spectrum of ACS6CN (b)UV–Visible absorption spectra of 20 μ M ACS6CN in presence of different concentrations of DNA:(μ M): (a)0.0 ;(b) 8; (c)10; (d)12;(e)14;(f)16 ;(g)18.....	60
Figure 19 (a) Absorption spectrum of ACS5CN (b)UV–Visible absorption spectra of 20 μ M ACS5CN in presence of different concentrations of DNA:(μ M): (a)0.0 ;(b) 4; (c)6; (d)8;(e)10;(f)12 ;(g)14;(h) 16	60
Figure 20. Molecular docked structures of 7ESTAC01 with ctDNA.a)Duplex Strand. Dodecamer duplex sequence (CGCGAATTCGCG) ₂ (PDB ID: 1BNA) was used in the docking studies b) Molecular docked model of 7ESTAC01	61
Figure 21 a) Molecular Docked structure of 7ESTAC01 with A strand b) Molecular Docked structure of 7ESTAC01 with B strand	61
Figure 23 a) Molecular Docked structure of 6ESTAC01 with A strand b)) Molecular Docked structure of 7ESTAC01 with B strand	62
Figure 22 Molecular docked structures of 6ESTAC01 with ctDNA.a) Duplex Strand. Dodecamer duplex sequence (CGCGAATTCGCG) ₂ (PDB ID: 1BNA) was used in the docking studies b) Molecular docked model of 6ESTAC01 showing significant hydrophobic interactions with ctDNA.	62
Figure 24 Molecular docked structures of 7CNAC01 with ctDNA.a) Duplex Strand. Dodecamer duplex sequence (CGCGAATTCGCG) ₂ (PDB ID: 1BNA) was used in the docking studies b) Molecular docked model of 7CNAC01	63
Figure 25 Molecular Docked structure of 7CNAC01 with A strand b)) Molecular Docked structure of 7CNAC01 with B strand	63
Figure 26 . Molecular docked structures of 6CNAC01 with ctDNA.a) Duplex Strand. Dodecamer duplex sequence (CGCGAATTCGCG) ₂ (PDB ID: 1BNA) was used in the docking studies b) Molecular docked model of 6CNAC01	64
Figure 27 a) Molecular Docked structure of 6CNAC01 with A strand b)) Molecular Docked structure of 6CNAC01 with B strand	64
Figure 29 . a) Molecular Docked structure of ACS6CN with A strand b)) Molecular Docked structure of ACS6CN with B strand	65
Figure 28 Molecular docked structures of ACS6N with ctDNA.a)Duplex Strand. Dodecamer duplex sequence (CGCGAATTCGCG) ₂ (PDB ID: 1BNA) was used in the docking studies b) Molecular docked model of ACS6N	65
Figure 30 Proposed mechanism for the electrochemical oxidation of guanine.....	73

Figure 31 Schematic drawing of (a) A,2-oxoA, and 2,8-dioxoA orientation during the oxidation and (b) G,8-oxoG, and 8-oxoGOX oxidized orientation during the oxidation.	74
Figure 32 a) Cyclic voltammogram of 10 mmol L ⁻¹ hybrid drugs 7estac01 in mixture of pH 7.2 , aqueous phosphate buffer and 20%DMF at a glassy Carbon Electrode(GCE) , with a Ag/AgCl reference electrode (RE), and the scan rate 0.1 V/s, E = potential, V = volt, A = ampere b) Cyclic voltammogram of 10 mmol L ⁻¹ hybrid drugs 7estac01 in mixture of pH 7.2 , aqueous phosphate buffer and 20%DMF at a Gold electrode(GE). C) Cyclic Voltamogram of 10 mmol L ⁻¹ 9-aminoacridine.....	80
Figure 33 MeB Signal On (SL-DNA-Before Hybridized) and MeB signal OFF (dsDNA-Hybridized). Cyclic voltammogram in Immobilization Buffer of 0.1 uM SL-DNA and dsDNA at Gold electrode at different Scan rates a) 1V/s b) 10V/s c) 100V/s.....	81
Figure 34 Cathodic(a,b) and Anodic Current(c,d) versus Scan rate of the 0.1 uM SL-DNA and dsDNA . Data took from the Cyclic voltammogram in Immobilization Buffer of 0.1 uM SL-DNA and dsDNA at Gold electrode at different Scan rates	84
Figure 35 MeB Signal On (SL-DNA-Before Hybridized) and MeB signal OFF (dsDNA-Hybridized). Cyclic voltammogram in Immobilization Buffer of 1 uM SL-DNA and dsDNA at Gold electrode at different Scan rates a) 1V/s b) 10V/s c) 100V/s.....	86
Figure 36 Cathodic(a,b) and Anodic Current(c,d) versus Scan rate of the 1 uM SL-DNA and dsDNA . Data took from the Cyclic voltammogram in Immobilization Buffer of 1 uM SL-DNA and dsDNA at Gold electrode at different Scan rates	88
Figure 37 A) ΔE separation of oxidation and reduction peaks before and after hybridization / SL-T-P =0.1uM B) ΔE separation of oxidation and reduction peaks before and after hybridization / SL-T-P =1 uM	89
Figure 38 Interaction of 7ESTAC01 with SL-DNA immobilized on the Gold Electrode.Cyclic voltammogram in Immobilization Buffer of 1 uM SL-DNA and 7ESTAC01 at different concentrations	90
Figure 39 Stem-Loop DNA on the gold electrode and Intercalation of 7ESTAC01 a) Cyclic Voltammetry in immobilization Buffer b)VPD in Acetate Buffer pH. 4.2 with different concentration of 7ESTAC01.....	92
Figure 41 SL-DNA and different concentration of 7ESTAC01 .Compound immobilized on the surface of the electrode for a) 1 h b)2 hours c) 24 hours SL-DNA and different concentration of 7ESTAC01 .Compound immobilized on the surface of the electrode for a) 1 h b)2 hours c) 24 hours	93
Figure 42 VPD of SL-DNA/GE and dsDNA/GE in Ph. 4.2 acetate buffer a) 400 uM 7estac01 in solution, acetate buffer with 1 hour of interaction: vpd oxidation applying -0.122 v of reduction potential of 7ESATC01 during 300 sec in stem-loop biosensor b) vpd oxidation applying -0.122 v of reduction potential of 7estac01 during 300 sec in 2wj biosensor for 10 um 7estac01 in solution, acetate buffer with 1 hour of interaction	94
Figure 43 . a) I(100 uM 7ESTAC01),II (400uM 7ESTAC01). 7ESTAC01 in solution using Acetate buffer with 2 hour of interaction: VPD oxidation .Reduce form of 7estac01 was obtained applying - 0.122 v of reduction potential during 300 sec in Stem-loop biosensor after the hour of interaction between 7esatc01 and SL-DNA	95
Figure 44 . DNA immobilized on the surface of the Gold Electrode. VPD in Acetate Buffer pH. 4.2	96

ABBREVIATIONS

A	Adenine
T	Thymine
G	Guanine
C	Cytosine
CT-DNA	Calf thymus DNA
dsDNA	Double stranded DNA
ssDNA	Single stranded DNA
DPV	Differential pulse voltammetry
CV	Cyclic voltammetry
DMF	Dimethylformamide
BP	Phosphate buffer
GCE	Glassy carbon electrode
GE	Gold Electrode
MHC	Mercatohexanol
SL-DNA	Stem Loop DNA
MeB	Methylene Blue
RE	Reference electrode
CE	Counter electrode
IB	Immobilization Buffer
HB	Hybridization buffer
TBAP	Tetrabutyl ammonium perchlorate
Ea	Anodic Potential

E_c	Cathodic Potential
ΔE_{peaks}	Peak potential difference
$E_{1/2}$	half wave potential
v	Scan rate
I_{pc}	Cathodic Current
I_{pa}	Anodic Current

SUMMARY

CHAPTER 1	15
ELECTROCHEMICAL, MOLECULAR DOCKING AND UV-VIS ABSORPTION SPECTROSCOPY ON THE INTERACTION ACRIDINE-THIOPHENE DERIVATES WITH dsDNA AND ssDNA.....	15
1.1 INTRODUCTION	16
1.1.2 Importance of the Acridine and thiophene in cancer treatment	16
1.1.3 Hybrid Drug to improve Cancer Treatment	17
1.1.4 Electrochemical DNA biosensor and DNA conductivity.....	18
1.2. OBJECTIVES.....	20
1.3. METHODOLOGY	21
1.3.1 Chemical Compounds	21
1.3.2 Reagents	22
1.3.3 Electrochemical studies.....	22
1.3.3.1 Standard Cleaning of Carbon Electrodes Vitreous.....	22
1.3.3.2 Studies in aprotic media	23
1.3.3.3 Studies in aprotic media in Oxygen Presence	23
1.3.3.4 Studies in protic media.....	24
1.3.4 Electrochemical DNA interaction assay.....	24
1.3.4.1 Electrochemical dsDNA biosensor	24
1.3.4.2 Study of interaction with ssDNA	25
1.3.5 UV–Visible absorption spectroscopy	25
1. 3.6 Molecular Docking.....	26
1. 4. RESULT AND DISCUSSION.....	28
1.4.1 Electrochemical studies.....	28
1.4.1.1 Electrochemistry in aprotic media of Acridine-thiophene conjugates	28
1.4.1.2 Electrochemistry in aprotic media of Acridine-thiophene conjugates	33
1.4.1.3 Reactivity with oxygen of acridine-thiophene derivate in aprotic media.....	41
1.4.3 Intercalation using ssDNA in solution	47
1.4.5 Molecular docking.....	60
1.4.5.1 Interaction of 7ESTAC01 and Duplex stranded.....	61
1.4.5.2 Interaction of 6ESTAC01 and Duplex stranded.....	61

1.4.5.3 6ESTAC01 and A/B Strand	62
1.4.5.4 Interaction of 7CNAC01 and Duplex stranded	63
1.4.5.5 7CNAC01 and A/B Strand	63
1.4.5.6 Interaction of 6CNAC01 and Duplex stranded	64
1.4.5.7 6CNAC01 and A/B Strand	64
1.4.5.8 Interaction of ACS6N and Duplex stranded.....	65
1.5 CONCLUSION	67
CHAPTER 2	69
AN ELECTROCHEMICAL BIOSENSOR BASED ON HAIRPIN-DNA MODIFIED GOLD ELECTRODE FOR DETECTION OF DNA DAMAGE FOR A NEW ACRIDINE-THIOPHENE CANCER DRUG.	69
2.1. INTRODUCTION	70
2.1.1 DNA biosensor for detection of Cancer- drug	70
2.1.2 SL-DNA Biosensor at Gold Electrode: Improvement of the Surface conductivity	70
2.1.3 Chemical and physical interaction of DNA and small molecules.....	72
2.1.4 Electrochemistry of guanine and 8-oxoguanine at gold electrodes.....	73
Source: From Reference (FERAPONTOVA,2004).....	73
2.1.4.1 Orientation of Guanine during Oxidation	74
Source: From Reference (IBAÑEZ, D. et al.,2015).....	74
2.2. OBJECTIVES.....	75
2.3. METHODOLOGY	76
2.3.1 Reagents	76
2.3.2 STEM-LOOP DNA (SL-DNA) and double strand DNA (dsDNA) biosensor on the gold electrode surface.....	77
2.3.2.1 Preparation of SL-DNA/GE and dsDNA/GE.....	77
2.3.2.2 Immobilization of Stem-Loop DNA and dsDNA.	77
2.3.2.3 Optimization of SL-DNA Probe, DNA complementary	77
2.3.3 Optimization of 7ESTAC01 concentration and experimental Timing.....	78
2.3.4 Electrochemical Measurements.....	79
2.4.1 Synergic activity of 7ESTAC01	80
2.4.2 Optimization of concentration of Stem-Loop DNA	81
a) b)	81
2.4.2.1 Optimization of DNA/GE and dsDNA/GE	85
2.4.2.3 Detection of DNA damage evaluated by oxidation.....	91
2.4.3 Interaction of SL-DNA/dsDNA with 7ESTAC01 inducing oxidative DNA damage.....	92

2.4.3.1 7estac01 in solution and reduced form of 7ESTAC01	94
2.4.3.2 Reduced form of 7ESTAC01 against Blanks.....	95
2.5. CONCLUSION.....	97
REFERENCES	98

CHAPTER 1

ELECTROCHEMICAL, MOLECULAR DOCKING AND UV-VIS ABSORPTION SPECTROSCOPY ON THE INTERACTION ACRIDINE-THIOPHENE DERIVATES WITH dsDNA AND ssDNA.

1.1 INTRODUCTION

As the mechanisms underlying the development of cancer were uncovered, it became clear that DNA is the critical target against tumorigenesis. Nowadays with the complete knowledge of the structure of DNA, there were several established therapeutic modalities targeting DNA: Antimetabolites, which can deplete nucleotides; alkylation agents, which cause direct DNA damage and intercalators, which bind DNA and inhibit the activity of many enzymes involucre in DNA replication process. The most successfully and widely used anticancer agents based on intercalation binding. The interest in DNA-intercalating ligands as anti-cancer drugs has developed greatly since the clinical success of doxorubicin. Many acridine/acridone compounds, which have anticancer activity have been synthesized, including the following: acridine-carboxamides, nitro acridines, nitro pyrazole-acridine, bis(acridines); and amsacrine (NEPALI,et al., 2014). However, despite a great deal of rational design of synthetic DNA-intercalators, only a few compounds have proved to be clinically useful.

For these reasons, there are useful future goals for the development of more specific DNA-intercalators as anti-cancer drugs. These include the production of improved topoisomerase inhibitors using DNA intercalation and the development of reductively-activated chromophores with high reactivity with oxygen. Then hybrid drug which comprises the incorporation of two drug pharmacophores in one single molecule are designed to have possible synergistic effects, and multiple targets have been studied (BRETT,et al.,2013). The use is of small molecules able to induce Topoisomerase inhibition and telomere dysfunction in cancer cells. The binding affinity and selectivity of these molecules depend on properties of chromophores and substituted groups.

1.1.2 Importance of the Acridine and thiophene in cancer treatment

Acridines are planar heterocyclic structures widely studied as antitumor and antiparasitic agent and have been shown to stabilize DNA structure that can promote telomerase inhibition in cancer cells (OUBERAI, et al.,2006). The biological activity of acridines has been attributed to the core polyaromatic ring, which can intercalate within double stranded DNA. The

mechanism of their intercalation into DNA is based on π -stacking interaction with base pairs of dsDNA. In cancer chemotherapy, the biological targets of acridines include DNA topoisomerases I, II; telomerase/telomeres and protein kinases. (WANG, et al.,2008). In addition to that, acridine-based anticancer or antimicrobial drugs, which bind to DNA by intercalation, might either donate electrons to or accept electrons from, the double helix, thus actively participating in electron transfer reactions. In fact, how important are contributions from electron transfer was demonstrated with several cancer drugs used in the market. (BAGULEY, et al.,2003). We focus in particular on two acridine-based drugs that have been tested against human cancer in the clinic. Amsacrine was the first synthetic drug of the DNA-intercalating type. Amsacrine is a 9-anilinoacridine derivative that appears to act as an electron donor in Electron transfer (ET) reactions on DNA, while N-[2-(dimethylamino)ethyl]acridine-4-carboxamide (DACA) may act as an electron acceptor. Such reactions may make important contributions to the antitumor activity of these drugs. Amsacrine and Nitracrine were used with clinical efficiency.

1.1.3 Hybrid Drug to improve Cancer Treatment

Several types of research were focused in synthesized acridine derivatives having nitro, methoxy, methyl, aminoalkyl and amino substituents have been tested as potential anticancer agents (PONTINHA, ET AL.,2013). In addition to that have been tested acridine conjugate linked with another pharmacophore to improve binding affinity and selectivity (NEPALI, et al.,2014 and GOODELL, et al.,2006).

Pontinha et al., 2013; designed series of substituted triazole linked acridine compounds. Thiophene-derivates are a new group of compounds with very interesting properties. The biological activity of some thiophene-derivates against some cancer cells might be attributable to a slight but continued deoxygenation of the compounds. The potential anticancer activity of thiophene-S-oxide has investigated a study of the use of estradiol derivatives as carriers of thiophene-S-oxides to breast cancer cells was also tested in a full 60 tumors cell lines (BRETT, et al.,2003)

J Noh et al.,2015; reported a promising dual Stimuli-responsive hybrid drug (QCA) as an anticancer therapeutic agent. This hybrid drug took advantage of the presence of H_2O_2 and

acidic pH, main features in cancer cells. In fact, the Quinone methide and cinnamaldehyde act in a synergistic manner to amplify oxidative stress.

1.1.4 Electrochemical DNA biosensor and DNA conductivity

Electrochemistry is a promising method suitable for rapid detection of specific dsDNA and ssDNA sequence, combining high sensitivity. Techniques, such as differential pulse (DPV) and cyclic voltammetry (CV), are suitable for studies of the biological system using aprotic and protic media, with very little or no sample pre-treatment. Special attention is paid to application carbon (pyrolytic graphite, glassy carbon) electrodes for monitoring reduction and oxidation processes (label-free detection) (DOGAN-TOPAL, et al., 2014). Moreover, there has been a growing interest in the electrochemical investigation of the interaction between anticancer drugs and DNA. Electrochemical DNA biosensor enables us to predict and evaluate anticancer drugs-DNA interaction. Also, the needed of analyses of several structures (pharmacophores), gene sequences, oxidative damage to DNA and the understanding of DNA interactions with molecules to the development of DNA-electrochemical biosensor is a priority for Anticancer drug research (KALANUR,; KATRAHALLI; SEETHARAMAPPA, 2009)

A dsDNA electrochemical biosensor is a receptor-transducer device that uses dsDNA that incorporates immobilized DNA on the electrode surface, and measure specific binding processes with DNA using an electrochemical transducer. A typical biosensor construct has three features a recognition element, a signal transducing structure and an amplification element. Electrochemical DNA biosensors exploit the affinity of single-stranded DNA, which is immobilized over an electrochemical transducer, for complementary strands of DNA and are used in the detection of specific sequences of DNA or small molecules like drugs candidates. (HUANG, et al., 2016).

The most important factor for the preparation of efficient DNA electrochemical biosensor is the immobilization of the DNA. Different adsorption immobilization procedures such as electrostatic or evaporation adsorption, forming monolayer DNA films have been used. This crucial immobilization of DNA onto an electrode surface is in many ways the most important aspect of the development of DNA biosensors for monitoring drug interaction because it will determinate the efficient electron transfer and accessibility of the DNA to drugs in solution.

The dsDNA electrochemical biosensor, using differential pulse voltammetry(DPV), has been successfully utilized to evaluate the interaction of several molecules with dsDNA (SAZHNIKOV, et al.,2013).Observing the electrochemical signal related to DNA-DNA interactions or DNA-drug interactions can provide; the nature of complex formed, binding site size and the role of free radicals generated during interaction in the drug action.

The electrochemical DNA biosensor has been used to sense oxidative damage to DNA. The electrochemical behavior of the oxidation of dsDNA has been studied on carbon electrodes and showed that can be oxidized more easily.The occurrence of oxidative damage to dsDNA leads to the breaking of the hydrogen bonds and the opening of the double helix.In fact, this causes the bases to come into contact with the electrode surface and enables the detection of oxidative damage by monitoring the oxidation of the guanine and adenine (RADI.; EISSA.; NASSEF,2014).

Another important advantage of using this biosensor is the possibility of generation of highly reactive intermediates *in situ*, on the electrode surface, and the electrochemical detection of their direct interaction with dsDNA . It is important to mention that there are still problems in an efficient immobilization of DNA on the electrode.For this reason, this step is considered vital during the DNA attaching. Few cases were reported when the immobilization was performed using electrochemical conditioning like polarization.Then, it concluded a weak point of electrostatic immobilization is the randomly oriented dsDNA over the surface of the electrode, diffculting the electrons transfer.However, the new generation of the electrochemical biosensor is focused in a covalent link between the DNA on the surface of the electrode.

The electrochemical studies using DPV to investigate reactivity with the oxygen of small molecules in aprotic media has been successfully studied. (BRETT,et al.,2003). Electrochemical studied of small molecule–DNA interactions can provide a useful complement to the results obtained by the UV-Vis spectroscopic methods. Relationship between constant binding and reduction potential recorded in aqueous media can help to understand structure-activity (SIRAJUDDIN; ALI S FAU - BADSHAH; BADSHAH,2014)

Six synthetic DNA intercalators of a series of acridine-thiophene conjugate compounds, designed as 7CNAC01, 6CNAC01,7ESTAC01,6ESTAC01, ACS6CN and ACS5CN that linked two important anti-cancer pharmacophores, were chosen for electrochemical characterization in aprotic and aqueous media using Cyclic voltammetry. We thus performed

an electrochemical study using dsDNA-biosensor to investigate the interaction of acridine-thiophene conjugate with dsDNA. The aim is to provide for the first time, new data concerning DNA damage using six acridine-thiophene conjugates.

To clarify the nature of the interaction between the six acridine-thiophene conjugate and DNA, UV-Vis spectroscopy was also performed using dsDNA calf thymus (ctDNA). Also, *in silico* molecular docking was performed to corroborate the experimental results and elucidated specific binding mode, between acridine derivatives and ctDNA.

1.2. OBJECTIVES

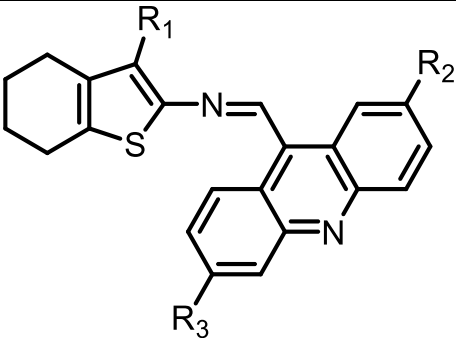
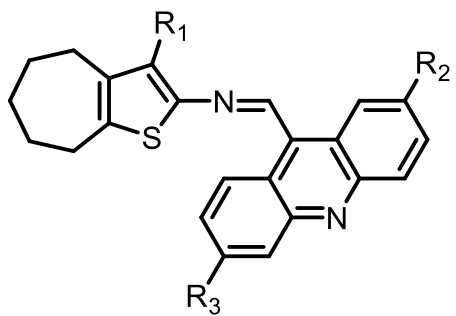
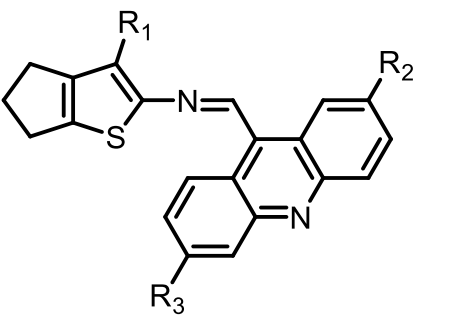
- ✓ Electrochemical, Molecular docking and UV-Vis absorption spectroscopy characterization of six synthetic DNA intercalators based on the linked of Acridine and Thiophene derivatives.
- ✓ Detection of the damage caused to DNA by Acridine-thiophene derivatives using an electrochemical DNA-biosensor on the surface of the Glassy carbon electrode.

1.3. METHODOLOGY

1.3.1 Chemical Compounds

All series of components were synthesized by Professor Thiago Mendonça de Aquino from Magnetic Resonance Laboratory at the Federal University of Alagoas-Brazil. The features of structure, formula and molecular weight, are shown in the following table.

Table 1 List of compounds based on the linked of acridine and thiophene derivatives.

Compounds	Substituents	Code	Molecular Formula	Molecular weight
	$R_1 = \text{CN}$ $R_2 = \text{H}$ $R_3 = \text{H}$	6CNAC01	$\text{C}_{23}\text{N}_3\text{SH}_{17}$	$367,46 \text{ g mol}^{-1}$
	$R_1 = \text{CN}$ $R_2 = \text{OMe}$ $R_3 = \text{Cl}$	ACS6CN	$\text{C}_{24}\text{N}_3\text{SOClH}_{18}$	$431,94 \text{ g mol}^{-1}$
	$R_1 = \text{CO}_2\text{CH}_2\text{CH}_3$ $R_2 = \text{H}$ $R_3 = \text{H}$	6ESTAC01	$\text{C}_{25}\text{N}_2\text{SO}_2\text{H}_{22}$	$414,52 \text{ g mol}^{-1}$
	$R_1 = \text{CN}$ $R_2 = \text{H}$ $R_3 = \text{H}$	7CNAC01	$\text{C}_{24}\text{N}_3\text{SH}_{19}$	$381,49 \text{ g mol}^{-1}$
	$R_1 = \text{CO}_2\text{CH}_2\text{CH}_3$ $R_2 = \text{H}$ $R_3 = \text{H}$	7ESTAC01	$\text{C}_{26}\text{N}_2\text{SO}_2\text{H}_{24}$	$428,55 \text{ g mol}^{-1}$
	$R_1 = \text{CN}$ $R_2 = \text{OMe}$ $R_3 = \text{Cl}$	ACS5CN	$\text{C}_{23}\text{N}_3\text{SOClH}_{16}$	$417,91 \text{ g mol}^{-1}$

1.3.2 Reagents

Calf Thymus DNA (Sodium salt, Type I) were obtained from Sigma Chemical Co.

Acetate buffer solutions of ionic strength 0.2 at pH 4.5 were used in all DNA experiments and were prepared using analytical grade reagents and purified water from a Millipore Milli-Q system.

All the electrochemical measurements in aqueous media were made in 10^{-1} mol. L⁻¹ phosphate buffer (PB) solutions prepared with Na₂HPO₄ and NaH₂PO₄.

Tetra butyl ammonium perchlorate(TBAP, 0.1mol L⁻¹). For TBAP synthesis proceeded as follows: 101.44 g of tetrabutylammonium bromide (TBABr) was slowly dissolved in 300 ml of distilled water, and then added to the aqueous solution TBABr, an aliquot of 30 mL perchloric acid resulting in a white suspension. The formed product was filtered under vacuum, giving small white crystals. The mother liquor of this filtration process had pH = 1.0; the precipitate was washed until the filtrate gets pH=7.0. For recrystallization, the crystals were filtered, dissolved in hot ethyl acetate and the mixture placed in a separatory funnel to remove residual water. The ethyl acetate phase was then placed in an ice bath for crystallization, and then the crystals formed were dried under reduced pressure.

1.3.3 Electrochemical studies

Electrochemical studies were performed using an AUTOLAB PGSTAT (AUT73222) with GPES version 4.3, software PG (Metrohm Autolab) using glassy carbon GCE (6 mm diameter) as the working electrode, a platinum wire as a counter electrode and an Ag/AgCl/Cl⁻¹ as a reference electrode. The measurements were performed at a temperature of 25 ± 1 °C. Further processing of graphics was performed by Origin 8.0 software.

The electrochemical techniques used were cyclic voltammetry(CV) and differential pulse voltammetry (DPV).

1.3.3.1 Standard Cleaning of Carbon Electrodes Vitreous

The glassy carbon electrode (GCE) has undergone a mechanical polishing cleaning after being left overnight in a solution of nitric acid 10% (v / v) to eliminate possible impurities adsorbed on the electrode surface.

The glassy carbon electrode was polished with alumina (1.0, 0.5 and 0.3 μM) and washed with water; later the electrodes were taken to ultrasound for 30 s in ethanol to remove the residual particles.

After the cleaning procedure, the glassy carbon electrode was performed with a standard solution of Potassium Ferricyanide ($\text{K}_3 [\text{Fe} (\text{CN})_6]$) / Potassium ferriyanide ($1.0 \times 10^{-3} \text{ mol L}^{-1} \text{ K}_4 [\text{Fe} (\text{CN})_6] \cdot 3\text{H}_2\text{O}$) in $0.1 \text{ mol L}^{-1} \text{ KCl}$ to verify the electroactive area of the electrode. Then the electrodes were used in electrochemical studies.

1.3.3.2 Studies in aprotic media

Cyclic voltammetry was performed using three electrodes: Glassy carbon electrode (GCE), platinum wire counter electrode (CE), and $\text{Ag}/\text{AgCl}/\text{Cl}^{-1}$ reference electrode (RE).

The analyzes in aprotic media were conducted using as the supporting electrolyte solution of N, N- dimethylformamide (DMF) and tetrabutylammonium perchlorate (TBAP, 0.1 mol L^{-1}). All compounds were tested at 1.0 mmol L^{-1} . The atmosphere and particularly the absence of traces of oxygen were controlled using nitrogen.

In the electrolytic cell, added to the supporting electrolyte (DMF + TBAP), under N_2 gas for 15-20 minutes. The potentials of oxidation (anodic E, E_a) and reduction (cathodic , E_c) values were measured for each substrate at window scan from -2.0 to 1.0 V. CVs of 1.0 mM of each compounds recorded at scan rates of 0.01 to 1 Vs^{-1} ,in the scanning window (between -2.5 and $+1.0 \text{ V}$ vs. Ag/AgCl). We thus studied the influence of the scanning scan rate(scan rate of $0.01 ; 0.03 ; 0.05 ; 0.075 ; 0.1 ; 0.2 ; 0.3 ; 0.5 ; 1 \text{ V s}^{-1}$).

1.3.3.3 Studies in aprotic media in Oxygen Presence

Electrochemical studies in aprotic media (DMF/ 0.1 mol L^{-1} TBAP) were performed in the presence and absence of oxygen to determine the reactivity, upon reduction of acridine-thiophene derivates front the oxygen. Were analyzed electrochemical parameters such as the peak potential and current for the first reduction wave . Each component was added to the supporting electrolyte, and the solution was degassed with N_2 before the measurement by cyclic voltammetry. Oxygen was bubbled into the cell, and their concentration was monitored with Oximeter (Digimed DM-4). Cyclic voltammograms were recorded at different oxygen concentrations with scan rate 0.5 V s^{-1} .

1.3.3.4 Studies in protic media

Cyclic voltammetry was performed using three electrodes: Glassy carbon electrode (GCE), platinum wire counter electrode (CE), and Ag/AgCl reference electrode (RE).

In electrochemical analysis was used as supporting electrolyte 0.2 mol L⁻¹ phosphate buffer solution (pH 7.0).

The electrochemical behavior of six compounds was investigated using Cyclic voltammetry in pH=7.2 Phosphate buffer and 20% DMF in N₂ saturated solutions using a GCE. CVs of 0.1 mM of each compound recorded at scan rates of 0.01 to 1 Vs⁻¹, in the scanning window (between -1.2 and +1.0 V vs. Ag/AgCl)

1.3.4 Electrochemical DNA interaction assay

All electrochemical studies testing DNA interaction was performed using differential pulse voltammetry(DPV).The working electrodes were a GCE of 6-mm diameter. The counter electrode was a platinum wire, and the reference electrode was Ag|AgCl|CL⁻¹. The optimized differential pulse voltammetry parameters were as follows: pulse amplitude of 50 mV, the pulse width of 70 ms⁻¹ and a scan rate of 5 mV s⁻¹ using a step potential [ΔE_s] of 2 mV.

1.3.4.1 Electrochemical dsDNA biosensor

The following experiments were conducted to evaluate the interaction of acridine-thiophene conjugate with DNA by differential pulse voltammetry.The electrochemical procedure for the investigation of the acridine-thiophene derivatives and dsDNA interaction involved three steps: preparation of the electrode surface, immobilization of the dsDNA gel and voltammetric transduction. The electrode was first polished with alumina. After mechanical cleaning the electrode was electrochemically pretreated the with a sequence of five cyclic potential scans from 0 to + 1.5 V (scan rate of 5 mV s⁻¹ and 120 seconds of conditioning time) versus Ag|AgCl|CL⁻¹ in the mixture of 0.2 M acetate buffer at pH 4.5 and 30% ethanol solution. This conditioning ensures immobilization of the DNA to the electrode surface.

To immobilize dsDNA (calf thymus, type 1), the surface of the electrode was coated with 10 uL of calf thymus DNA solution (12.0 mg of dsDNA in 1.0 mL acetate buffer at pH 4.5) and leaving the electrode to dry for 15 minutes with nitrogen .

The prepared biosensor was then put into the cell in scan rate 0.005 V s^{-1} with potential scans from 0 to +1.4 V and 120 seconds of conditioning time. The Conditioning potential for each substrate is being shown at the end of the paragraph. For each series of experiments, an identical dsDNA electrode was prepared as a reference blank as a control; this blank received the same pre- and post-treatments as the test electrode. Each substrate was worked with 10^{-5} M . The Interaction time for all substrates and DNA biosensor before the potential application was 20 min.

1.3.4.2 Study of interaction with ssDNA

Single-stranded DNA (ssDNA) was prepared by dissolving 3.0 mg of dsDNA in 1.0 mL of hydrochloric acid (1 M) and heating for one h until complete dissolution. This treatment was followed by neutralizing the solution with 1.0 mL of sodium hydroxide (1 M) and 9 mL of acetate buffer was then added. Freshly prepared ssDNA solution was added to the cell, and single-scan DPV experiments were conducted in the range of 0 to +1.4 V versus $\text{Ag}|\text{AgCl}|\text{Cl}^{-1}$ 120 seconds of conditioning time. Two peaks corresponding to the oxidation of the guanine and adenine bases appeared at potentials of +0.815 and +1.131 V, respectively. To ensure reproducibility, this assay format was repeated at least three times, and the oxidation current and potential of the bases were very similar (RSD of 5%). After this process, the GCE modified with acridine-thiophene derivatives was inserted into the ssDNA solution, and the DPV experiment was performed. An unmodified glassy carbon electrode was also employed in the DPV experiments involving the ssDNA solution and was used for comparison.

1.3.5 UV–Visible absorption spectroscopy

We performed UV-Vis absorption spectroscopy using calf thymus DNA. We chose to keep the concentration of the compound in and vary the DNA.

The study was performed in Tris-HCl buffer (50 mM NaCl, five mM Tris-HCl, pH 7.2), the concentration of compounds constant ($20 \mu\text{M}$) while varying the ct-DNA concentration from 0 to $20 \mu\text{M}$.

The DNA was prepared for dissolution of 12 mg.mL^{-1} ct-DNA in acetate buffer (pH 4.5, 1.0 mol.L^{-1}). The stock solution was kept at 8°C for 24 h, and stirred at certain intervals to ensure homogeneity of the final DNA solution.

The concentration of the stock solution of ctDNA (0.38 mM per nucleotide) was determined by the UV absorption at 260 nm using the molar extinction coefficient of 6600 M⁻¹ cm⁻¹. UV-Vis spectroscopy checked your purity by monitoring the ratio of absorbance values at 260/280 nm, ratio > 1.8 at A₂₆₀/A₂₈₀ was obtained is indicative that DNA was sufficiently free from proteins. The intrinsic binding constant K_b of the compounds with CT-DNA was calculated according to Wolfe-Shimer equation:

$$\frac{[DNA]}{(\epsilon_a - \epsilon_f)} = \frac{[DNA]}{(\epsilon_b - \epsilon_f)} + \frac{1}{K_b(\epsilon_b - \epsilon_f)} \quad (1)$$

Where [DNA] is the concentration of DNA by nucleotides, ϵ_a is the molar absorption coefficient of the complex at a given DNA concentration ($A_{obs}/[Compound]$), ϵ_f is the molar absorption coefficient of the complex in free solution, and ϵ_b is the molar absorption coefficient of the complex when fully bound to DNA. A plot of $[DNA]/(\epsilon_a - \epsilon_f)$ vs. [DNA] allows the determination of the intrinsic binding constant K_b , obtained by the linear data fit. The value of constant was calculated as the ratio between slope and intercept.

1. 3.6 Molecular Docking

The structures of acridine derivatives were first treated by semi-empirical theory at level PM3 using ArgusLab v. 4.0.1 software. The optimized structures with the lowest energy were used for the molecular docking calculations.

DNA and ligand (drug) files were provided using AutoDock Tools. The DNA was treated as a rigid molecule, whereas the ligands were treated as flexible, which means that all non-ring torsions were maintained.

The MGL tools 1.5.4 with AutoGrid4 and AutoDock4 were used to set up and perform blind docking calculations between drugs and DNA sequence. The Calf thymus DNA (ctDNA) sequence (CGCGAATTCGCG)₂ dodecamer (PDB ID: 1BNA) obtained from the Protein Data Bank (<http://www.rcsb.org/pdb/home/home.do>). First, the heteroatoms including water molecules were deleted. The polar hydrogen atoms were added into ctDNA molecules. Then, the partial atomic charges of the ctDNA and acridine derivatives were calculated using Gasteiger-marsili and Kollman methods, respectively. The ctDNA was put inside a box with some grid points in x × y × z directions, 94 × 104 × 126 and a grid spacing of 0.375 Å. Lamarckian genetic algorithms, as implemented in AutoDock, were employed to perform

docking calculations. The number of genetic algorithm runs and the number of evaluations were set to 100 and 2.5 million, respectively. All other parameters were default settings. For each of the docking cases, the lowest energy docked conformation, according to the AutoDock scoring function, was selected as the binding mode. The output from AutoDock was rendered with PyMol.

Molecular models were built to discuss the binding modes by docking using an AutoDock program for the interactions of acridine derivatives with multiple ctDNA fragments. The resulting complex was used for calculating the energy parameters which can substantiate the spectroscopic results. For better accuracy in results, the energy calculations using AutoDock Vina were performed from the 20 most important conformations for each acridine compounds studied. From the Vina calculations, the conformer with minimum binding energy is picked up from the one minimum energy (root mean square deviation; RMSD = 0.0) conformers from the 20 runs.

1. 4. RESULT AND DISCUSSION

1.4.1 Electrochemical studies

1.4.1.1 Electrochemistry in aprotic media of Acridine-thiophene conjugates

The first electrochemical characterization was performed using dimethylformamide (DMF) and 0.1 M Tetrabutyl ammonium perchlorate (TBAP) as the supporting electrolyte. The atmosphere and particularly the absence of traces of oxygen were controlled using nitrogen. CVs of 1.0 mM of each compound recorded at scan rates of 100 mV s⁻¹ in the scanning window (between -2.5 and +1.0 V vs. Ag/AgCl).

Cyclic Voltammogram of 7CNAC01 shows one quasi-reversible reduction wave in the cathodic region. The reduction region shows that the one quasi-reversible wave centered on $E_c = -0.73$ V vs. Ag/AgCl with corresponding $\Delta E_{\text{peaks}}(E_a - E_c) = 178$ mV. The peak separation value is about 131 mV at low scan (10 mV s⁻¹) but ΔE_{peaks} values increase progressively with the scan rate (225 to 300 mV/s) showing a non-negligible kinetic limitation in comparison with an ideally fast electron transfer. Therefore, it is likely that 2 electrons are involved as expected for this kind of molecule in aprotic conditions (12). The I_{pa}/I_{pc} ratio for all voltammetric processes was dependent on the scan rate and in all cases was near unity, suggesting and confirming that the reduction of 7CNAC01 is a quasi-reversible process. (Fig. 1(a) and Fig 3(a)). A similar result was obtained for 6CNAC01. The CV of 6CNAC01 shows one quasi-reversible reduction in the cathodic region. This wave is observed on $E_c = -0.74$ V with a peak separation of $\Delta E_{\text{peaks}}(E_{1a} - E_{1c}) = 415$ mV. The large peak to peak potential difference (ΔE_{peaks}) of 495 mV is suggestive of electrochemical reaction coupled with a chemical reaction. Fig. 1(b) and Fig. 4 (a). Identical $E_{1c} = -0.73$ V and $E_{1c} = -0.74$ V cathodic potential in the reduction region for 7CNAC01 and 6CNAC01, respectively. It is expected because both molecules have the same substituents. (Table 2).

The compound 7ESTAC01 exhibits one quasi-reversible reduction in the cathodic region centered on $E_c = -0.88$ V vs. Ag/AgCl with a peak separation of $\Delta E_{\text{peaks}}(E_{1a} - E_{1c}) = 79$ mV. Reversing the scan direction, showed two waves. The first one, corresponded to anodic peak centered on $E_a = -0.80$ V. The second one anodic peak, exhibit one irreversible oxidation wave at $E_{2a} = -0.32$ V. On the other hand, 6ESTAC01 shows two waves in the cathodic region. The first one wave shows an Irreversible reduction at $E_{1c} = -0.54$ V vs. Ag/AgCl. The second one wave showed a quasi-reversible reduction in the cathodic region centered on $E_{2c} = -0.82$ V vs.

Ag/AgCl with a peak separation of $\Delta E_{\text{peaks}}(E_a-E_c)=100\text{mV}$. Fig 1(c). Identical E_{1c} (-0.88V and -0.82 V) for 7ESTAC01 and 6ESTAC01 are expected because both molecules have the same substituent (Table 1). On the other hand to understand the more negative E_{1c} to 7ESTAC01 and 6ESTAC01 than 7CNAC01 and 6CNAC01. We localized one difference of the R1 substituent on the thiophene pharmacophore (Table 1). R1=CN (to 7CNAC01 and 6CNAC01) and R1= $\text{C}_0\text{H}_2\text{CH}_2\text{CH}_3$ (7ESTAC01 and 6ESTAC01). Then we propose that the good nucleophilicity of the (CN^-) can be facilitated the reduction potential of 7CNAC01 and 6CNAC01.

The CVs of ACS6CN and ACS5CN showed different patterns of electrochemical waves due to the presence of different substituent's on both pharmacophores (R1=CN, R2=OMe, R3=Cl). ACS6CN, shows two irreversible reduction in the cathodic region centered on $E_c = -1.27\text{ V}$ and $E_c = -0.58\text{ V}$ vs. Ag/AgCl . In the electrochemical window [0 – 1.0 V vs. Ag/AgCl], the CV highlights one irreversible anodic wave centered on $E_a = +0.29\text{ V}$ vs. Ag/AgCl, which have not been investigated further more. Nevertheless, that signals can be possibly assigned to the oxidation and dimerization of the unsaturated carbon atoms (Fig. 1(e) and Fig 1(f)) . The compound ACS5CN exhibits two waves in the cathodic region. The first one exhibits quasi-reversible reduction centered on $E_{2c} = -1.19\text{ V}$ vs. Ag/AgCl with a peak separation of $\Delta E_{\text{peaks}}(E_a-E_c)=140\text{mV}$. The second one exhibits quasi-reversible reduction centered on $E_{3c} = -1.78\text{ V}$ vs. Ag/AgCl with a peak separation of $\Delta E_{\text{peaks}}(E_a-E_c)=150\text{mV}$. On the anodic region (between 0 and +1.0 V vs. Ag/AgCl), shows one quasi-reversible oxidation centered on $E_{1c} = +0.05\text{ V}$ vs. Ag/AgCl with a peak separation of $\Delta E_{\text{peaks}}(E_a-E_c)=110\text{mV}$. Fig. 1(e)

Concerning the electrochemistry of acridines derivatives, with same substituents (9-chloro-6-hydroxymethyl-4-methoxy-7H-pyrido[4,3,2-kl]acridine) of our compound ACS6CN and ACS5CN, two paper have been previously characterized in aprotic media (11,19). P.W. Crawford et al, 1997 and Laurent Bouffier et al., 2012 and et al., recorded a CV of 10^{-3} M of Diplamine 11 in dimethylformamide (DMF) with TBAHFP (10^{-1} mol/L) as the supporting electrolyte. The CV was consistent with two sequential one-electron transfers, the first reduction forming reversible wave ($E_{1/2} = -1.092\text{ V}$) and the second generating a chemically unstable di-anionic species ($E_c = -1.554\text{ V}$) by an irreversible way. The characteristic potentials are in good accordance with our values of ACS5CN in aprotic media. (Table 2 and Fig 1(f))

Finally, to prove if the electrochemical wave is due the diffusion of our substrates to the electrode. We evaluated the peak current, varies linearly to the square root of the scan rate.

It shows that the electrode reaction is due to the diffusion of 7CNAC01, 6CNAC01, 7ESTAC01, 6ESTAC01, ACS6CN and ACS5CN in the solution (Fig 3(a), Fig 4(a), Fig 5(a), Fig 6(a), Fig 17(a), Fig 8(a))

Table 2 Mean parameter of Cyclic voltammetry in aprotic media, DMF/TBAP solution $\nu=0.1$ V/s. Experimental conditions as for Fig. 1 (Cathodic (E_c) and anodic (E_a) potentials

Aprotic media (DMF/TBAP)	E_{1c} (V)	E_{1a} (V)	$E_{1/2}$ (V)	$\Delta E(E_{1a} - E_{1c})$ mV
7CNAC01	-0.73	-0.54	-0.57	190
6CNAC01	-0.74	-0.30	-0.46	440
7ESTAC01	-0.88	-0.80	-0.75	80
6ESTAC01	-0.82	-0.72	-0.74	100
ACS6CN	-1.27	---	-1.17	---
ACS5CN	-1.19	-1.05	-1.10	140

Figure1 Cyclic voltammetry of 1 mM of each compound in dimethylformamide (DMF) plus 0.1 M Tetrabutyl ammonium perchlorate (TBAP), with a Ag/AgCl reference electrode (RE), and the scan rate 0.1 V/s, E = electrochemical potential, V = volt, A = ampere. Using Glass carbon electrode (GCE)

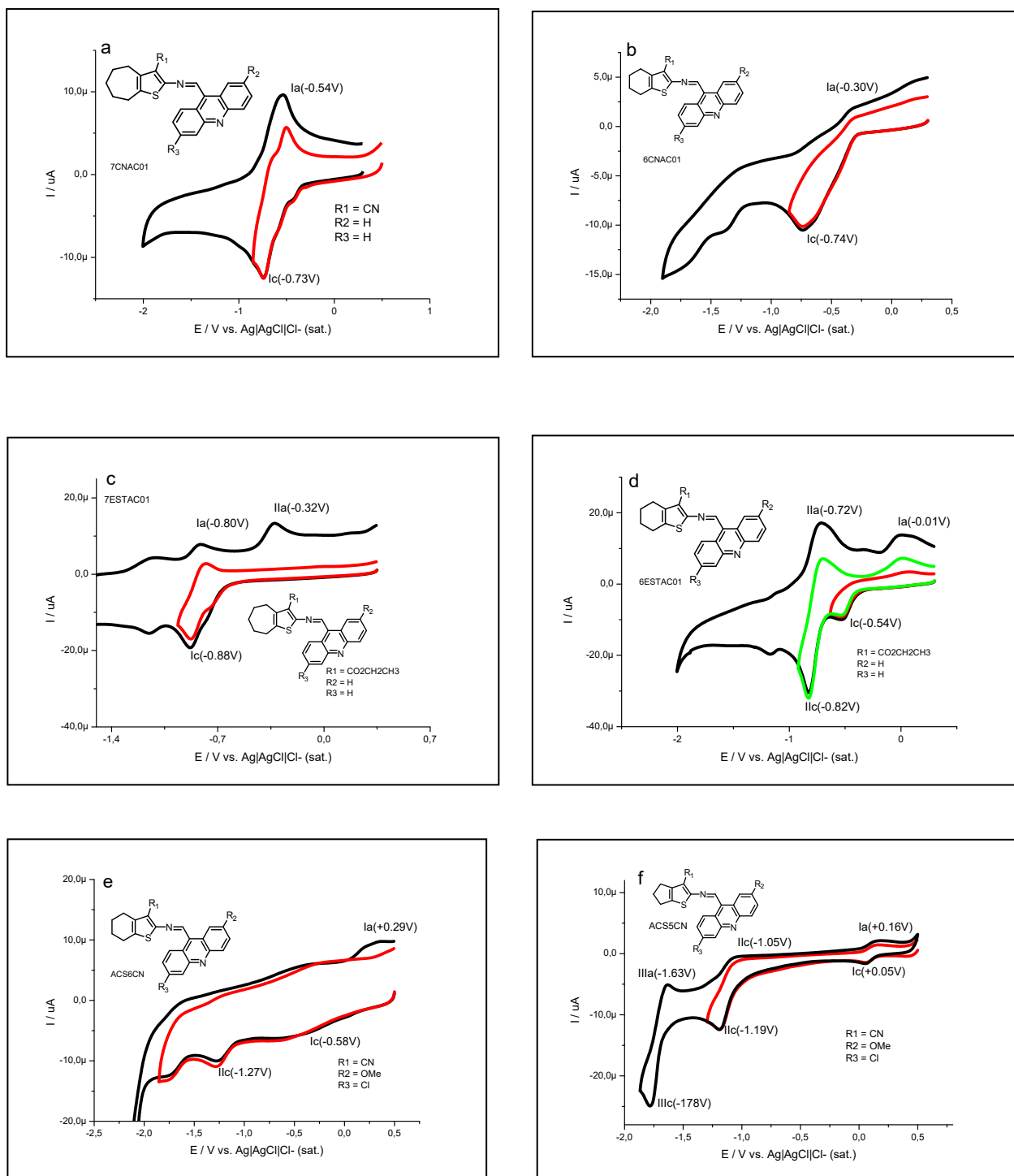
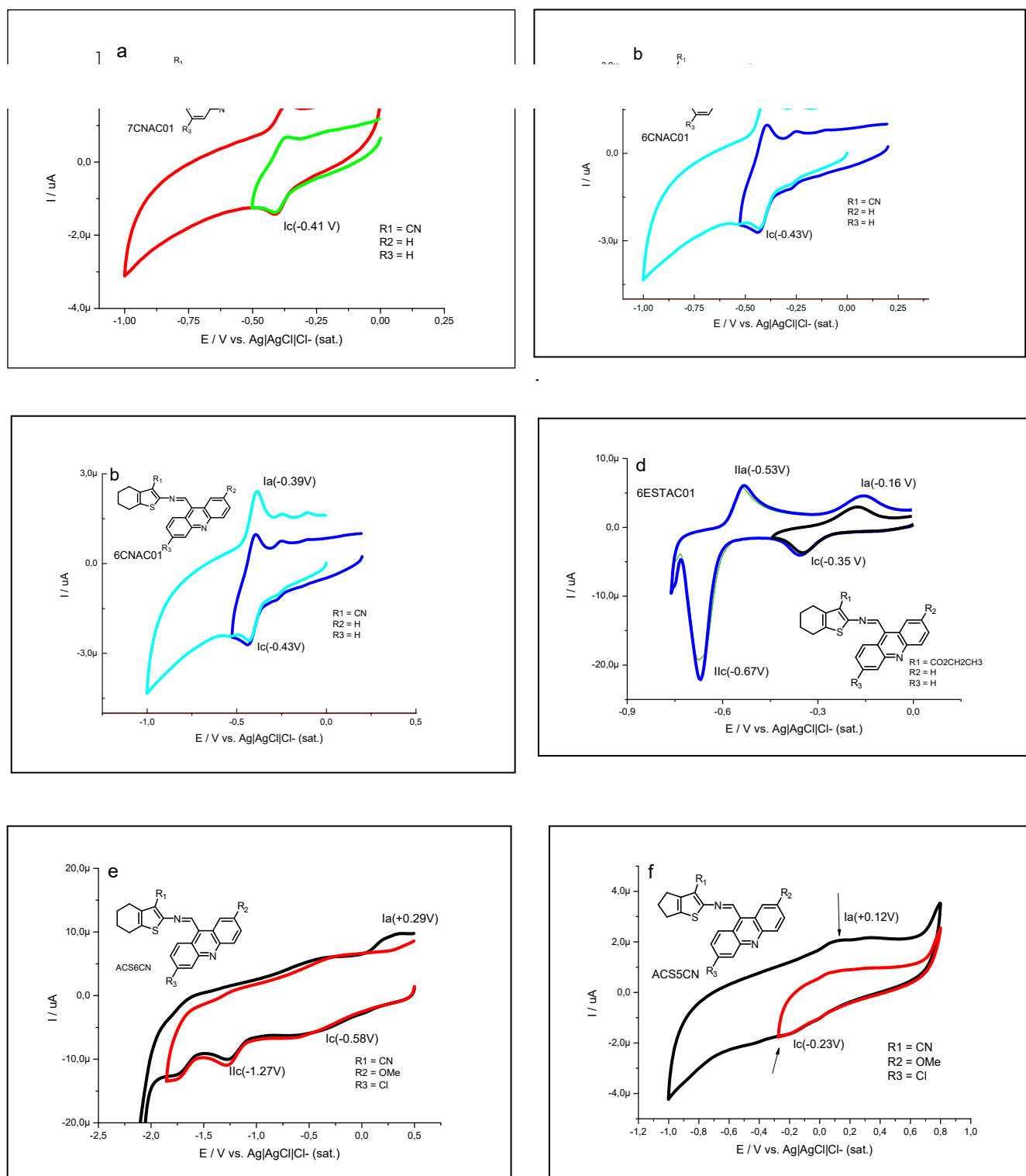


Figure2 Cyclic voltammogram of 10 mmol L⁻¹ hybrid drugs in mixture of pH 7.2 , aqueous phosphate buffer and 20%DMF at a GCE electrode , with a Ag/AgCl reference electrode (RE), and the scan rate 0.1 V/s, E = potential, V = volt, A = ampere



1.4.1.2 Electrochemistry in aprotic media of Acridine-thiophene conjugates

The electrochemical behavior of six compounds was investigated using CV in pH=7.2 Phosphate buffer and 20% DMF in N₂ saturated solutions using a GCE. CVs were recorded in the interval, -1.2 V to +1.0 V (Fig. 2). The results showed that six 7CNAC01, 6CNAC01, 7ESTAC01, 6ESTAC01, ACS6CN and ACS5CN compounds, undergo electrochemical reduction and both ACS6CN and ACS5CN undergo electrochemical oxidation.

7CNAC01 shows one semi-defined quasi-reversible system can be observed at $E_c = -0.41$ V vs. Ag/AgCl with a peak separation of $\Delta E_{\text{peaks}}(E_a - E_c) = 140$ mV. The reduction region of 6CNAC01 showed one quasi-reversible system at $E_c = -0.43$ V vs. Ag/AgCl with a peak separation of $\Delta E_{\text{peaks}}(E_a - E_c) = 40$ mV. Both results confirmed the electrochemical studies in aprotic media to 7CNAC01 and 6CNAC01. (Fig. 2(a) and (b)).

In Fig. 2(c) and (d). The reduction region of 7ESTAC01 showed two waves. The first one exhibits quasi-reversible reduction wave is centered on $E_c = -0.38$ V vs. Ag/AgCl with a peak separation of $\Delta E_{\text{peaks}}(E_a - E_c) = 210$ mV. The second one exhibits irreversible reduction is showed on $E_{2c} = -0.71$ V vs. Ag/AgCl. Similarly, the reduction region of 6ESTAC01, showed two waves. The first one exhibits quasi-reversible reduction wave is centered on $E_c = -0.35$ V vs. Ag/AgCl with a peak separation of $\Delta E_{\text{peaks}}(E_a - E_c) = 190$ mV. The second one exhibits quasi-reversible is observed on $E_{2c} = -0.67$ V vs. Ag/AgCl with a peak separation of $\Delta E_{\text{peaks}}(E_a - E_c) = 140$ mV.

Fig. 2(e). The reduction region of ACS6CN exhibit one quasi-reversible semi defined-wave is observed on $E_c = -0.40$ V vs. Ag/AgCl with a peak separation of $\Delta E_{\text{peaks}}(E_a - E_c) = 50$ mV. In the electrochemical window [0 – 1.0 V], the CV highlights one irreversible anodic wave centered on $E_a = +0.78$ V vs. Ag/AgCl. ACS5CN shows, one semi-defined irreversible wave at $E_c = -0.23$ V and a half potential $E_{1/2} = -0.14$ V (Table 3) in the cathodic region and another irreversible wave in the anodic region $E_a = +0.12$ V, (Fig. 2 (f)).

The main reason is explaining the very limited number of electrochemical reports in this acridine family of compounds linked to the intrinsic poor solubility in aqueous solutions. However and due the quite importance of acridine and thiophene pharmacophores, one

important and relevant paper in aqueous media to acridine derivatives, were studied by PONTINHA et al., 2013. They investigated the electrochemical behavior of two Triazole-acridine conjugates (GL15 and GL7) using CV in pH=7.0 (0.1 M phosphate buffer) in N₂ saturated solutions using a glassy carbon electrode.

Figure3 Studies in aprotic media. (a) Scan speeds in aprotic media of 7CNAC01.(b) Graph of I_{pc} vs $v^{1/2}$; (c) Graph of E_{pc} vs. $\log v$. [7CNAC01] = 1,0 mmol L⁻¹ in DMF/TBAP (0,1mol L⁻¹);glassy carbon electrode. N₂ atmosphere.

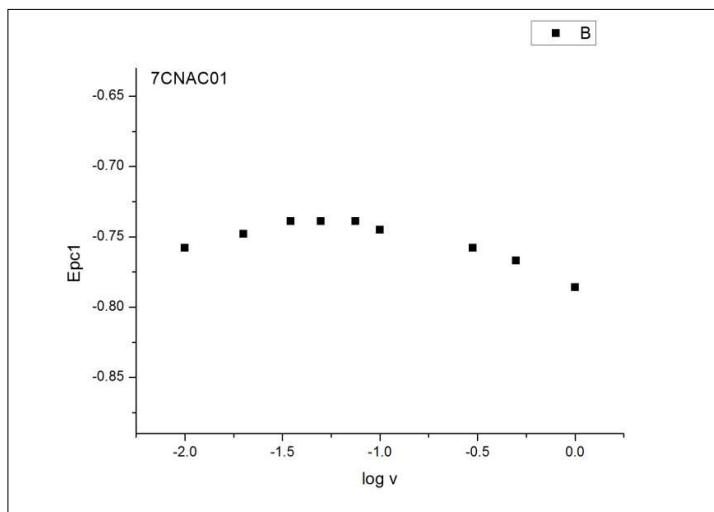
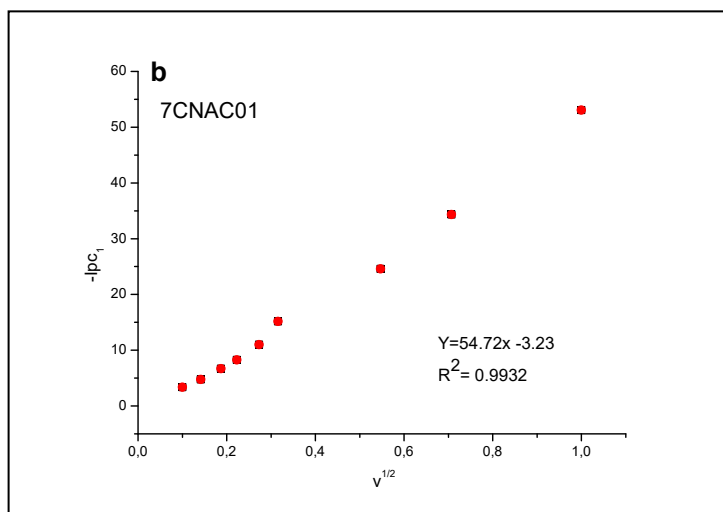
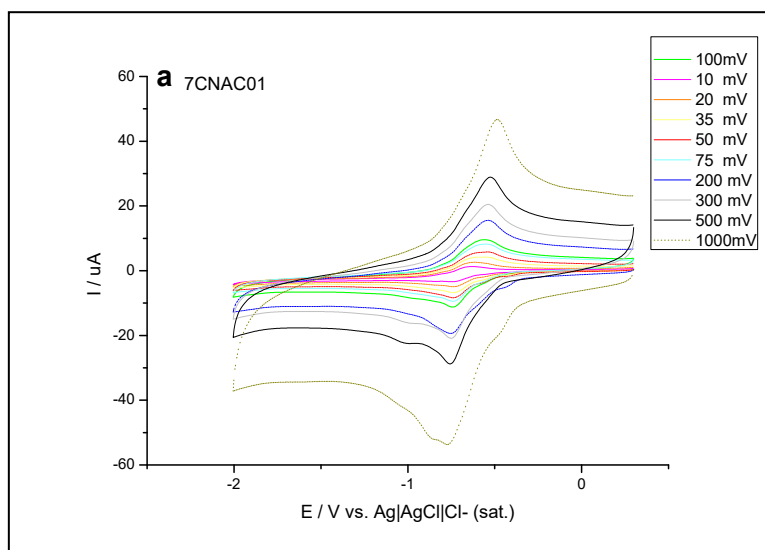
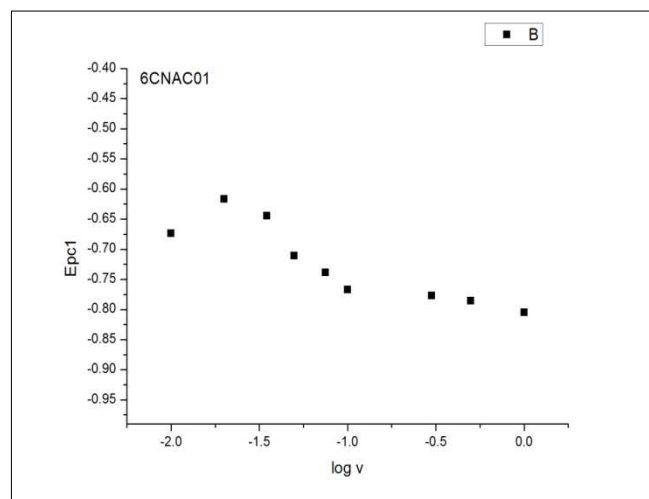
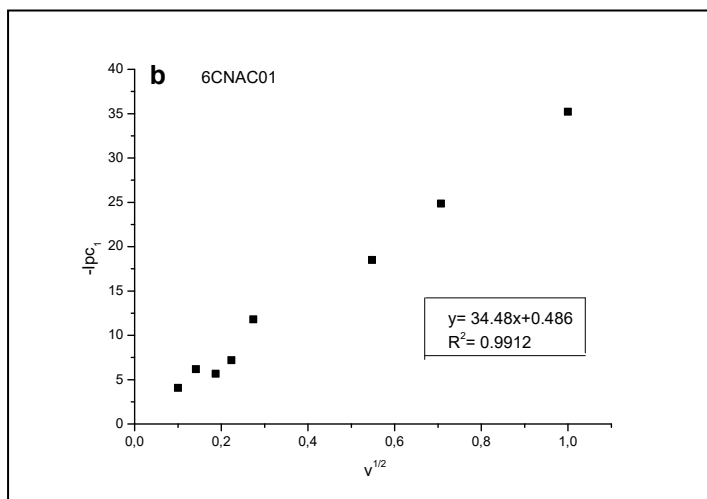
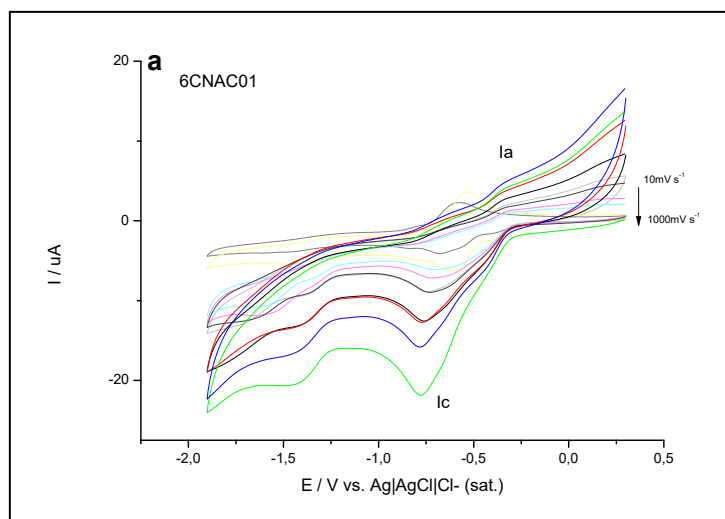


Figure4 Studies in aprotic media . (a) Scan speeds in aprotic media of 6CNAC01.(b) Graph of I_{pc} vs $v^{1/2}$; (c) Graph of E_{pc} vs $\log v$. [6CNAC01] = 1,0 mmol L in DMF/TBAP (0,1 molL⁻¹);glassy carbon electrode



The reduction of GL15 and GL17 showed similar potential. The reduction of GL15 and GL17 showed two peaks, peak $E_{1c} = -0.47$ V and peak 2c at $E_{2c} = -0.76$ V. The ΔE for two waves indicates the quasi-reversibility process to two Triazole-acridine conjugates. According to with our result in protic solution (Table 3 and Fig.2), the characteristic potentials are in good accordance with our E_{1c} values of 7CNAC01, 6CNAC01, 7ESTAC01, 6ESTAC01, ACS6CN and with the quasi-reversibility process.

Finally, in our electrochemical studies for acridine-thiophene derivates, we found that the electrochemical behavior of these active redox drugs is influenced by the nature of the solvent. It was clearly observed at Fig.1, Fig.2, Table 2, and Table 3.

Table 3 Mean parameter of Cyclic voltammetry electrochemical studies in aqueous solution, pH 7.2 Phosphate buffer, and 20%DMF. $\nu=0.1$ V/s. Experimental conditions as for Fig. 2

pH 7.2 Phosphate buffer	E_{1c} (V)	E_{1a} (V)	$E_{1/2}$ (V)	$\Delta E(E_{1a} - E_{1c})$ mV
7CNAC01	-0.41	-0.27	-0.38	140
6CNAC01	-0.43	-0.39	-0.39	40
7ESTAC01	-0.38	-0.17	-0.34	210
6ESTAC01	-0.35	-0.16	-0.31	190
ACS6CN	-0.40	-0.35	-0.37	50
ACS5CN	-0.23	----	-0.14	-----

Figure5 Studies in aprotic media . (a) Scan speeds in aprotic media of 7ESTAC01.(b) Graph of I_{pc} vs $v^{1/2}$; (c) Graph of E_{pc} vs $\log v$. [7ESTAC01] = 1,0 mmol L⁻¹ in DMF/TBAP (0,1 mol L⁻¹);glassy carbon electrode

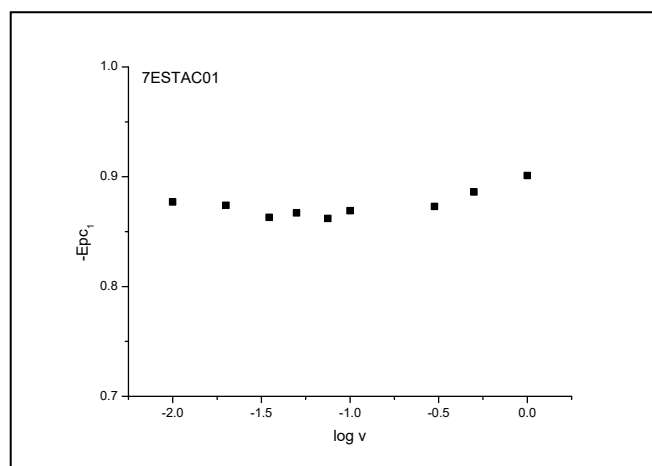
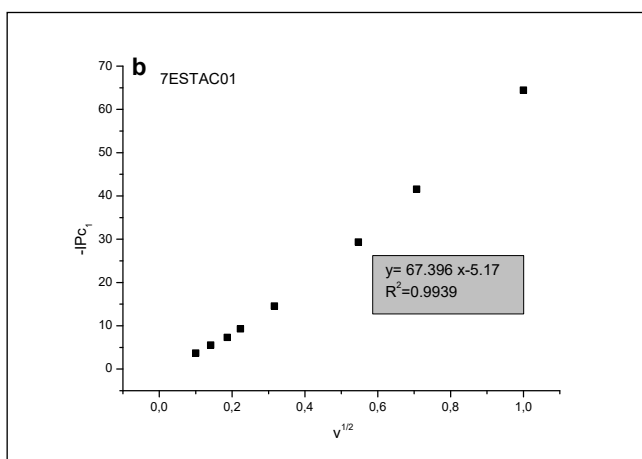
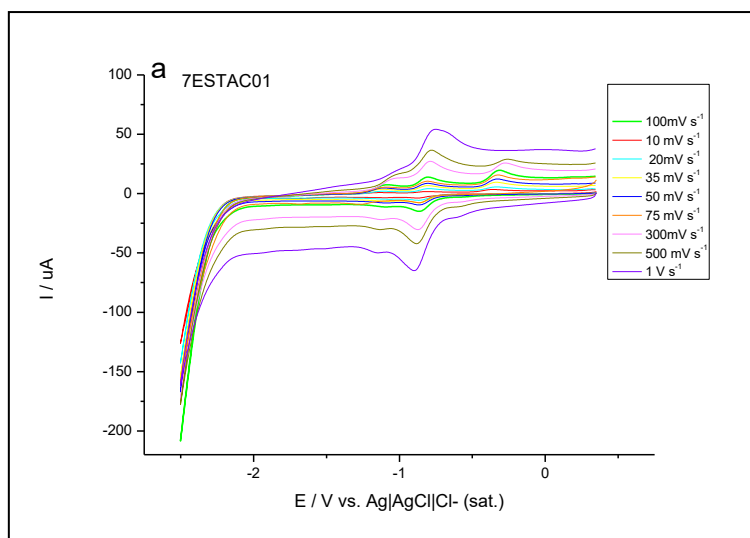


Figure6 Studies in aprotic media. (a) Scan speeds in aprotic media of 6ESTAC01. (b) Graph of I_{pc} vs $v^{1/2}$; (c) Graph E_{pc} vs $\log v$. [6ESTAC01] = 1,0 mmol L⁻¹ in DMF/TBAP (0,1 molL⁻¹); glassy carbon electrode.

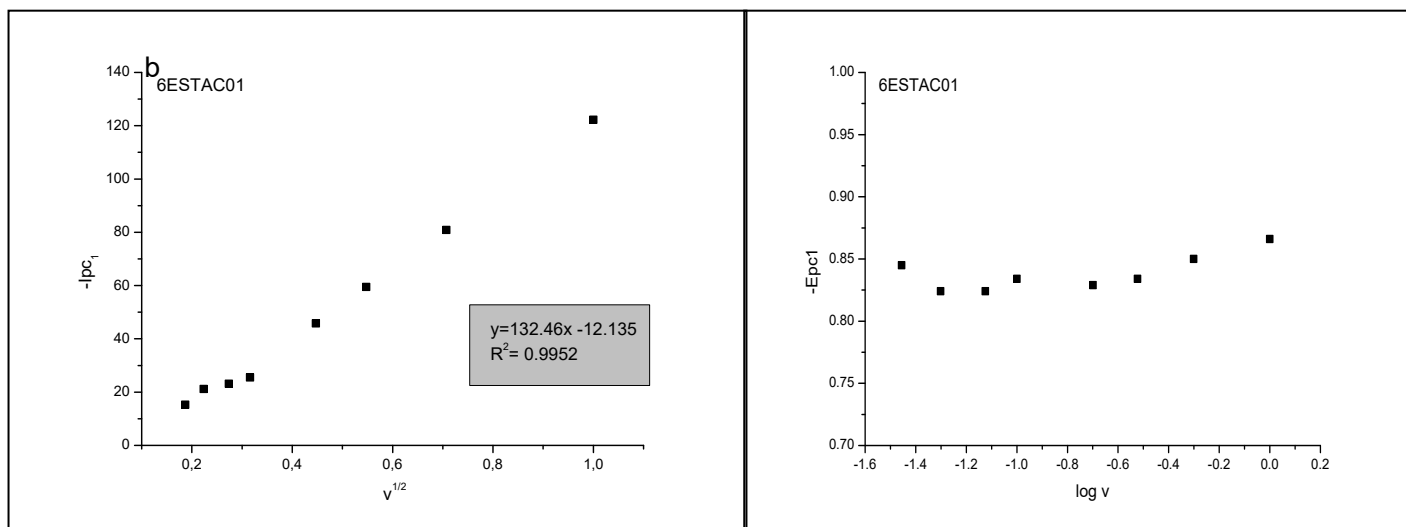
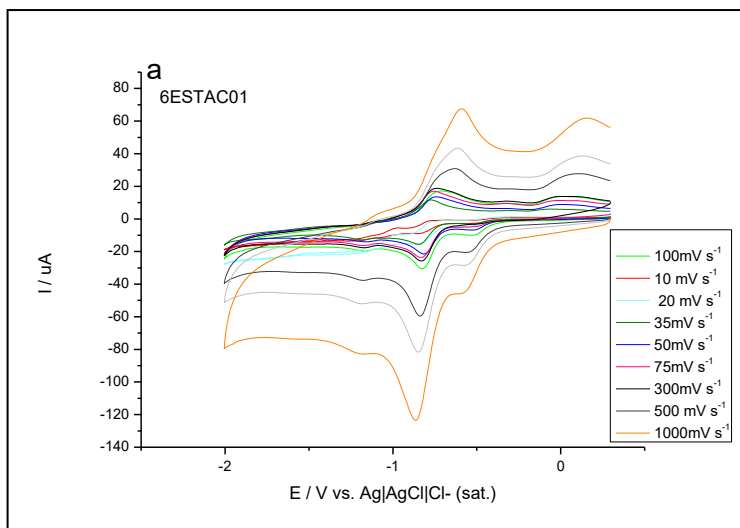


Figure 7 Studies in aprotic media. (a) Scan speeds in aprotic media of ACS6CN. (b) Graph of I_{pc1} vs $v^{1/2}$; (c) Graph E_{pc} vs $\log v$. [ACS6CN] = $1,0 \text{ mmol L}^{-1}$ in DMF/TBAP ($0,1 \text{ mol L}^{-1}$); glassy carbon electrode.

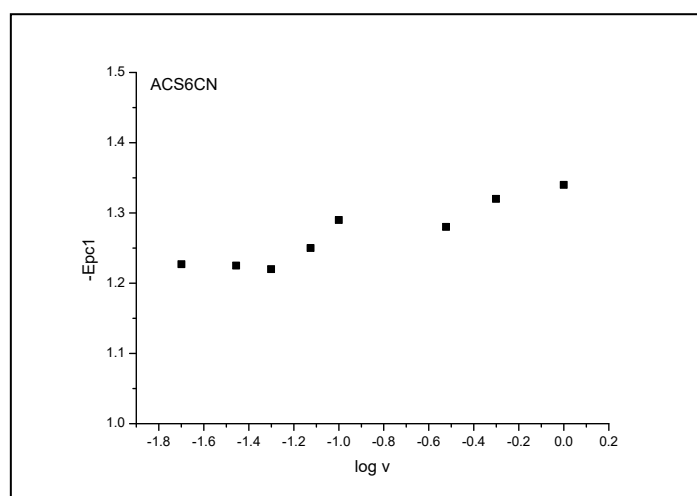
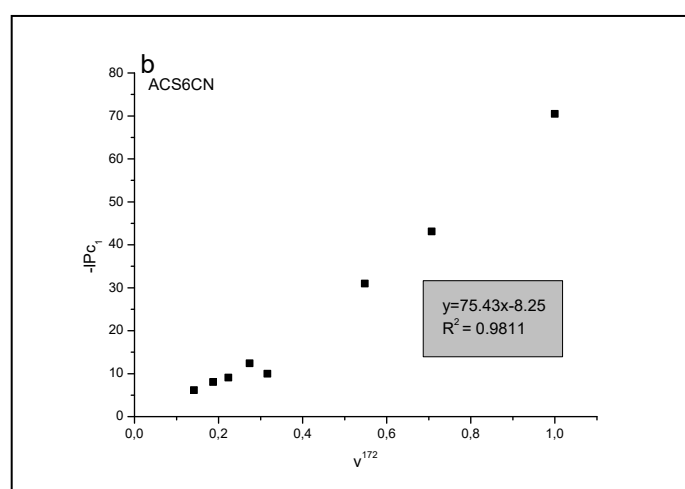
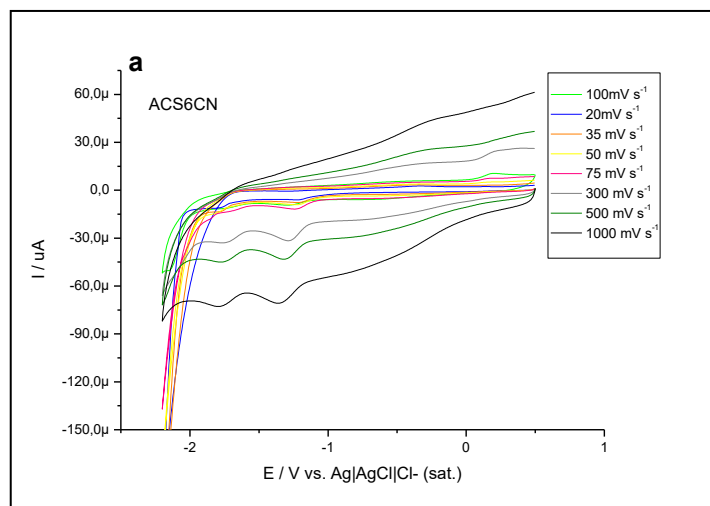
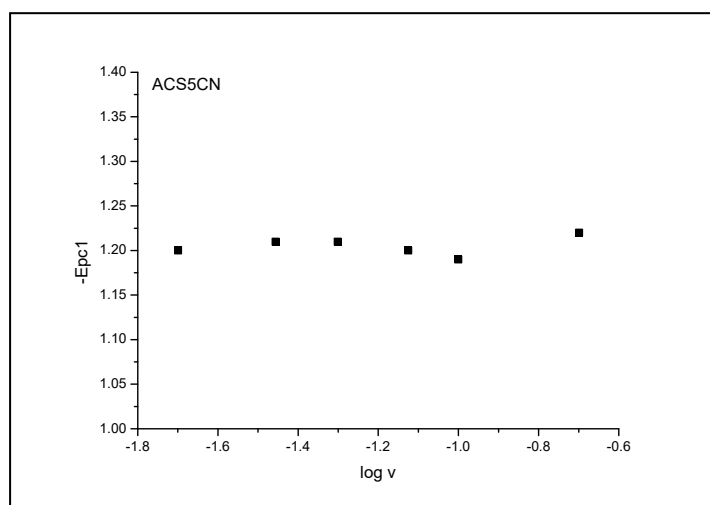
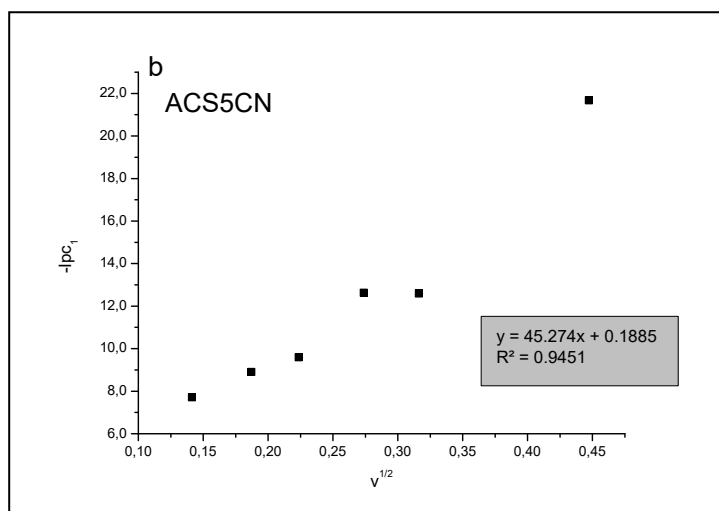
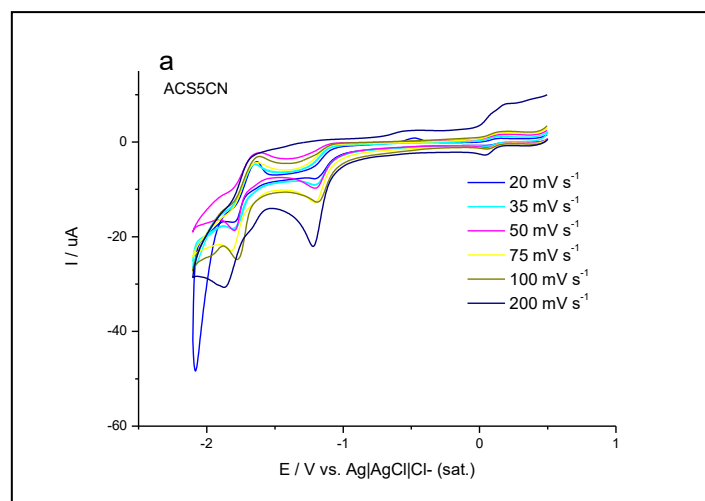


Figure8 Studies in aprotic media. (a) Scan speeds in aprotic media of ACS5CN. (b) Graph of I_{pc1} vs $v^{1/2}$; (c) Graph E_{pc} vs $\log v$. [ACS5CN] = 1,0 mmol L⁻¹ in DMF/TBAP (0,1 mol L⁻¹);glassy carbon electrode



1.4.1.3 Reactivity with oxygen of acridine-thiophene derivate in aprotic media

The acridine-thiophenes derivatives were also evaluated for their reactivity towards oxygen. This was investigated by cyclic voltammetry in aprotic media due to the stability of the radical generated after reduction process, thus constituting, the best model for the study of cell membrane environment where the process of peroxidation occurs lipid. In Figure 9, show several cyclic voltammograms of six compounds recorded at scan rates of 50 mV s^{-1} in the scanning window (between -2.5 and $+1.0 \text{ V}$ vs. Ag/AgCl). Each compound was evaluated with a different concentration level of oxygen. In our result, it is clear for all compounds that there is no shift potential despite the high oxygen presence. Also, the current values to each wave do not show changes (Fig 9(a), Fig 9(b), Fig 9(c), Fig 9(d), Fig 9(e), Fig 9(f)).

Then our result exhibit, which our six compounds no show apparently reactivity with oxygen (aprotic media). This result is corroborated for other papers, which found a very low reactivity of thiophene. However; BRETT, et al., 2003 found that Thiophene-derivates can get high reactivity, this was an exhibit for thiophene-S-oxide. Unfortunately, there are no studies of reactivity of hybrid drugs.

Table 4 Electrochemical parameters obtained for 7CNAC01 in aprotic media. Study on function of scan rate.

V (V s ⁻¹)	-E _{pc1} (V)	-E _{pa1} (V)	-I _{pc1} (μA)	ΔE _p (E _{pa1} -E _{pc1}) (V)
10mV s ⁻¹	0.758	0.627	3.35	0.131
20mV s ⁻¹	0.748	0.617	4.74	0.131
35mV s ⁻¹	0.739	0.570	6.68	0.169
50mV s ⁻¹	0.739	0.551	8.24	0.188
100mV s ⁻¹	0.739	0.561	9.74	0.178
200mV s ⁻¹	0.745	0.548	16.14	0.197
300mV s ⁻¹	0.758	0.533	24.59	0.225
500mV s ⁻¹	0.767	0.514	34.33	0.253
1000mV s ⁻¹	0.786	0.486	53.05	0.300

Table5 Electrochemical parameters obtained for 6CNAC01 in aprotic media. Study on the function of scan rate.

V (V s ⁻¹)	-E _{pc1} (V)	-E _{pa1}	-I _{pc1} (μA)	ΔE _p (E _{pa1} -E _{pc1}) (V)
10mV s ⁻¹	0.679	0.571	4.11	0.108
20mV s ⁻¹	0.614	0.533	6.28	0.081
35mV s ⁻¹	0.689	0.500	6.18	0.189
50mV s ⁻¹	0.711	0.302	7.20	0.409
75mV s ⁻¹	0.722	0.300	8.95	0.422
100mV s ⁻¹	0.738	0.323	8.85	0.415
200mV s ⁻¹	0.754	0.291	12.25	0.463
300mV s ⁻¹	0.775	0.290	12.56	0.485
500mV s ⁻¹	0.790	0.291	15.74	0.499
1000mV s ⁻¹	0.8026	0.309	35.07	0.493

Table 6 Electrochemical parameters obtained for 7ESTAC01 in aprotic media. Study on function of scan rate.

V (V s⁻¹)	-E_{pc1} (V)	-E_{pa1}	-I_{pc1} (μA)	ΔE_p(E_{pc1}-E_{pa1}) (V)
10mV s ⁻¹	0.877	0.818	3.70	0.06
20mV s ⁻¹	0.874	0.805	5.55	0.07
35mV s ⁻¹	0.863	0.811	7.32	0.05
50mV s ⁻¹	0.867	0.808	9.29	0.06
75mV s ⁻¹	0.862	0.809	7.38	0.05
100mV s ⁻¹	0.879	0.800	14.57	0.06
300mV s ⁻¹	0.873	0.795	29.34	0.08
500mV s ⁻¹	0.886	0.784	41.55	0.10
1000mV s ⁻¹	0.901	0.75	64.43	0.15

Table 7 Electrochemical parameters obtained for 7ESTAC01 in aprotic media. Study on the function of scan rate.

V (V s⁻¹)	-E_{pc1}	-E_{pa1}	-I_{pc1} (μA)	ΔE_p(E_{pc1}-E_{pa1}) (V)
35mV s ⁻¹	0.845	0.77	15.27	0.075
50mV s ⁻¹	0.824	0.743	21.17	0.081
75 mV s ⁻¹	0.824	0.743	23.15	0.081
100mV s ⁻¹	0.834	0.732	25.47	0.102
200mV s ⁻¹	0.829	0.657	45.75	0.172
300mV s ⁻¹	0.834	0.625	59.49	0.209
500mV s ⁻¹	0.85	0.614	80.89	0.236
1000mV s ⁻¹	0.866	0.592	122.19	0.274

1.4.2 Electrochemical dsDNA biosensor

The acridines-thiophene derivatives and DNA interaction were investigated using the DNA-biosensor prepared by immobilizing DNA onto the glassy carbon surface. The electrochemical reduction of each substrate of acridines-thiophene derivatives generate radicals that interact with DNA causing damage. This interaction detected by electrochemical sensing of the oxidation of the DNA purine bases. In fact, several works showed which DNA-biosensor using GCE can detect small modification in the double strand of DNA.

For our six compounds, the reduced form was obtained applying a reduction potential for each compound in acetate buffer with a Glassy carbon electrode. The reduction potential was carry out from $E_p=0$ to $-1.5V$ to get the specific reduced potential of each compound. For 7CNAC01 and 6CNAC01 recorded a $E(V) = -0.404$ and -0.531 respectively. For the 7ESTAC01 and 6ESTAC01 showed a $E(V) = -0.122$ and -0.562 respectively. For the ACS6CN and ACS5CN recorded a $E(V) = -0.440$ and -0.649 respectively.

Our result from the dsDNA biosensor showed the interaction of dsDNA with reduced-substrates for each thiophene-acridine derivatives. According to the F.C. Abreu, 2002 and Burcu Dogan-Topal, 2014, for some anticancer drugs, the generations of those short-lived radicals are needed to interaction and damage DNA.

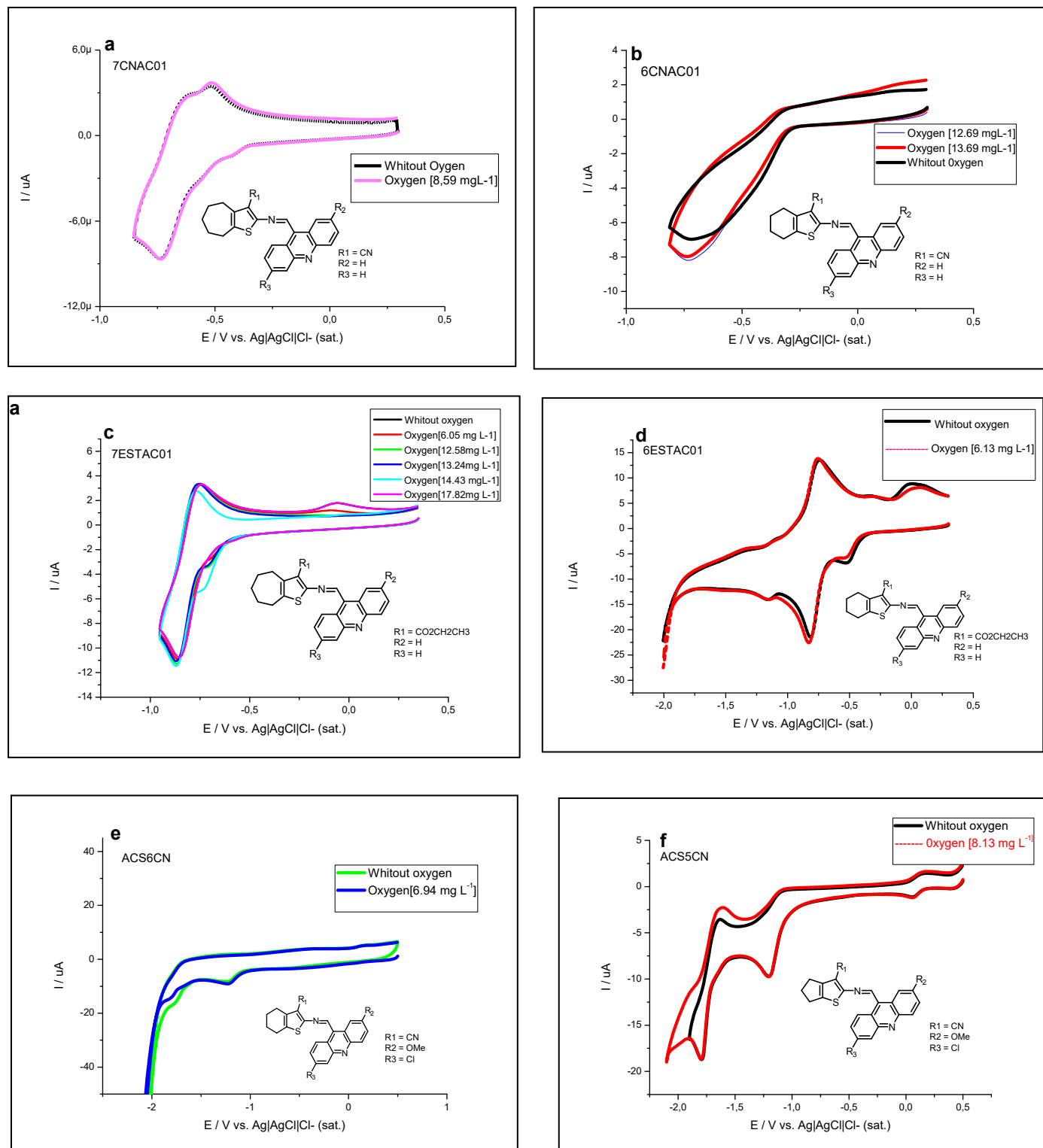
In our first result, the 7CNAC01-DNA interaction was investigated using the DNA-biosensor. For this especially compound we performed two experiment. The first one using the reduced form of 7CNAC01 and the second one using the non-reduced form of 7CNAC01 (Fig. 10(a) and Fig. 13(b)). DPV of non reduced form of 7CNAC01 oxidation using a DNA-biosensor (Fig. 10(a)) shows no interaction with DNA. Then only after 7CNAC01 is reduced, at $E_p = -0.4V$ for $t = 120$ seconds, does it generated radicals that interact with dsDNA (Fig. 10(b)). This interaction was detected by electrochemical sensing of the oxidation of the DNA purine bases the appearance of guanine, $E_p = 0.97 V$, and adenine, $E_p = 1.33 V$, peaks, demonstrates clearly that the damage by the radicals caused distortion of the double helix and exposure of the bases that can be oxidised. In fact, with this results, we performed and worked only with the reduced form of each compound.

Another results from the dsDNA biosensor show positive interactions for 7CNAC01, 6CNAC01 and ACS5CN, as represented by the appearance of guanine ($E_p = 0.99$; $E_p = 1.03$; $E_p = 0.83 V$, respectively) and adenine ($E_p = 1.24$; $E_p = 1.29$; $E_p = 1.26V$, respectively)

peaks (Figs.10 (a), Figs.11 (a), Fig.15 (a)). This clearly demonstrates that damage from the compounds caused a distortion of the double helix and exposure of the bases to oxidation.

There are three models of binding of small molecules to DNA double helix, intercalation binding, groove binding and electrostatic binding. Among these, intercalation and groove binding modes are dependent on DNA double helix. But, the electrostatic binding occurs out of the groove of the DNA. If the interaction models are intercalation and groove binding, the interaction capability would decrease in the presence of denatured DNA. However, the electrostatic interactions may continue to operate even after DNA denaturation. Then for our experiment to evaluate and determine what kind of binding have our substrates with DNA, and if the intercalation would decrease or disappear the anodic peak of guanine and adenine bases, we performed the analyses of intercalation using denatured DNA (ssDNA in solution).

Figure 9 Reactivity with oxygen .Cyclic voltammetry of 1 mM Acridine-thiophene in dimethylformamide (DMF) plus 0.1 M Tetrabutyl ammonium perchlorate (TBAP), with a Ag/AgCl reference electrode (RE), and the scan rate 50 mV.s⁻¹



1.4.3 Intercalation using ssDNA in solution

In the experiments using ssDNA in pH=4.5 acetate buffer, a decrease of the oxidation waves of the bases, guanine and adenine, with anodic potential shifts, were observed, confirming the interaction with single strand of DNA for 7CNAC01, 6CNAC01, 7ESTAC01, 6ESTAC01, ACS6CN and ACS5CN. After acridine-thiophene derivatives interaction with ssDNA at CGE surface, there was a clear decrease at guanine oxidation peak using three concentration level of compound ($1.0 \times 10^{-6} \text{M}$; $1.0 \times 10^{-5} \text{M}$; $1.0 \times 10^{-4} \text{M}$). The peak current values of the ssDNA solution decreased with increasing substrates concentrations level. This decrease marked a possible damage in the oxidizable groups of guanine and adenine that could be caused structural change on guanine and adenine bases.

The electrochemical detection of DNA interacting was evaluated by the change in the guanine and adenine oxidation peak. Electrochemical signals of compounds were examined after the interaction with ssDNA solution and obtained current values. To find quantitative values about interaction mechanism of acridine-thiophene derivatives with DNA, the calculation of coefficient using the current values for each bases, is an important information.

This factor was investigated in two papers by **Ozkan et al, 2008 and 2010** and **G. Bagni et al.** where using dsDNA modified and ssDNA to determine the behavior of bound and free Mitomycin molecules towards DNA. In our study the coefficient value was calculated using current signals for each bases to three different concentration levels of each substrate.

$$\text{Coefficient} = \text{Compound}_{\text{bound}} / \text{Compound}_{\text{free}}$$

$\text{Coefficient (G\%, A\%)} = (I_{\text{bound}} - I_{\text{free}}) / I_{\text{free}} $
--

In the equation, I_{free} is the oxidation peak height of only ssDNA solution without substrate, I_{bound} is the oxidation peak current of compound obtained after interaction with ssDNA.

In our result, the decrease in the peak height of both bases, were estimated with interactions between compounds and ssDNA, the current ratio of adenine and guanine interaction were calculated for each compound. The guanine or adenine oxidation signal obtained with DPV in absence of compound served as 100%. Then our result were evaluated using this coefficient

of interaction. According to our results 7CNAC01, 6CNAC01, 7ESTAC01, 6ESTAC01, ACS6CN and ACS5CN exhibited oxidation signal and shift potential to guanine and adenine (Fig.10(b), Fig.11(b), Fig.12(b), Fig.13(b), Fig.14(b), Fig.15(b)). Each result was evaluated for each compound. A common feature for all compounds when interacts with ssDNA, showed the concentration level of sample is proportional to the increased binding coefficient for each base. Also and more important feature is that the reduced form of each compound exhibit greater oxidation signal to guanine and adenine bases. (Table 9 to Table 13)

The oxidation signal was analyzed for each compound using the coefficient for guanine and adenine. For 1.0×10^{-4} M of 7CNAC01, exhibit interaction with guanine and adenine at 37.31% and 20.39% respectively. Also the reduced form of 1.0×10^{-4} M of 7CNAC01 showed stronger oxidation signal and shift potential to both bases (Table 8). Similar result showed the table 10, where 1.0×10^{-4} M of 6CNAC01 exhibit interaction with guanine and adenine at 16.45% and 19.95 % respectively. Also the reduced form showed stronger oxidation signal and shift potential to both bases. For 7ESTAC01, showed slight oxidation signal only to Guanine, however to reduced form showed oxidation signal to both bases (%G=37.41 and A% =8.79). On the other hand to 6ESTAC01 exhibit signal oxidation to both bases either to non reduced and reduced form of 6ESTAC01 (Table 11 and Table 12). To ACS6CN and ACS5CN, observed signal oxidation to both bases and shift potential. Our result showed the oxidation signal to guanine were %G=41.63 and 47.09% for ACS6CN and ACS5CN, respectively and the oxidation signal to adenine were %A=18.41 and 27.3% for ACS6CN and ACS5CN, respectively.

The electrochemical reduction of each substrate of acridines-thiophenes derivatives generate radicals that interact with DNA causing damage. Indeed our results of interaction of ssDNA and radicals for each reduced compound exhibit a better interaction with single strand of DNA.

On the other hand for all compounds worked in this work the guanine interaction was more recorded than the adenine interaction. This result can show two possibilities. The first, that exists a preference bond with Guanine than adenine for our acridine-thiophene derivatives or the second that shows that the guanine is an electroactive DNA base that is more easily oxidized than others. Indeed it was used for some electrochemical works, as a marker for the voltammetric detection of DNA-drug interactions (SIRAJUDDIN; ALI S FAU - BADSHAH; BADSHAH, 2013).

Finally, important information from our result is the shift peak potential recorded for the six compounds (Table 9). In our result showed shift potential either to guanine and adenine.

For 7CNAC01, 6CNAC01, 7ESTAC01, 6ESTAC01, ACS6CN, ACS5CN showed shift potential to more cathodic value. Slight shift potential was recorded to 6CNAC01 and 7ESTAC01 (16 to 29 mV). Significant shift potential was recorded to 7CNAC01, 6ESTAC01, ACS6CN and ACS5CN (38 to 79mV).

RAUF, S. et al.,2005; have reported three kinds of modes for small molecules binding to DNA, if E_p shifted to more anodic value when small molecules interacted with DNA; the interaction mode was electrostatic binding. On the other hand, if E_p shifted to more positive value, the interaction mode was intercalative binding. In fact several works concluded that significant shift potential is typical of the intercalation. The shift in peak potential toward positive side could be attributed to the intercalation of compounds 7CNAC01, 6ESTAC01, ACS6CN and ACS5CN into the stacked base pair pockets of DNA but also is probably to 6CNAC01 and 7ESTAC01.

ctDNA Interaction with 7CNAC01

Figure 10 a) DPV, at pH 4.5 in acetate buffer with 30% ethanol, of the dsDNA biosensor in the absence and in the presence of 7CNAC01 reduced in solution (1.0×10^{-5} M) at $E_p = -0.4$ V; $t = 120$ s; $\nu = 5$ mV s $^{-1}$ (b) DPV with the same parameter of (a) in the absence and in the presence of 7CNAC01 without reduction. (c) DPV at pH 4.5 in acetate buffer with 30% ethanol for the oxidation of 7CNAC01 attached to the surface of glass carbon electrode (GCE) in the presence of ssDNA solution.

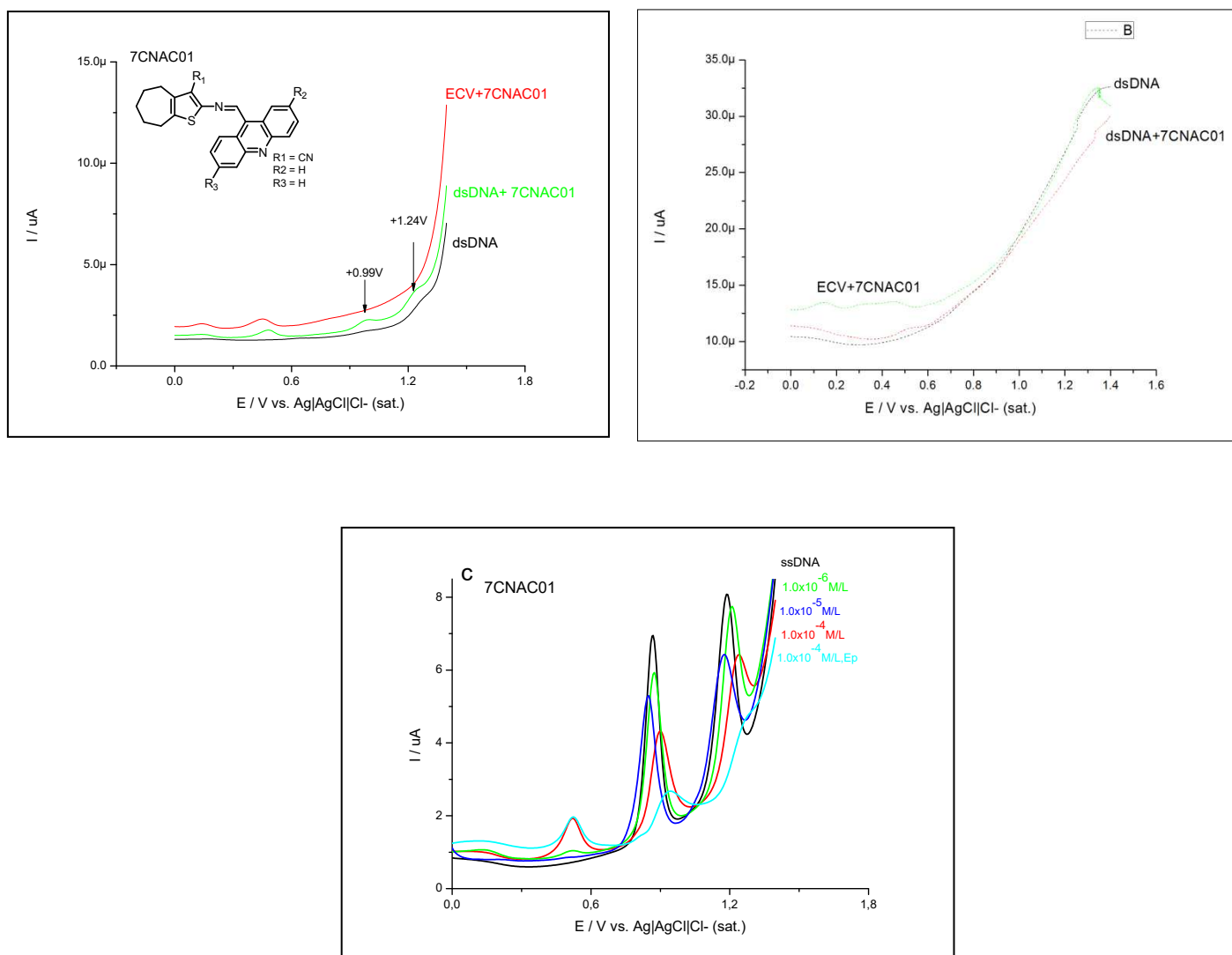


Table 8 Detection of DNA damage at the ssDNA/7CNAC01 caused by three concentrations level of 7CNAC01 ($1.0 \times 10^{-6} \text{M}$, $1.0 \times 10^{-5} \text{M}$, $1.0 \times 10^{-4} \text{M}$) and short-lived radicals generated by electrochemical reduction of 7CNAC01 ($c = 1.0 \times 10^{-4} \text{M}$) during DPV between 0 and 0 and +1.4 V (scan rate 5 mV s^{-1}). Experimental conditions as for Fig. 10 (IG, IA, represent anodic peak currents of guanine and adenine)

Compound 7CNAC01	IG	I _{b,G}	G% (I _{b,G} /I _{f,G})x100	I A	I _{b,A}	A% (I _{b,A} /I _{f,A})x100
0 $\mu\text{mol L}^{-1}$	6.9195	0	0	8.046	0	0
1 $\mu\text{mol L}^{-1}$	5.9064	1.0131	14.64	7.738	0.308	3.83
10 $\mu\text{mol L}^{-1}$	5.2881	1.6314	23.58	6.427	1.619	20.12
100 $\mu\text{mol L}^{-1}$	4.3408	2.5787	37.31	6.406	1.640	20.39
100 $\mu\text{mol L}^{-1}$ Potential	2.6459	4.2736	61.76	4.606	3.439	42.75

Table 9 The shift potential of oxidation signal for guanine and adenine in ssDNA solution.

Compound	ssDNA	
7CNAC01	G= 37.31 %	$\Delta E = 0.038 \text{V}$
	A= 20.39 %	$\Delta E = 0.051 \text{V}$
6CNAC01	G= 16.45 %	$\Delta E = 0.024 \text{V}$
	A= 19.95 %	$\Delta E = 0.029 \text{V}$
7ESTAC01	G= 14.69 %	$\Delta E = 0.026 \text{V}$
	A= 0,3 %	$\Delta E = 0.016 \text{V}$
6ESTAC01	G= 37.56 %	$\Delta E = 0.067 \text{V}$
	A= 7.45 %	$\Delta E = 0.071 \text{V}$
ACS6CN	G= 41.63 %	$\Delta E = 0.046 \text{V}$
	A= 18.43 %	$\Delta E = 0.061 \text{V}$
ACS5CN	G= 47.09 %	$\Delta E = 0.061 \text{V}$
	A= 27.03 %	$\Delta E = 0.079 \text{V}$

ctDNA Interaction with 6CNAC01

Figure 11 (a) Differential pulse voltammogram(DPV), at pH 4.5 in acetate buffer with 30% ethanol, of the dsDNA biosensor in the absence and in the presence of 6CNAC01 in solution (1.0×10^{-5} M) (b) DPV at pH4.5 in acetate buffer with 30% ethanol for the oxidation of 6CNAC01 attached to the surface of glassy carbon electrode (GCE) in the presence of a ssDNA solution.

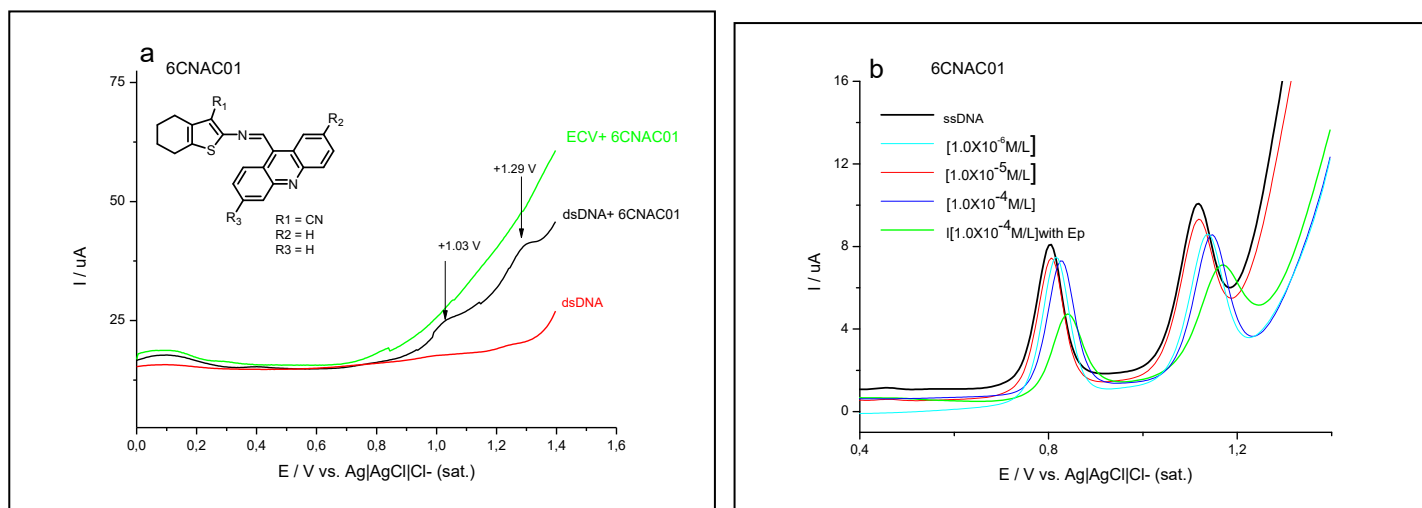


Table 10 Detection of DNA damage at the ssDNA/6CNAC01 caused by three concentrations level of 6CNAC01 ($1.0 \times 10^{-6} M$, $1.0 \times 10^{-5} M$, $1.0 \times 10^{-4} M$) and short-lived radicals generated by electrochemical reduction of 6CNAC01 ($c = 1.0 \times 10^{-4} M$) during DPV between 0 and +1.4 V (scan rate 5 mV s^{-1}). Experimental conditions as for Fig. 11 (IG, IA, represent anodic peak currents of guanine and adenine).

Compound 6CNAC01	IG	I _{b,G}	G% (I _{b,G} /I _{f,G})x100	IA	I _{b,A}	A% (I _{b,A} /I _{f,A})x100
0 $\mu\text{mol L}^{-1}$	8.6681	0	0	10.6463	0	0
1 $\mu\text{mol L}^{-1}$	8.1457	0.5224	6.02	9.883	0.7633	7.169
10 $\mu\text{mol L}^{-1}$	8.0753	0.5928	6.84	9.2561	1.3902	13.05
100 $\mu\text{mol L}^{-1}$	7.2418	1.4263	16.45	8.5227	2.1236	19.95
100 $\mu\text{mol L}^{-1}$ (Ep)	5.923	2.7451	31.66	8.3532	2.2931	21.54

ctDNA Interaction with 7ESTAC01

Figure 12 (b) Differential pulse voltammogram (DPV) at pH 4.5 in acetate buffer with 30% ethanol for the oxidation of 7ESTAC01 attached to the surface of glassy carbon electrode (GCE) in the presence of ssDNA solution. (a) Differential pulse voltammogram, at pH 4.5 in acetate buffer with 30% ethanol, of the dsDNA biosensor in the absence and in the presence of 7ESTAC01 in solution (1.0×10^{-5} M).

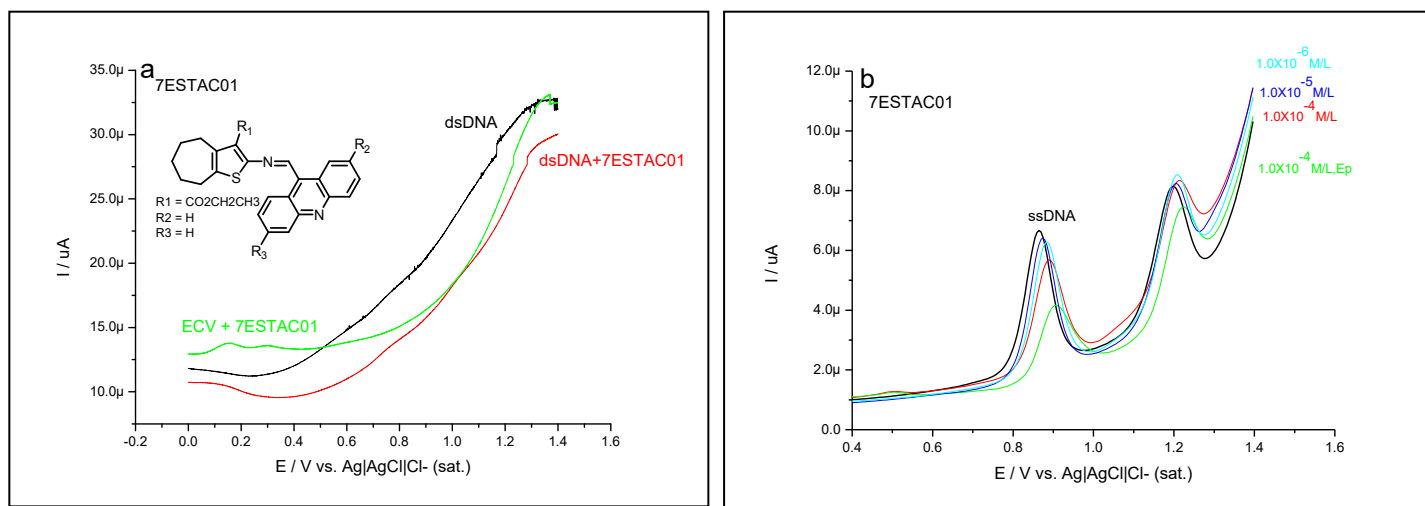


Table 11 Detection of DNA damage at the ssDNA/7ESTAC01 caused by three concentrations level of 7ESTAC01 (1.0×10^{-6} M, 1.0×10^{-5} M, 1.0×10^{-4} M) and short-lived radicals generated by electrochemical reduction of 7ESTAC01 ($c = 1.0 \times 10^{-4}$ M) during DPV between 0 and +1.4 V (scan rate 5 mV s^{-1}). Experimental conditions as for Fig. 12 (IG, IA, represent anodic peak currents of guanine and adenine).

Compound	IG	Ib,G	G% (Ib,G / If,G)x100	IA	Ib,A	A% (Ib,A / If,A)x100
7ESTAC01						
0 $\mu\text{mol L}^{-1}$	6.647	0	0	8.153	0	0
1 $\mu\text{mol L}^{-1}$	6.37	0.277	4.17	8.153	0	0
10 $\mu\text{mol L}^{-1}$	6.24	0.407	6.13	8.153	0	0
100 $\mu\text{mol L}^{-1}$	5.67	0.977	14.69	8.153	0	0
100 $\mu\text{mol L}^{-1}$ (Ep)	4.16	2.487	37.41	7.436	0.717	8.79

ctDNA Interaction with 6ESTAC01

Figure 13 (a) Differential pulse voltammogram, at pH 4.5 in acetate buffer with 30% ethanol, of the dsDNA biosensor in the absence and in the presence of 6ESTAC01 in solution (1.0×10^{-5} M) (b) Differential pulse voltammogram (DPV) at pH 4.5 in acetate buffer with 30% ethanol for the oxidation of 6ESTAC01 attached to the surface of glassy carbon electrode (GCE) in the presence of a ssDNA solution.

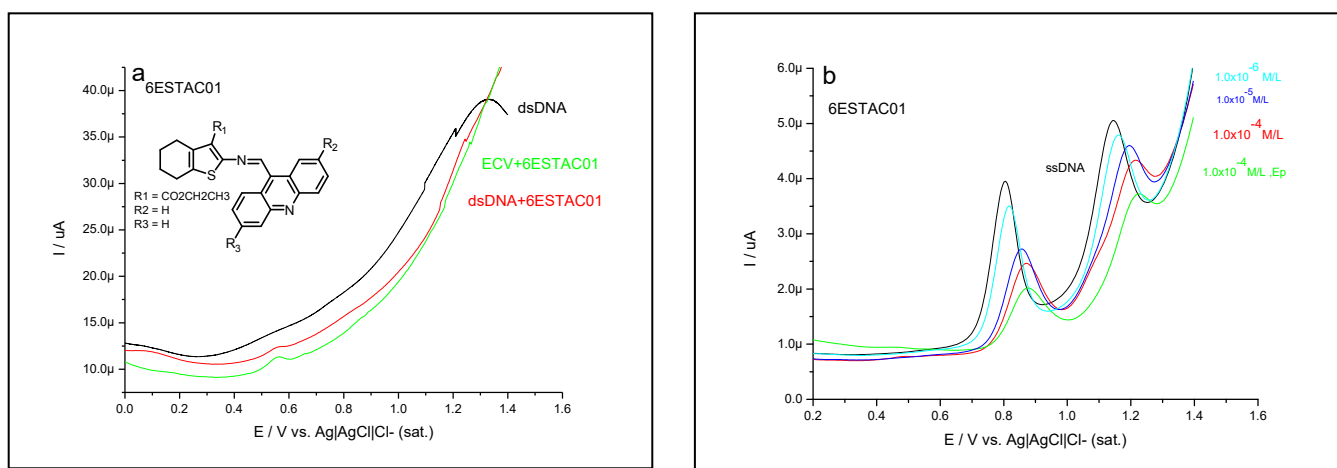


Table 12 Detection of DNA damage at the ssDNA/6ESTAC01 caused by three concentrations level of 6ESTAC01 (1.0×10^{-6} M, 1.0×10^{-5} M, 1.0×10^{-4} M) and short-lived radicals generated by electrochemical reduction of 6ESTAC01 ($c = 1.0 \times 10^{-4}$ M) during DPV between 0 and +1.4 V (scan rate 5 mV s^{-1}). Experimental conditions as for Fig. 13 (IG, IA, represent anodic peak currents of guanine and adenine).

Compound 6ESTAC01	IG	Ib,G	G% (Ib,G / If,G)x100	IA	Ib,A	A% (Ib,A / If,A)x100
0 $\mu\text{mol L}^{-1}$	3.924	0	0	5.042	0	0
1 $\mu\text{mol L}^{-1}$	3.486	0.438	11.16	4.78	0.262	5.19
10 $\mu\text{mol L}^{-1}$	2.73	1.194	30.42	4.58	0.462	9.16
100 $\mu\text{mol L}^{-1}$	2.45	1.474	37.56	4.34	0.702	7.45
100 $\mu\text{mol L}^{-1}$ (Potential)	2	1.924	49.03	3.71	1.332	26.41

ctDNA Interaction with ACS6CN

Figure 14 (a) Differential pulse voltammogram, at pH 4.5 in acetate buffer with 30% ethanol, of the dsDNA biosensor in the absence and in the presence of ACS6CN in solution (1.0×10^{-5} M) (b) Differential pulse voltammogram (DPV) at pH 4.5 in acetate buffer with 30% ethanol for the oxidation of ACS6CN attached to the surface of glassy carbon electrode (GCE) in the presence of a ssDNA solution.

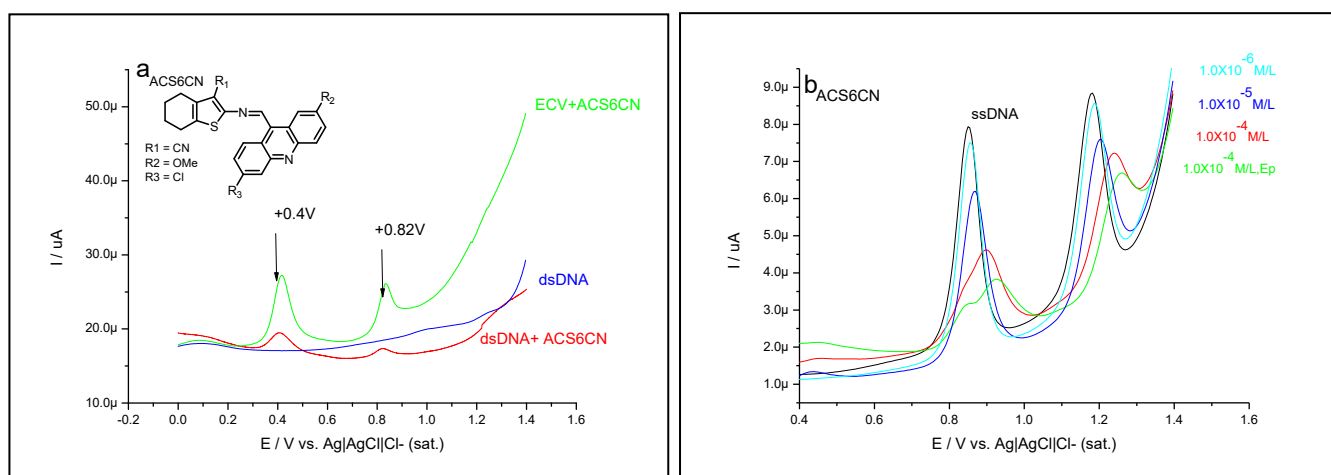


Table 13 Detection of DNA damage at the ssDNA/ACS6CN caused by three concentrations level of ACS6CN (1.0×10^{-6} M, 1.0×10^{-5} M, 1.0×10^{-4} M) and short-lived radicals generated by electrochemical reduction of ACS6CN ($c = 1.0 \times 10^{-4}$ M) during DPV between 0 and +1.4 V (scan rate 5 mV s^{-1}). Experimental conditions as for Fig. 14 (IG, IA, represent anodic peak currents of guanine and adenine

Compound ACS6CN	IG	I _{b,G}	G% (I _{b,G} /I _{f,G})x100	I _A	I _{b,A}	A% (I _{b,A} /I _{f,A})x100
0 $\mu\text{mol L}^{-1}$	7.9123	0	0	8.8304	0	0
1 $\mu\text{mol L}^{-1}$	7.4948	0.4175	5.28	8.5284	0.302	3.42
10 $\mu\text{mol L}^{-1}$	6.1811	1.7312	21.88	7.5789	1.2515	14.17
100 $\mu\text{mol L}^{-1}$	4.6182	3.2941	41.63	7.2045	1.6259	18.41
100 $\mu\text{mol L}^{-1}$ (Potential)	3.8114	4.1009	51.83	6.6849	2.1455	24.30

ctDNA Interaction with ACS5CN

Figure 15 (a) Differential pulse voltammogram(DPV), at pH 4.5 in acetate buffer with 30% ethanol, of the dsDNA biosensor in the absence and in the presence of ACS5CN in solution (1.0×10^{-5} M) (b) DPV at pH4.5 in acetate buffer with 30% ethanol for the oxidation of ACS5CN attached to the surface of glassy carbon electrode (GCE) in the presence of a ssDNA solution.

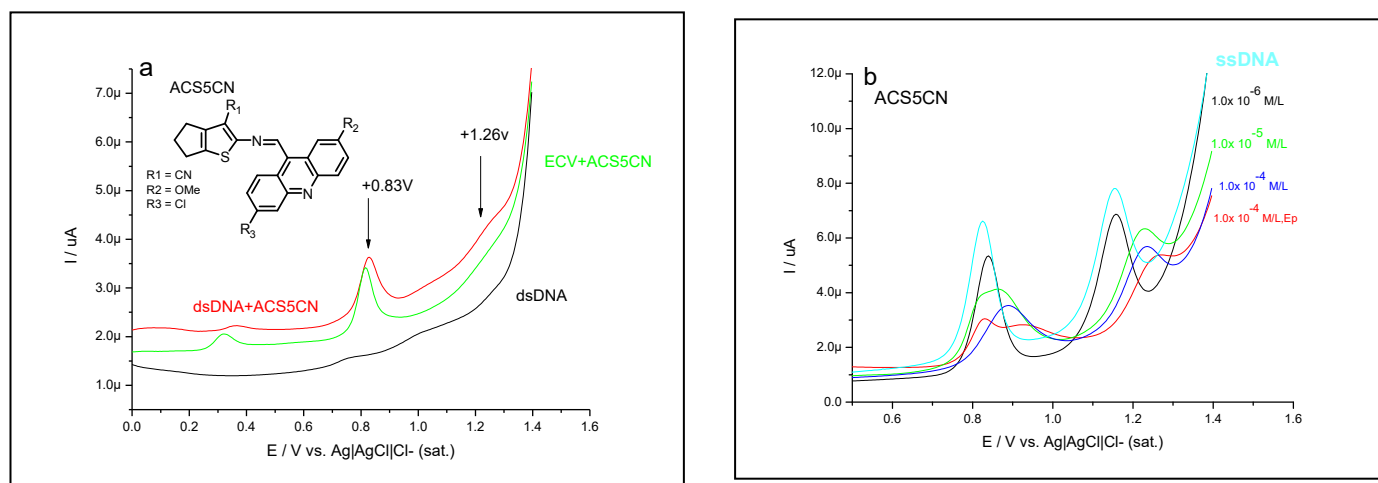


Table 14 Detection of DNA damage at the ssDNA/ACS5CN caused by three concentrations level of ACS5CN (1.0×10^{-6} M, 1.0×10^{-5} M, 1.0×10^{-4} M) and short-lived radicals generated by electrochemical reduction of ACS5CN ($c = 1.0 \times 10^{-4}$ M) during DPV between 0 and +1.4 V (scan rate 5 mV s^{-1}). Experimental conditions as for Fig. 15 (IG, IA, represent anodic peak currents of guanine and adenine).

Compound	IG	Ib,G	G% (Ib,G / If,G) x 100	IA	Ib,A	A% (Ib,A / If,A) x 100
ACS5CN						
0 $\mu\text{mol L}^{-1}$	7.912	0	0	7.8	0	0
1 $\mu\text{mol L}^{-1}$	7.47	0.442	19.34	6.84	0.96	12.3
10 $\mu\text{mol L}^{-1}$	6.1811	1.7309	38	6.31	1.49	19.1
100 $\mu\text{mol L}^{-1}$	3.49	4.422	47.09	5.67	2.13	27.3
100 $\mu\text{mol L}^{-1}$ (Potential)	3	4.912	54.52	5.33	2.47	31.66

1.4.4 UV-Vis Absorption Spectroscopy

To visualize the effectiveness of the intercalation process within ds-DNA, we have recorded the UV–visible for each compound absorption spectra of 7ESTAC01, 6ESTAC01, ACS6CN, ACS5CN (20 μM) in the absence and presence of ds-DNA in phosphate buffer. Based on variations in absorbance spectra of our acridine-thiophene derivatives upon binding to DNA, the binding constant, K_b , was calculated using the Wolfe-Shimer equation. The value of binding constant K_b was obtained from the intercept to slope ratio of $[\text{DNA}]/[(\epsilon_a - \epsilon_f)]$ vs. $[\text{DNA}]$.

The absorption spectrum of 7ESTAC01 and 6ESTAC01 exhibited bands at 228, 252 and 442 nm (Fig.16 and Fig.17). As evident from Fig.16 (a), the absorbance of 7ESTAC01 increased at 228 nm while those at 442 nm decreased slightly with the successive addition of DNA. For 6ESTAC01, the absorbance increased at 228 nm and decreased with the successive addition of dsDNA (2, 10, 12, 14, 16, 20 μM). The binding constant K_b of 7ESTAC01 and 6ESTAC01 were evaluated to $K_b = 6,57 \times 10^4 \text{ L mol}^{-1}$ and $K_b = 1,33 \times 10^5 \text{ L mol}^{-1}$, respectively (Fig 16(b) and Fig.17(b)). An isosbestic point has been observed at 297 nm (for 7ESTAC01 and 6ESTAC01), indicated spectroscopically distinct chromophores. Such spectral behavior is associated with the intercalation as a dominant binding mode.

Table 15 Correlation values between binding constant (K_b) from UV-Vis and half-wave potential ($E_{1/2}$) from cyclic voltammetry in protic media (pH=7.2 phosphate buffer)

Compound	K_b	$E_{1/2} \text{ (V)}$
7ESTAC01	$K_b = 6,57 \times 10^4 \text{ L mol}^{-1}$	- 0.34
6ESTAC01	$K_b = 1,33 \times 10^5 \text{ L mol}^{-1}$	-0.31
ACS6CN	$K_b = 2,8 \times 10^4 \text{ L mol}^{-1}$	-0.37
ACS5CN	$K_b = 2,23 \times 10^5 \text{ L mol}^{-1}$	-0.14

Figure 17. (a) Absorption spectrum of 7ESTAC01 (b)UV–Visible absorption spectra of 20 μM 7ESTAC01 in presence of different concentrations of DNA:(μM): (a)0.0 ;(b) 2; (c)10; (d)12;(e)14;(f)16 ;(g)18;(h) 20 .

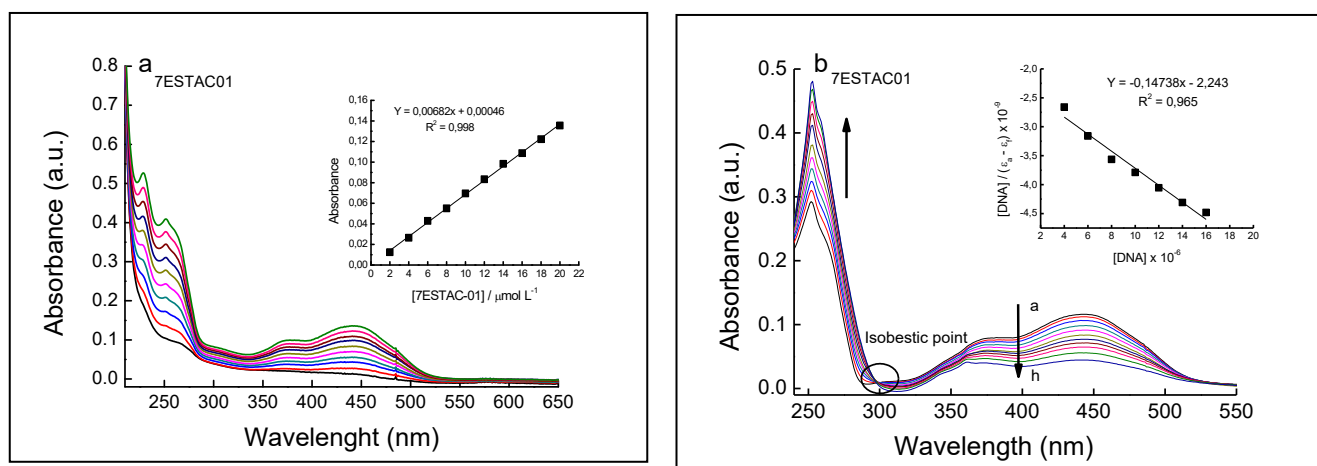
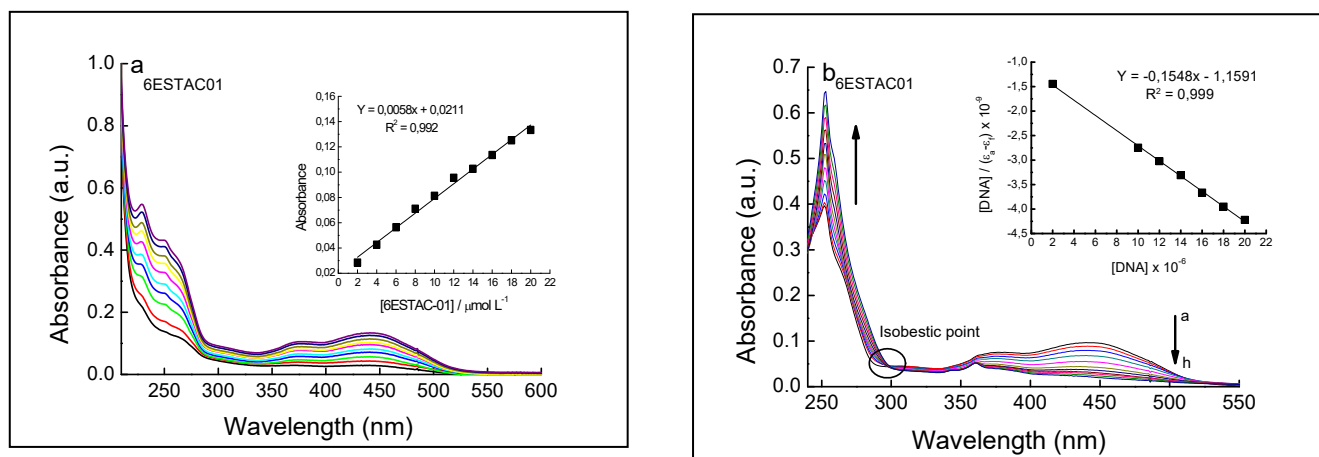


Figure 16 (a) Absorption spectrum of 6ESTAC01 (b)UV–Visible absorption spectra of 20 μM 6ESTAC01 in presence of different concentrations of DNA:(μM): (a)0.0 ;(b) 4; (c)6; (d)8;(e)10;(f)12 ;(g)14;(h) 16 .



Absorption spectra of 20 μM of ACS6CN and ACS5CN, showed a decrease in molar absorptivity at 417 nm for both, with no change in band position on the addition of DNA. (Fig 18(a) and Fig.19 (a)). The binding constant K_b of ACS6CN and ACS5CN were evaluated to $K_b = 2,8 \times 10^4 \text{ L mol}^{-1}$ and $K_b = 2,23 \times 10^5 \text{ L mol}^{-1}$, respectively (Fig 18(b) and Fig.19(b)). No appreciable shift in wavelength due to the interaction with a different concentration level of DNA had been found in the absorption spectrum of 7ESTAC01, 6ESTAC01, ACS6CN, and ACS5CN.

Finally, to evaluate a possible correlation between K_b and $E_{1/2}$. We obtained a linear correlation with $R^2 = 0.9114$ (Table 15). Then the apparent correlation between a binding constant and half potential in aqueous media was showed. We proposed for the first time an apparent correlation between K_b and $E_{1/2}$ in the case of 7ESTAC01, 6ESTAC01, ACS6CN, and ACS5CN.

Figure 18 (a) Absorption spectrum of ACS6CN (b)UV–Visible absorption spectra of 20 μM ACS6CN in presence of different concentrations of DNA: (μM): (a)0.0 ;(b) 8; (c)10; (d)12;(e)14;(f)16 ;(g)18.

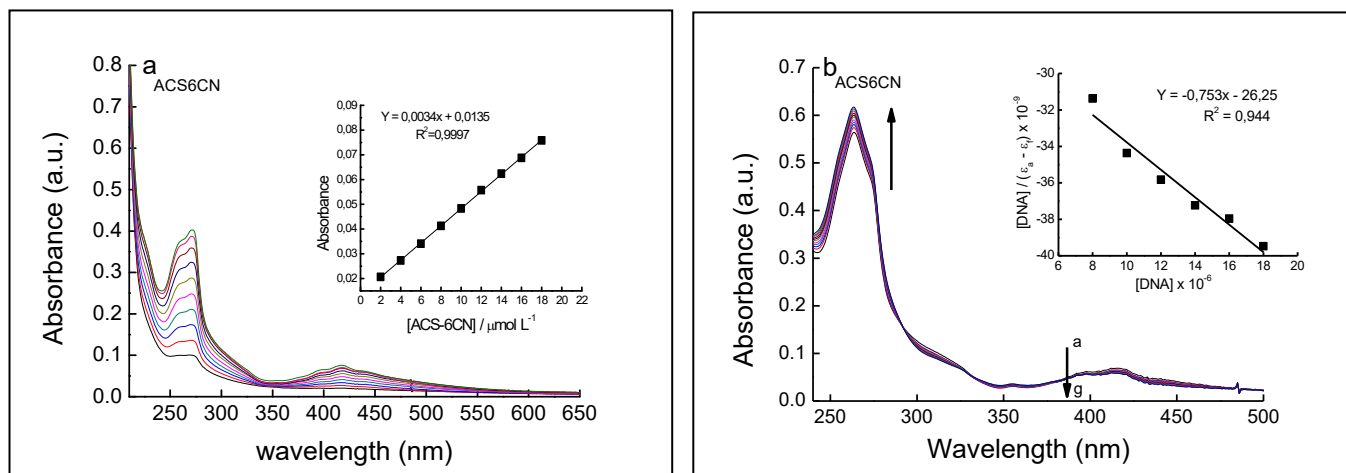
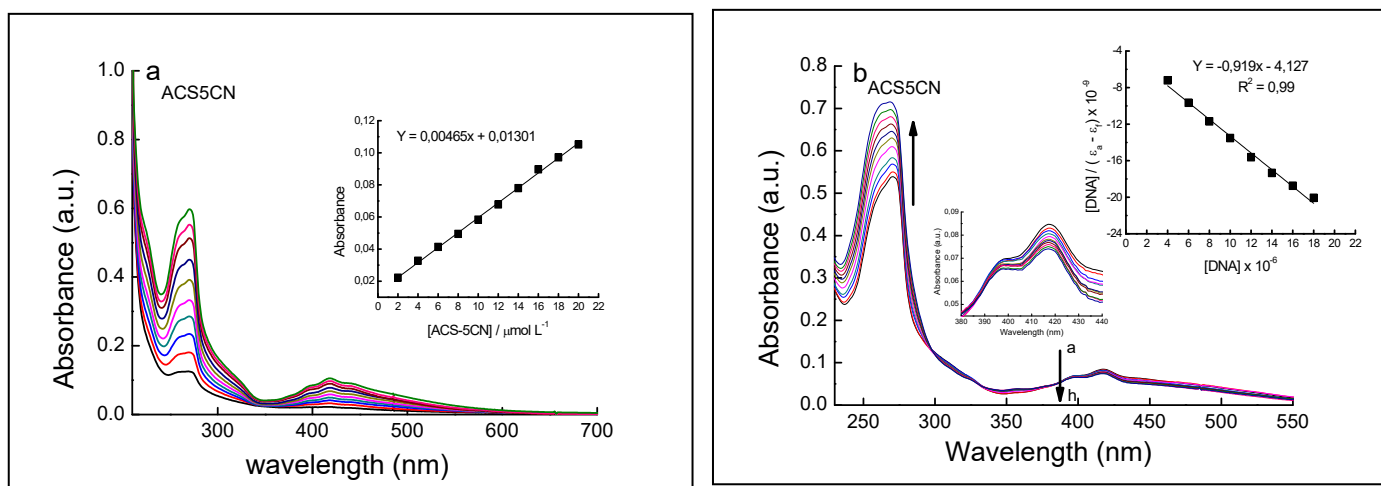


Figure 19 (a) Absorption spectrum of ACS5CN (b)UV–Visible absorption spectra of 20 μM ACS5CN in presence of different concentrations of DNA: (μM): (a)0.0 ;(b) 4; (c)6; (d)8;(e)10;(f)12 ;(g)14;(h) 16 .

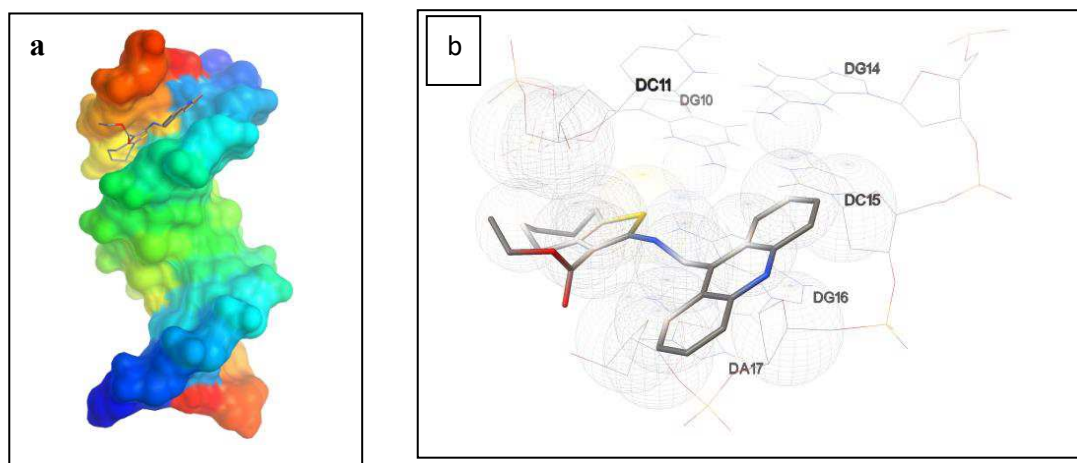


1.4.5 Molecular docking

1.4.5.1 Interaction of 7ESTAC01 and Duplex stranded

A Strand: As shown in Fig 20. C15, G16, A17 Intercalation in the minor groove. Hydrophobic interactions involving the Cyclo thiophene, acridine, imine function. **B Strand: C11 and G10:** hydrogen binding between carbonyl and C21 and oxygen. 1.4.5.2 7ESTAC01 and A/B Strand

Figure 20. Molecular docked structures of 7ESTAC01 with ctDNA. a) Duplex Strand. Dodecamer duplex sequence (CGCGAATTCGCG)₂ (PDB ID: 1BNA) was used in the docking studies b) Molecular docked model of 7ESTAC01



A Strand: As shown in Fig 21a, presence of Hydrogen binding between A6 and Ester carbonyl. Also there is Hydrophobic interactions involving the Cyclo Alkyl, cyclo thiophene, imine function and ester carbonyl between A5, A6, T7, T8. **B Strand:** Involving hydrogen binding between the Oxygen ester and C21. Also Hydrophobic interactions involving **C21 and G22** with, acridine, ester carbonyl and imine function (Fig. 21b)

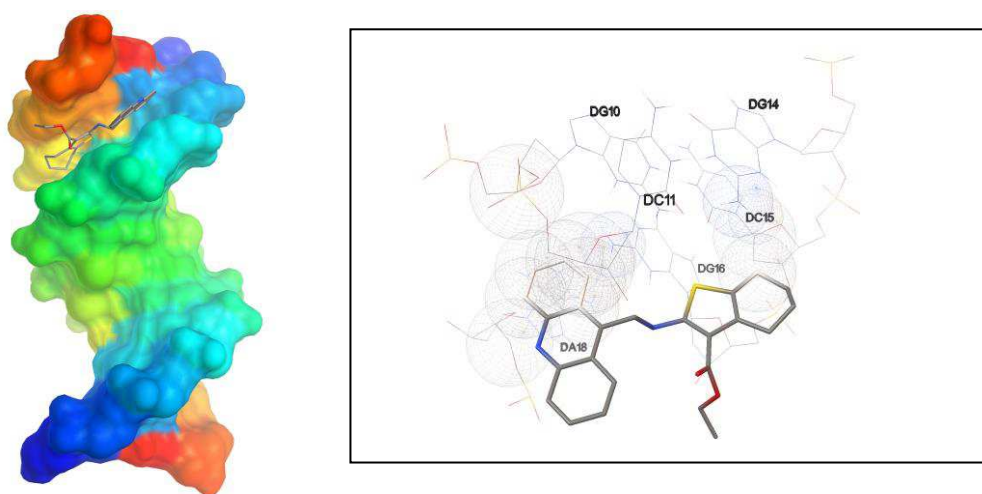
Figure 21 a) Molecular Docked structure of 7ESTAC01 with A strand b) Molecular Docked structure of 7ESTAC01 with B strand



1.4.5.2 Interaction of 6ESTAC01 and Duplex stranded

6estac01 with duplex strand: As shown in Fig 22, Intercalating in the minor groove . Involving Hydrophobic interactions between the Cyclo Alkyl and acridine with G10 and C11 on A Strand and G14, C15, G16, A18 on B strand.

Figure 22 Molecular docked structures of 6ESTAC01 with ctDNA.a) Duplex Strand. Dodecamer duplex sequence (CGCGAATTCGCG)₂ (PDB ID: 1BNA) was used in the docking studies b) Molecular docked model of 6ESTAC01 showing significant hydrophobic interactions with ctDNA.



1.4.5.3 6ESTAC01 and A/B Strand

A Strand: As shown in Fig 23a ,presence of Hydrogen binding between A6 and Ester carbonyl.Hydrophobic interactions involving the Cyclo Alkyl,cyclo thiophene ,imine function and ester carbonyl between G4, A5, A6 and T7 .**B Strand:**Involving hydrogen binding between the Oxygen ester and T19 and Hydrophobic interactions involving **A17, A18, T19, T20** with Cyclo Alkyl,acridine and ester carbonyl (Fig.23)

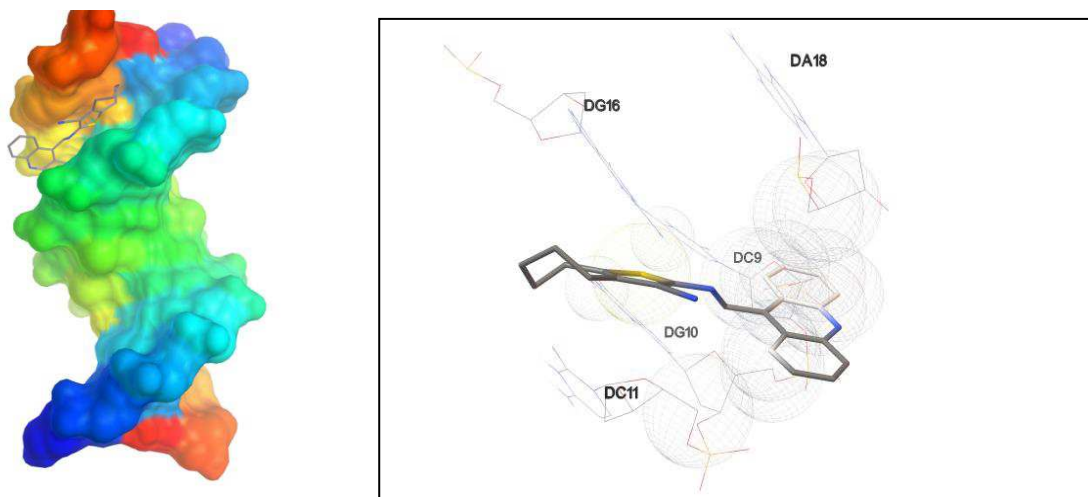
Figure 23 a) Molecular Docked structure of 6ESTAC01 with **A strand** b)) Molecular Docked structure of 7ESTAC01 with B strand



1.4.5.4 Interaction of 7CNAC01 and Duplex stranded

7CNAC01 with Duplex strand: Intercalating in the minor groove. **A Strand:** Involving Hydrophobic interactions between C9, G10, and C11 with the Cyclothiophene and acridine. **B Strand:** Showing Hydrophobic interactions with G16 and A18. And the Cyclothiophene and acridine.

Figure 24 Molecular docked structures of 7CNAC01 with ctDNA. a) Duplex Strand. Dodecamer duplex sequence (CGCGAATTCGCG)₂ (PDB ID: 1BNA) was used in the docking studies b) Molecular docked model of 7CNAC01



1.4.5.5 7CNAC01 and A/B Strand

A Strand: Involving Hydrophobic interaction of C3, G4, A5 and A6 with the Cyclo Alkyl, Cyclothiophene, acridine, and Imine FUNCTION groups. **B Strand:** Involving Hydrophobic interaction of A17, A18, T19 with the Cyclo Alkyl, Cyclothiophene, acridine, and Imine function

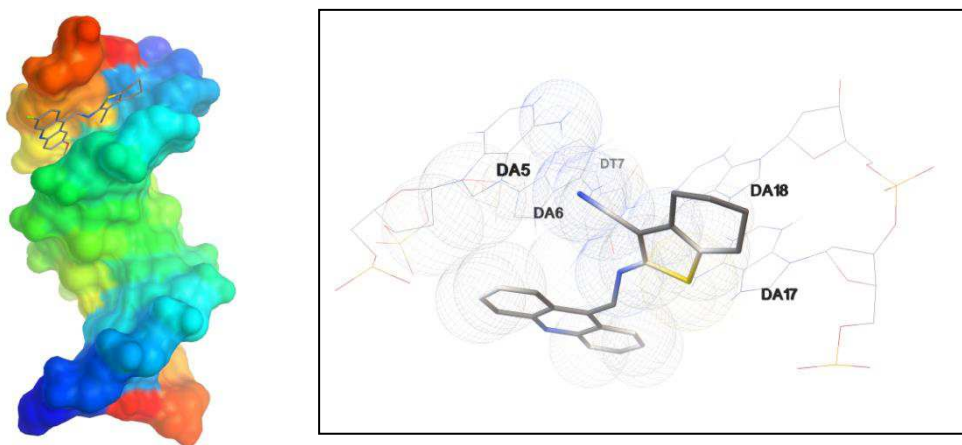
Figure 25 Molecular Docked structure of 7CNAC01 with A strand b)) Molecular Docked structure of 7CNAC01 with B strand



1.4.5.6 Interaction of 6CNAC01 and Duplex stranded

6CNAC01 with duplex strand: Intercalating in the major groove. **A Strand:** Involving interactions between A5, A6, and T7 with the Cyclo thiophene, acridine, imine function and cyano moiety. **B Strand:** Showing hydrophobic interactions between A17 and A18 with the Cyclo thiophene, acridine, imine function and cyano moiety.

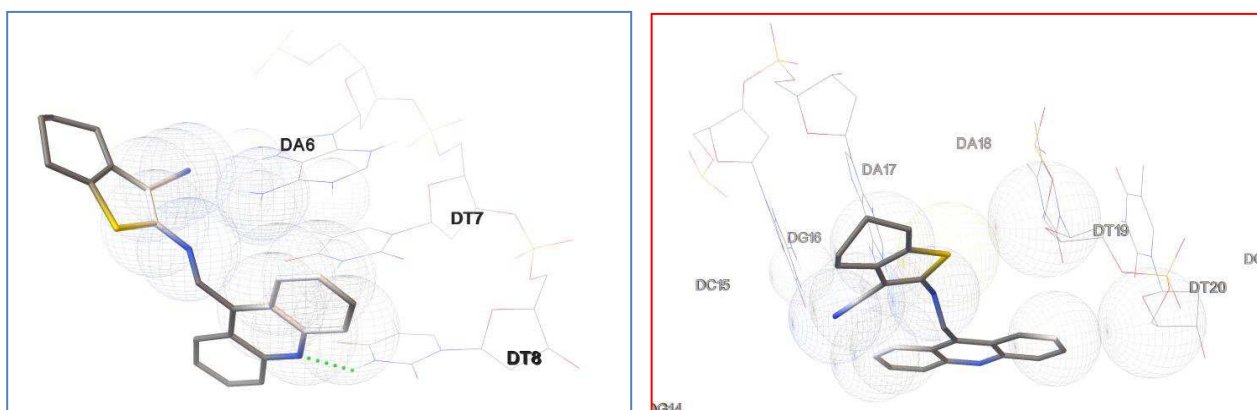
Figure 26 . Molecular docked structures of 6CNAC01 with ctDNA.a) Duplex Strand. Dodecamer duplex sequence (CGCGAATTCGCG)₂ (PDB ID: 1BNA) was used in the docking studies b) Molecular docked model of 6CNAC01



1.4.5.7 6CNAC01 and A/B Strand

A Strand: Involving Hydrophobic interaction of T7 and A6 with the Cyclo thiophene, acridine, imine function and cyano moiety and Hydrogenic bound between T8 and the Nitrogen of the **acridine**. **B Strand:** Involving Hydrophobic interaction of G16, A17, A18, 19

Figure 27 a) Molecular Docked structure of 6CNAC01 with A strand b)) Molecular Docked structure of 6CNAC01 with B strand .

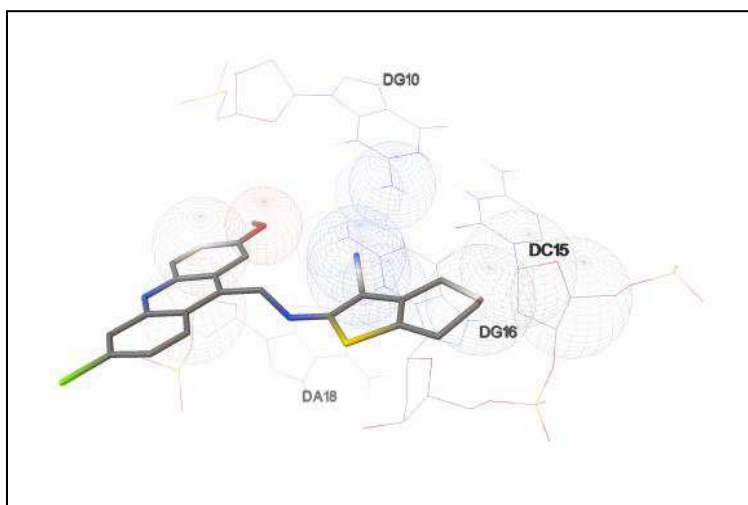
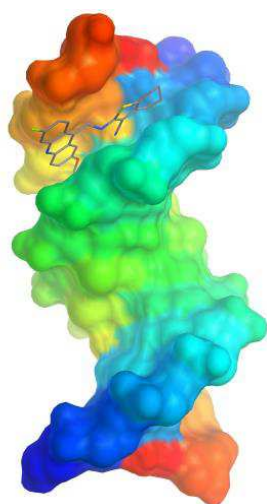


and T20 with the Cyclothiophene, acridine, imine function and cyano moiety

1.4.5.8 Interaction of ACS6N and Duplex stranded

ASC6CN with duplex strand: Interaction in the minor groove. **A Strand:** Involving interactions between G10 with the cyclo alkyl, acridine, cyano moiety and ester carbonyl. **B Strand:** Showing interactions between C15, G16, A18 with the cyclo alkyl, acridine, cyano

Figure 28 Molecular docked structures of ACS6N with ctDNA. a) Duplex Strand. Dodecamer duplex sequence (CGCGAATTCGCG)₂ (PDB ID: 1BNA) was used in the docking studies b) Molecular docked model of ACS6N



moiety and ester carbonyl.

1.4.5.9 ACS6CN and A/B Strand

A Strand: Involving Hydrophobic interaction of A5, A6, T7 and T8 with the Cyclo alkyl, acridine and ester carbonyl. **B Strand:** Involving hydrogen bond to the Nitrogen of the imine function with the G22 and Hydrophobic interaction involving T20, C21, G22 and C23 with the acridine, cyclo thiophene, and cyclo alkyl

Figure 29 . a) Molecular Docked structure of ACS6CN with A strand b)) Molecular Docked structure of ACS6CN with B strand .

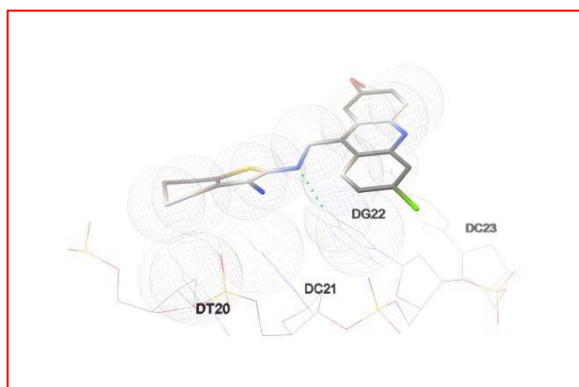
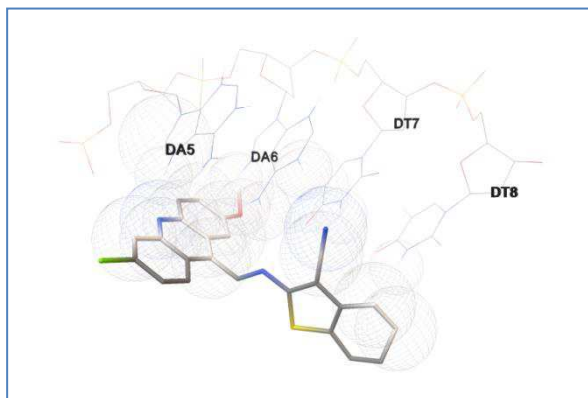


Table 16 Binding energy for acridine derivatives with ctDNA

Compound	Affinity (Kcal mol ⁻¹)		
	dsDNA	Astrand	BStrand
7CNAC01	-8,7	-5,9	-5,8
6CNAC01	-7,3	-5,6	-5,5
7ESTAC01	-7,6	-5,8	-5,3
6ESTAC01	-7,1	-5,6	-6,1
ASC6CN	-8,3	-6,3	-5,8
ASC5CN	-7,7	-5,9	-5,5

For all the compounds studied, a preference for the minor groove intercalation has found. The groove binding interactions involving possible electrostatic, hydrogen (7ESTAC01 and 6ESTAC01) and van der Waals bonds are clearly observed in the fig.20-29. On the other hand for all the acridine-thiophene compound the main interaction are hydrophobic interaction.

The negative values of the binding energies indicated a higher binding potential of the compounds with ctDNA, as well as were found to be consistent with the biological and spectroscopic studies (Table x). The compounds 7CNAC01, ASC6CN, and 7ESTAC01 showed the highest affinity -8.7, -8.3 and 7.6 Kcal mol⁻¹ docking energy and the main interactions in the binding process with ctDNA are hydrophobic interactions.

In this model, for the three compounds that exhibited best values of the binding energies, the GC DNA residues played a major role in the binding site. Important to mentioned on the molecular docking of 6ESTAC01 and A 7ESTAC01 a hydrogen binding between Adenine, Guanine and ester carbonyl and oxygen were showed.

1.5 CONCLUSION

Chapter 1

- We proposed for the first time a direct correlation between constant binding (K_b) and half-wave potential ($E_{1/2}$) for 7ESTAC01, 6ESTAC01, ACS6CN, and ACS5CN.
- We found that the nature of solvent strongly influences the electrochemical behavior of these active redox drugs.
- We found that our six acridine-derivates conjugates, no show apparently reactivity with oxygen (aprotic media).
- The reduction of 7CNAC01, 6CNAC01, 7ESTAC01, and 6ESTAC01 are similar in that four involve quasi-reversible process wich involves possibly the transfer of one electron and one proton.
- The electrochemical DNA-biosensor shows dsDNA damage for reduced form of 7CNAC01, 6CNAC01, and ACS5CN.
- 7CNAC01, 6CNAC01, 7ESTAC01, 6ESTAC01, ACS6CN, and ACS5CN exhibited oxidation signal and shifted potential to guanine and adenine that could be caused damage in singled stranded ssDNA.
- For the first time, there is evidence of interaction of acridine-thiophene derivates (7CNAC01, 6CNAC01, ACS5CN) and dsDNA, which suggests that possible toxicity can be caused by this interaction, after reductive activation.
- The electrochemical reduction of each substrate of acridines-thiophenes derivates generate radicals that interact better with singled stranded ssDNA causing damage. Then, the bio-reduction of the acridine-thiophene could be pointed out as an activation step generating the active form of the drug.
- The shift in peak potential toward positive side could be attributed to the intercalation of compounds 7CNAC01, 6ESTAC01, ACS6CN and ACS5CN with DNA.
- We proposed the intercalation as a dominant binding mode to 7ESTAC01 and 6ESTAC01
- In silico molecular docking further confirmed that acridine derivatives bind preferentially to the minor groove of the DNA, with a certain preference of the binding of GC region.
- The main interactions for our six candidates of acridine-thiophene with calf thymus DNA are hydrophobic interactions with a notable preference for the minor groove DNA.

- The compounds 7ESTAC01 and 7CNAC01 showed the highest affinity -7.6 and -8.7 Kcal mol⁻¹ docking energy and the main interactions in the binding process with ctDNA are hydrophobic interactions
- 7ESTAC01 showed a hydrogen binding between Adenine(A6) with ester carbonyl.
- 6ESTAC01 showed a hydrogen binding between Cytosine (C21) and ester carbonyl besides of Guanine (G22) with the oxygen.

CHAPTER 2

AN ELECTROCHEMICAL BIOSENSOR BASED ON HAIRPIN-DNA MODIFIED GOLD ELECTRODE FOR DETECTION OF DNA DAMAGE FOR A NEW ACRIDINE-THIOPHENE CANCER DRUG.

2.1. INTRODUCTION

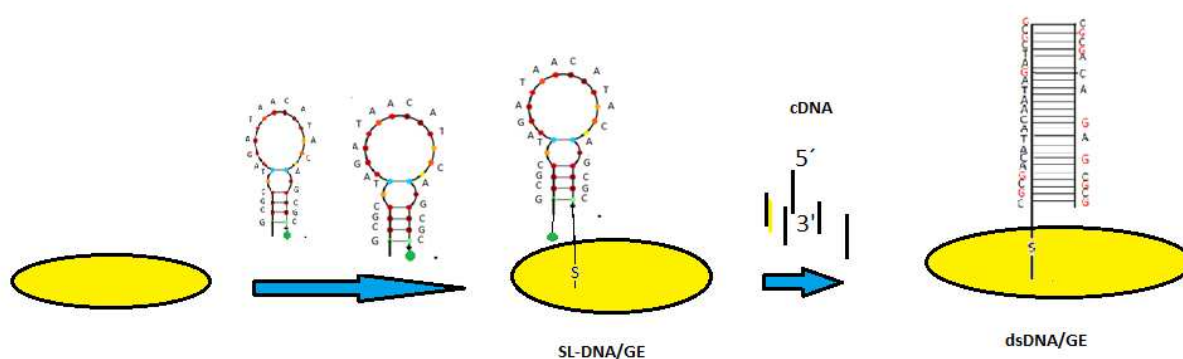
2.1.1 DNA biosensor for detection of Cancer- drug

The idea of integration without hybridization has been explored in the development of fast and accurate electrochemical biosensor to detect DNA damage. The uses of effective biosensors to detect interaction with small molecules like cancer drug have been studied and represent a new challenge in cancer drug development.

2.1.2 SL-DNA Biosensor at Gold Electrode: Improvement of the Surface conductivity

The develop of the new biosensor to detect small molecules are focused on improving DNA immobilization techniques on the surface of the electrode to get a better conductivity and accessibility for the drug.

Most of the literature concluded that the immobilization of the DNA on the surface of the electrode performed by electrochemical techniques don't ensure a uniform immobilization. It was suggested that randomly oriented dsDNA (from calf thymus) does not conduct electrons efficiently and can show issues in the accessibility of drugs to the DNA. In fact, non covalent binding immobilization of bases decreases the specificity of the recognition layer and therefore is not recommended. In front of this, the use of covalent bonding to link the DNA and form monolayer is obtaining better results. Attaching a thiol group to one end of an oligo deoxynucleotide made it possible to form self-assembled monolayers of dsDNAs on gold surfaces. (MILLS, et al., 2016 and YUN XIA; YA HU, 2005)



Scheme 1. Schematic of the fabrication process of SL-DNA/ dsDNA Biosensor at Gold electrode. **Source: Author**

Then to improve the conductivity and avoid nonspecific interactions a covalently bound probe would provide more opportunities to improve immobilization and easily removing the nonspecifically bound molecules. For this reason, two-component films have been used to contain a thiol-derived ssDNA and dsDNA and mercaptohexanol(MCH), which prevents nonspecific adsorption of the ssDNA. (Scheme 1)

Two important works using Atomic Force Microscopy and Scanning tunneling microscopy has characterized different immobilizations, hybridizations, and oxidation of synthetic DNA on pyrolytic graphite electrodes and Gold Electrodes.(MCEWEN; CHEN; ZHOU,2009). They concluded that the optimal electrochemical response of the DNA biosensor depends on pH, buffer compositions, ionic strength, immobilization procedure, adsorptions time, type and concentration of DNA. Then it was revealed that the best surface conductivity followed the order: dsS-DNA/Au < MCH/dsS-DNA/Au < Oxidized MCH/dsS-DNA/Au. Thus it showed importantly, the conjunction of dsDNA(double strand) attached by thiol on the surface of the Gold electrode with a posterior mercaptohexanol(MHC) treatment showed the best conductivity.

The present work takes advantage of all of these features to develop a Stem Loop-DNA biosensor for the detection of DNA damage.

Detection of DNA damage

Inspired by the DNA damage can be detected for direct determination of the oxidation of electroactive guanine and adenine bases, the number of biosensor studies pursuing a detection of DNA damage by oxidation have been increasing considerably since ten years ago. (HUANG, S. et al.,2016 and LABUDA; OVÁDEKOVÁ; GALANDOVÁ,2009)

The electrochemical processes involved in purine DNA base oxidation are similar to those involving enzymatic oxidation. Electrochemical oxidation on Carbon electrodes showed that all bases Guanine, adenine, thymine and cytosine could be oxidized following a pH-dependent mechanism, but both of the purine bases, guanine, and adenine, are of particular interest to electrochemists due to the relative ease with which they may oxidize(LUCARELLI, et al.,2004). The sensitive and specific electrochemical oxidation of guanine and adenine bases, exhibits, and enhanced differential pulse voltammogram(DPV)oxidation peak. (VYSKOČIL; LABUDA; BAREK, 2010)

These external small electroactive molecules have been applied to prove the electron transfer characteristic of DNA lesion was studied for many groups including modified solid electrodes such as gold electrode surface (BOAL.; BARTON, 2005), glassy carbon (LI; BATCHELOR-MCAULEY; COMPTON,2010) and mercury electrode (FOJTA.; PALEČEK,1997)

2.1.3 Chemical and physical interaction of DNA and small molecules

Three basic modes of non-covalent binding of small molecules to double-stranded (ds) DNA can be distinguished: i) electrostatic interactions of cationic species with phosphate anions ii) groove binding interactions (involving electrostatic, hydrogen and/ or van der Waals bonds); and iii) intercalation of planar condensed aromatic ring systems between adjacent base pairs (primarily involving stacking interactions). Noncovalent binding of various carcinogens or drugs often facilitates subsequent covalent DNA damage by the given agent. (BAGULEY, et al.,2003)

Damage to DNA arises from interactions of DNA with different chemical, or physical agents showed different electrochemical patterns of Charge transfer(WONG.; GOODING,2006) .In fact, decrease and a decrease of the DPV peak current and shift potential were showed in many works where depending on the type of interaction and type of the DNA immobilized have shown different DPV peak current. Strand breaks are formed as a result of the radical attack on the deoxyribose residues or due to acidic or enzymatic hydrolysis of the phosphodiester bonds. Hydrolysis of N-glycosidic bonds leads to the release of bases(purines more easily than pyrimidines) and formation of basic sites in DNA. Some simple chemicals including alkylating agents, electrophiles or nucleophiles react with DNA base residues thus changing their physical-chemical properties. More complex compounds possessing reactive groups (covalently binding to sites in DNA) and bulky side moieties, form DNA adducts that exhibit optical, electrochemical and immunochemical properties derived from the given modifier (KARADENIZ,et al.,2010 and MERIC, et al.,2002). Bifunctional agents may form inter- or inter strand cross-links of ten involving significant conformational changes of the DNA double helix. Besides agents interacting with DNA covalently, a broad range of potentially genotoxic species exhibits non-covalent DNA interactions.(NOH, J. et al.,2015)

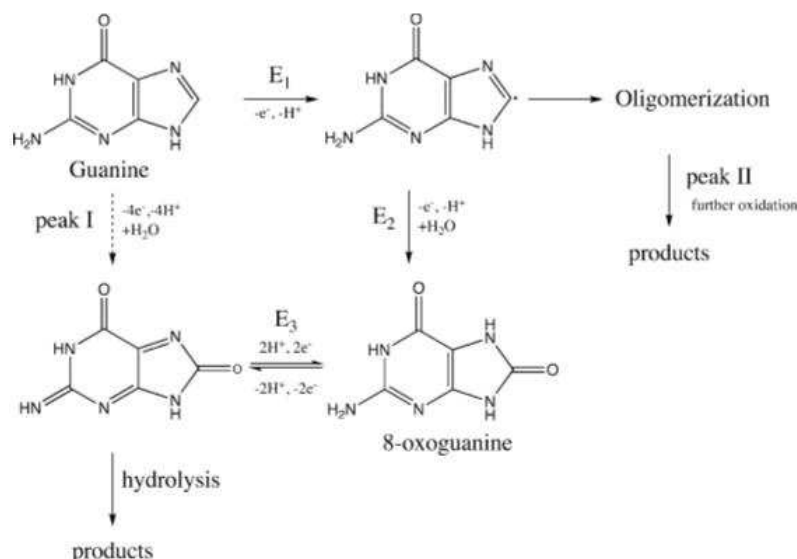
2.1.4 Electrochemistry of guanine and 8-oxoguanine at gold electrodes

Several authors have performed mechanism studies on the electrochemical behavior of purine derivatives. Electrochemical oxidation of DNA at a glassy carbon electrode using differential pulse voltammetry (DPV) shows two current peaks due to the oxidation of guanine and adenine residues at 1.0 V and 1.2 V, respectively. Also, the electrochemical oxidation of DNA at a gold electrode using DPV as well shows a positive shift (IBÁÑEZ, D. et al., 2015 and MCEWEN; CHEN; ZHOU, 2009)

Electrochemical oxidation of G has been studied at carbon/graphite surfaces, and it has been found to be analogous to that of other purines. Oxidation of G at pyrolytic graphite, glassy carbon electrodes implies consecutive irreversible pH-dependent $4e^-$ oxidation of G through the formation of intermediate 8-oxo-7,8-dihydroguanine (8-oxoG). (FERAPONTOVA, 2004)

According to with an oxidative mechanism of guanine at the gold electrode. Electrochemical oxidation of G and 8-oxoG on gold demonstrates that 8-oxoG can undergo a quasi-reversible $1e^-$ redox transformation at potentials less positive than irreversible $2e^-$ oxidation of G.

Figure 30 Proposed mechanism for the electrochemical oxidation of guanine.

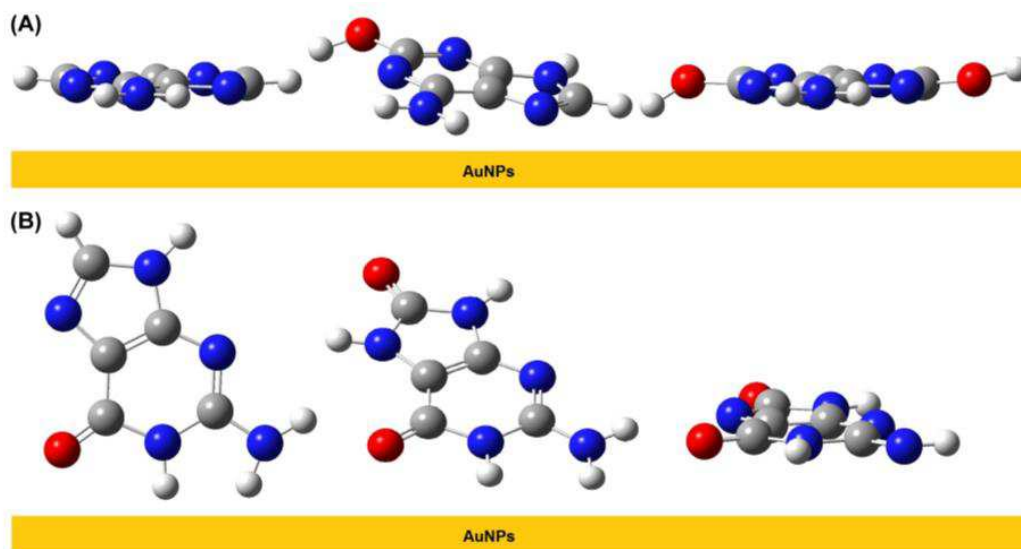


Source: From Reference (FERAPONTOVA, 2004)

2.1.4.1 Orientation of Guanine during Oxidation

In an elegant and useful work, IBÁÑEZ, et al., 2015, studied the adenine and guanine oxidation mechanism using gold nanoparticles by surface-enhanced Raman spectroelectrochemistry(SERS) . They showed a special and useful information about the orientations during the oxidation of this purine bases. Adenine shows a parallel orientation respect to the AuNPs surface at 0.00 V, when it is oxidized to 2-oxoA the molecule acquires a slightly tilted orientation, but after the second oxidation process to 2,8-dioxoA, the molecule recovers the parallel orientation. On the other hand, guanine orientation is perpendicular respect to the AuNPs surface at 0.00 V, but after the first oxidation at +0.10 V, 8-oxoG starts to be slightly tilted. The most important change in orientation is produced when the 8-oxoG is oxidized to 8-oxoGoxo, which acquires a parallel orientation respect to the AuNPs surface(Graph below)

Figure 31 Schematic drawing of (a) A,2-oxoA, and 2,8-dioxoA orientation during the oxidation and (b) G,8-oxoG, and 8-oxoGOX oxidized orientation during the oxidation.



Source: From Reference (IBÁÑEZ, D. et al.,2015)

In this second chapter, the electrochemical oxidation of DNA on a new Stem-Loop DNA/GE gold (attaching by a thiol group) to detect DNA damage through the interaction of a hybrid drug 7ESTAC01, is shown for the first time. The sensitive and specific electrochemical oxidation of guanine and adenine bases was analyzed, by DPV.

2.2. OBJECTIVES

1. Develop of electrochemical DNA sensor for the detection of DNA damage using the electrochemical signal of oxidation of purine DNA bases with redox activity, to detect DNA-drug interaction.
2. Try to understand the nature of the complex formed, binding constant, binding site size and the role of free radicals generated during interaction in the drug action.

2.3. METHODOLOGY

2.3.1 Reagents

All solutions were prepared with Milli-Q water using a Siemens PURELAB Ultra system (Lowell, USA). Several buffers were used in this work: A phosphate buffer saline (PBS) solution was used as the immobilization buffer (IB) contained 50mM Sodium Phosphate (Monobasic/Dibasic), 250mM NaCl and adjusted to a pH of 7.4; hybridization buffer contained 50 mM Tris-HCl, 25 mM NaCl, 50mM MgCl₂. Stock solutions of 1mM 7ESTAC01 were prepared in IB.

An Acetate buffer solution was used for the DNA oxidation. The pH was adjusted with either NaOH or HCl solution.

A gold electrode (GE) was purchased from CH Instruments (Austin, USA). Alumina slurry (1.0 mm, 0.3 mm and 0.05 mm) was obtained from Buehler (Lake Bluff, USA).

The SL-DNA, DNA complementary sequences were purchased from Integrated DNA Technologies (Coralville, USA) and used as received (Table x). Trizma hydrochloride (Tris-HCl), tris(2-carboxyethyl) phosphine hydrochloride (TCEP), sodium phosphate dibasic (Na₂HPO₄), sodium phosphate monobasic dihydrate (NaH₂PO₄·2H₂O), 6-mercapto-1-hexanol (MCH) and magnesium chloride (MgCl₂) were purchased from Sigma-Aldrich. Sodium chloride (NaCl), potassium chloride (KCl), Sodium hydroxide (NaOH) and sulfuric acid (H₂SO₄) were obtained from Fisher Scientific (Pittsburgh, USA).

All DNA sequences were purchased from Sigma-Aldrich. Their base sequences were listed as below

Stem-Loop DNA: 5'-C6-S-S-TC GCG ACA TAC AAT AGA TCG CG-Methylene Blue-3.'

DNA Complementary: 5'- CGA TCT ATT GTA TGT TAA CG -3.'

2.3.2 STEM-LOOP DNA (SL-DNA) and double strand DNA (dsDNA) biosensor on the gold electrode surface

2.3.2.1 Preparation of SL-DNA/GE and dsDNA/GE

Gold electrodes (GE) were used as substrates for SL-DNA and dsDNA probe immobilization. Immersion cleaned GE in a piranha solution (1:3 ratio of H₂O₂: H₂SO₄) for ten minutes. Then, the GE was presented by polishing on a micro cloth with 1.0 mm, 0.3 mm and 0.05 mm alumina slurry, rinsed thoroughly with ultrapure and then sonicated in ethanol to remove any residual alumina particles trapped at the surface of the electrode. The Gold Electrode was activated in 0.5 M H₂SO₄ via cyclic voltammetry from 1.6 to 0.1 V at a scan rate of 50 mV.s⁻¹

2.3.2.2 Immobilization of Stem-Loop DNA and dsDNA.

The SL-DNA, was immobilized on the electrode surface via a gold-thiol bond. The disulfide bonds of the SL-DNA probe were reduced with one mM TCEP by shaking the solution at room temperature for 1 hour. The solution was then diluted with IB to yield 1 uM of the SL-DNA probe and 15 uL of this solution was dropped on the electrode and incubated at room temperature for 30 min. Then, the electrodes were rinsed with IB and dried with nitrogen. To minimize nonspecific adsorption on the electrode surface, 15 uL of 2 mM MCH in Immobilization buffer was dropped on the electrode and incubated for 30 minutes. Then, the electrodes were rinsed with IB and dried with nitrogen. For dsDNA/GE preparation, SL-DNA modified GE was Hybridization dropping 15 ul of 50 mM DNA complementary in HB, which formed dsDNA at the surface of GE. To this hybridization 15 uL of this solution was drop cast to the electrode and incubated for 1.5 hours at room temperature. After hybridization, dsDNA was rinsed with HB and dried with nitrogen. Next 7ESTAC01 for 2 hours. Then, Apply VPD with oxidation potential from 0 to +1.6V.

2.3.2.3 Optimization of SL-DNA Probe, DNA complementary

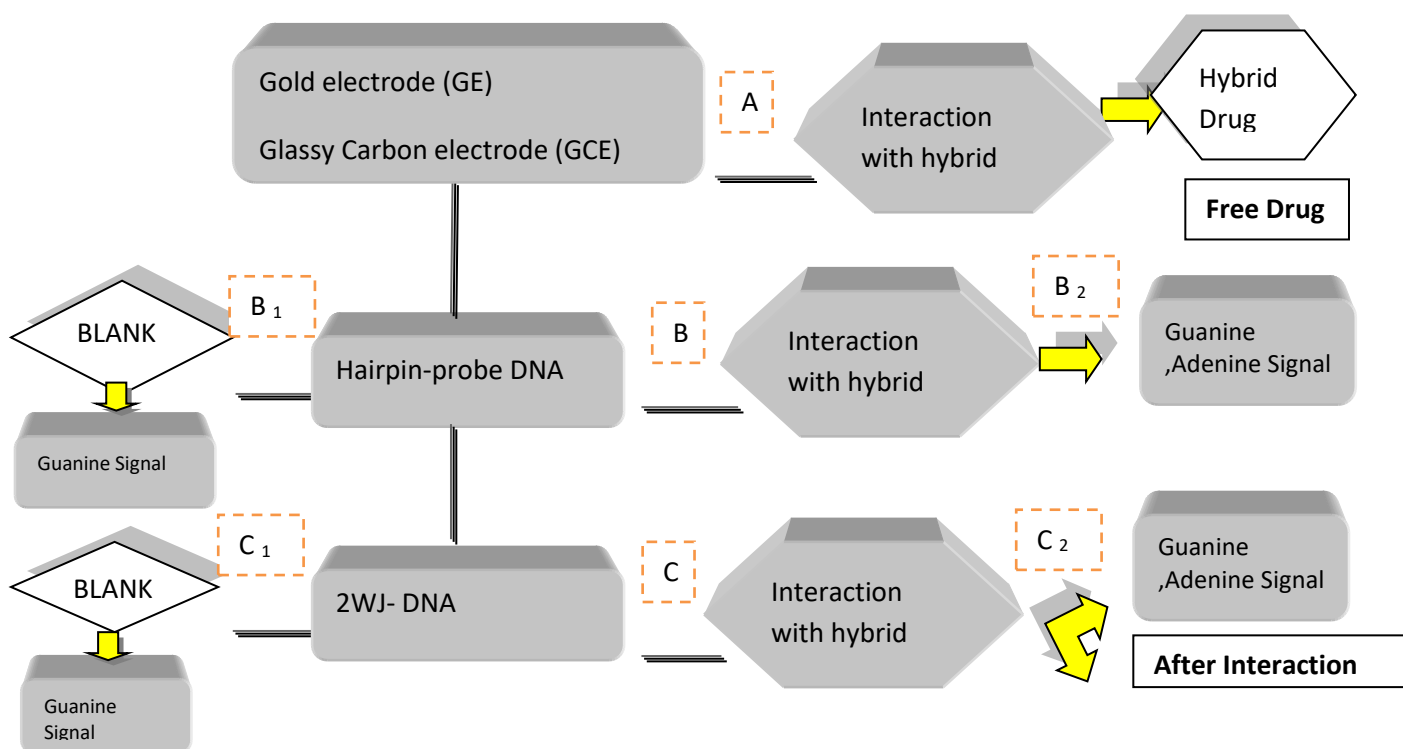
The concentrations of SL-DNA probe were tested for two concentrations, 0.1uM, and one uM and incubated with DNA complementary to get ds-DNA probe. Next, the concentration of the SL-DNA was varied in concentrations of 0.1uM and 1.0 uM, and incubated with 50 nM DNA complementary upon immobilization of SL-DNA probe. Finally, the concentration of the DNA complementary was held constant at 50nM.

2.3.3 Optimization of 7ESTAC01 concentration and experimental Timing

The SL-DNA and dsDNA modified GE was immersed into acetate buffer pH. 4.2 that containing 7ESTAC01. The optimization of 7ESTAC01 was varied in concentration 10uM, 100uM, and 400uM; whereas intercalation time of the compound with the SL-DNA/GE and dsDNA/GE was varied from 1h, 2h and 24 hours.

The procedure for GE-based biosensor consist of the following steps: i) measurement of free compound signal; ii) measurement of guanine signal obtained from Hairpin probe DNA-modified electrode before the interaction with the compound; iii) measurements of guanine and compound signal after interaction between compound and SL-DNA; iv) measurement of guanine signal obtained from dsDNA before the interaction with the compound) measurements of guanine and compound signal obtained from hybrid DNA after the interaction with the compound.(Scheme 2)

Identification of interaction mechanism of 7ESTAC01 and DNA



Scheme 2. The procedure for Identification of interaction mechanism of Compound 7ESTAC01 and SL-DNA/dsDNA. **Source:** Author

2.3.4 Electrochemical Measurements

A typical 3-electrode system was used where the modified gold electrode (GE) served as the working electrode, a platinum wire was used as the counter electrode, and Ag/AgCl (3 M KCl) was used as a reference.

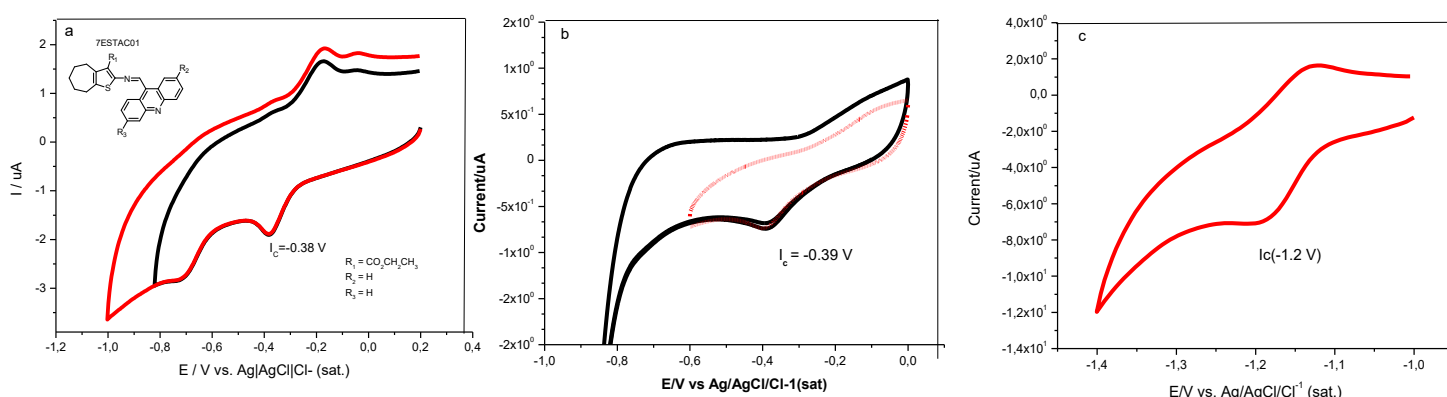
Electrochemical responses on SL-DNA/GE and dsDNA/GE to different concentration of 7ESTAC01 in IB were investigated by Differential potential voltammetry (DPV). DPV measurements were recorded in a pH 4.2 Acetate buffer at an oxidation potentials range from 0.0 to + 1.6V; pulse amplitude 0.05Vs; sample width 0.00167s; pulse period 0.5s; quiet time 2s; scan rate 0.005Vs⁻¹. All the intercalation measures of 7ESTAC01 and the DNA/GE biosensor was worked with the reduced 7ESTAC01. The reduced 7ESTAC01 was obtained applying VPD at a potential range from 0.0 to -0.122V for 100sec.

Cyclic voltammetry (CV) was performed to analyze the DNA immobilization on the electrode at a potential range from 0.0 to -0.5 V at a Scan rate of 0.1 V s⁻¹. CV measurements were carried out in IB. At least three electrodes were used for each experiment to provide statistically significant results.

2. 4. RESULT AND DISCUSSION

2.4.1 Synergic activity of 7ESTAC01

Figure 32 a) Cyclic voltammogram of 10 mmol L⁻¹ hybrid drugs 7estac01 in mixture of pH 7.2 , aqueous phosphate buffer and 20%DMF at a glassy Carbon Electrode(GCE) , with a Ag/AgCl reference electrode (RE), and the scan rate 0.1 V/s, E = potential, V = volt, A = ampere b) Cyclic voltammogram of 10 mmol L⁻¹ hybrid drugs 7estac01 in mixture of pH 7.2 , aqueous phosphate buffer and 20%DMF at a Gold electrode(GE). C) Cyclic Voltamogram of 10 mmol L⁻¹ 9- aminoacridine



The synergic activity of all the compound was analyzed. According to with all the potential recorded (E_c), our six acridine-thiophene derivates showed a less negative Potential than the Aminoacridine. (Table 3, Fig 32c). This result means that there is a synergic activity demonstrated for the hybrid compounds. As shown in the Fig. 32c the First cathodic potential for the Aminoacridine showed a peak $E_{ic} = -1.2V$. According to the literature, most of the bioactive compound including acridine derivates recorded a less negative potential of $-0.5V$ (33) . Those results mean synergic activity of acridine-thiophene derivates. Then according to our result (Table 3, Table 15), All the recorded potential were less than $-0.5V$. For the next experiments and according to the chapter 2 goals, we choose our best hybrid candidate: 7ESTAC01 to prove DNA damage on the SL-DNA Biosensor.

2.4.2 Optimization of concentration of Stem-Loop DNA

Figure 33 MeB Signal On (SL-DNA-Before Hybridized) and MeB signal OFF (dsDNA-Hybridized). Cyclic voltammogram in Immobilization Buffer of 0.1 μ M SL-DNA and dsDNA at Gold electrode at different Scan rates a) 1V/s b) 10V/s c) 100V/s

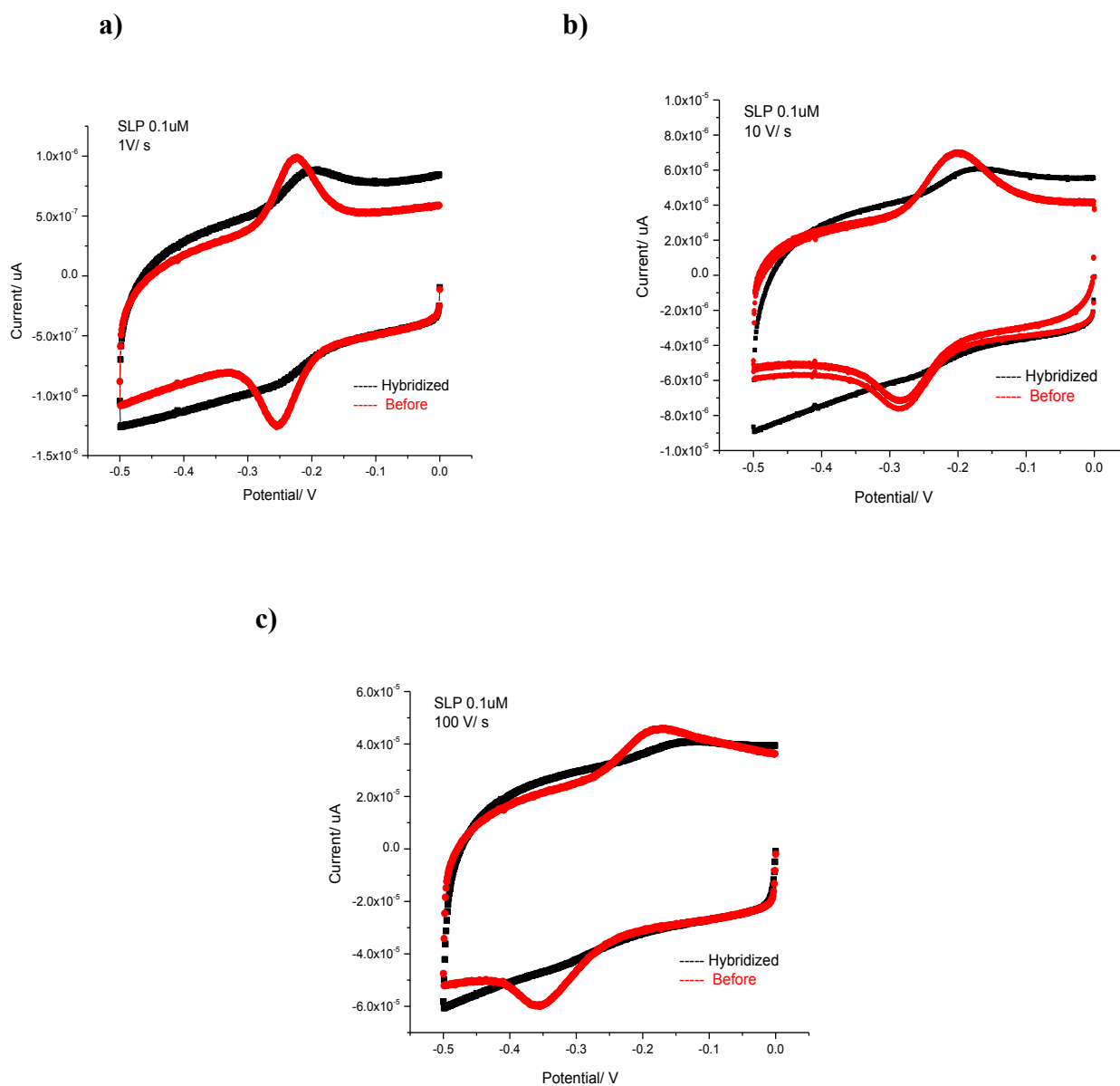
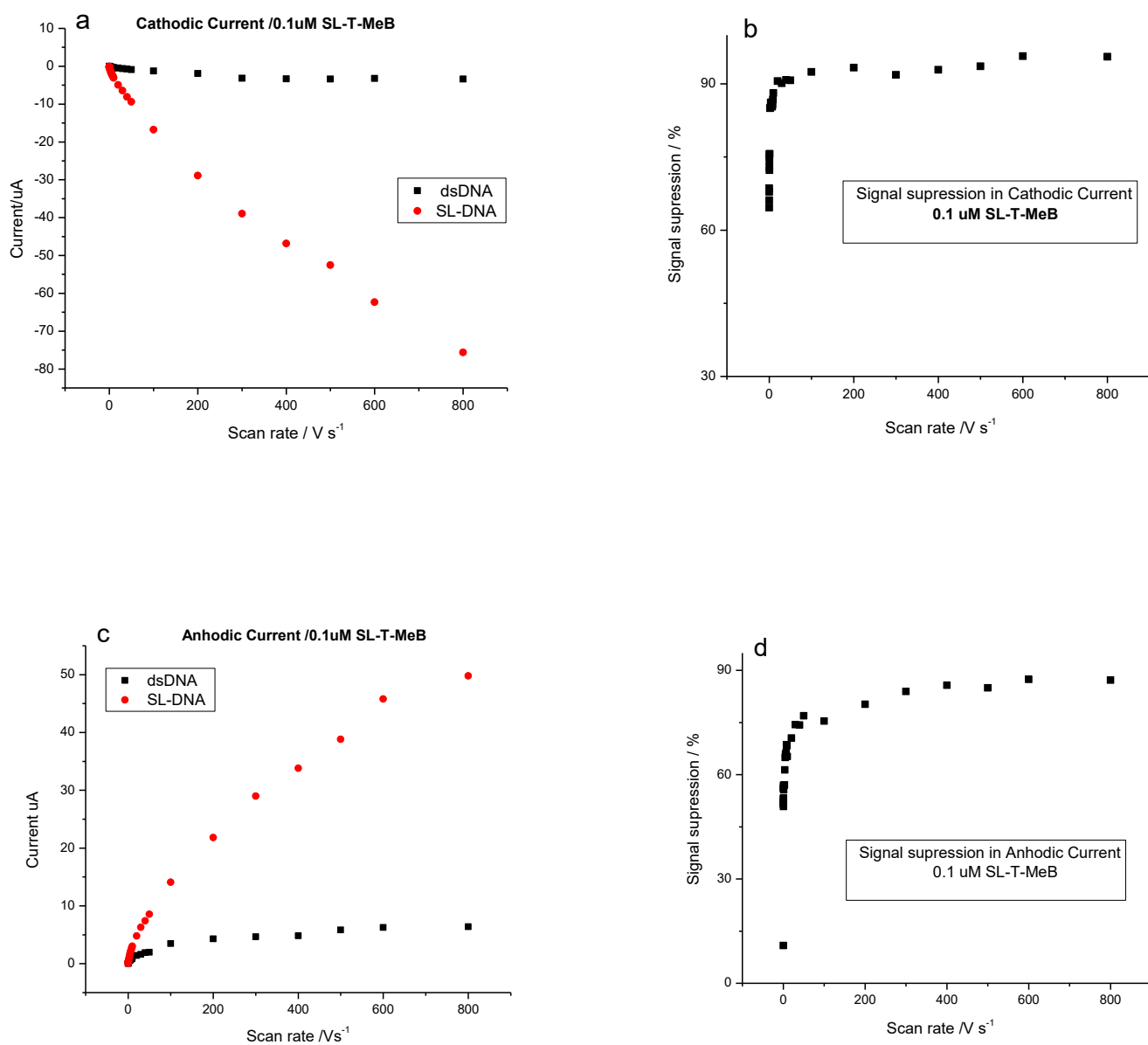


Table 17 Electrochemical parameters obtained from a CV of 0.1 μ M SL-DNA and dsDNA immobilized for different Scan rates.

Scan rate Vs^{-1}	I μA (cathodic)		I μA (anodic)	
	dsDNA	SL-DNA	dsDNA	SL-DNA
0.1	-0.017	-0.04805	0.02994	0.03358
0.2	-0.04468	-0.1422	0.04312	0.09818
0.3	-0.06758	-0.1997	0.07486	0.1546
0.4	-0.08262	-0.2571	0.101	0.2092
0.5	-0.0857	-0.3092	0.1256	0.2556
0.6	-0.09934	-0.3671	0.1474	0.3093
0.7	-0.1056	-0.409	0.1683	0.3598
0.8	-0.1156	-0.4622	0.1928	0.4107
0.9	-0.1222	-0.5003	0.1938	0.4497
1	-0.1364	-0.5606	0.2188	0.4927
2	-0.1454	-0.9708	0.3794	0.881
3	-0.1992	-1.335	0.5406	1.258
4	-0.2294	-1.658	0.5961	1.543
5	-0.2623	-1.893	0.6484	1.85
6	-0.2985	-2.166	0.7237	2.121
7	-0.354	-2.413	0.7848	2.336
8	-0.3797	-2.665	0.8277	2.635
9	-0.3731	-2.823	0.8774	2.77
10	-0.361	-3.044	1.049	3.014
20	-0.467	-4.946	1.411	4.789
30	-0.6349	-6.431	1.619	6.315
40	-0.7435	-8.08	1.902	7.399
50	-0.8689	-9.378	1.974	8.554
100	-1.263	-16.74	3.468	14.09
200	-1.932	-28.91	4.31	21.83
300	-3.173	-38.95	4.657	29.01
400	-3.337	-46.83	4.836	33.81
500	-3.356	-52.56	5.838	38.83
600	-3.245	-75.35	6.279	49.81
800	-3.3665	-75.64	6.385	49.78

The higher Scan rates from 1 to 800 Vs^{-1} were tested with a Sensitivity of 10^{-2} to avoid overflow in the Cyclic Voltammetry. Electrochemical parameters obtained from a CV such as cathodic and anodic current were recorded for each scan rate (Table 17 and 18). This data were obtained from a CV of 0.1 μM SL-DNA and 1 μM SL-DNA immobilized for different Scan rates. As shown in the Fig. 34 and 36 correlations between Current vs Scan rate were recorded.

Figure 34 Cathodic(a,b) and Anodic Current(c,d) versus Scan rate of the 0.1 μM SL-DNA and dsDNA . Data took from the Cyclic voltammogram in Immobilization Buffer of 0.1 μM SL-DNA and dsDNA at Gold electrode at different Scan rates



2.4.2.1 Optimization of DNA/GE and dsDNA/GE

To obtain the maximum sensitivity for trace 7ESTAC01 interaction, the influence of DNA type for the preparation of SL-DNA and dsDNA was firstly studied.

CVs of 0.1 μ M and 1 μ M SL-DNA/dsDNA in Immobilization Buffer were investigated at three several scan rate of 1V/s, 10V/s, and 100V/s. As shown in Fig 33 and Fig.35, SL-DNA and dsDNA exhibited a well-defined reversible redox behavior. Modification of SL-DNA to obtained dsDNA (using a DNA complementary) decrease the peak current difference between anodic peak and the cathodic peak Fig 34a,c and Fig36a, indicating that SL-DNA was successfully modified on the surface of GE and then decreased the effective area of GE. The decreased of the effective area is explained clearly for the signal ON of the Methylene Blue due it is converted into signal OFF during the hybridization of the DNA complementary with the SL-DNA.

The influence of DNA concentration on the electrochemical behavior was subsequently investigated analyzing Voltammograms, peak current and peak potential difference between cathodic and anodic potentials. As shown in Fig.33 and Fig.35, with the 0.1 μ M concentration of SL-DNA and dsDNA, the Cyclic voltammogram of the SL-DNA is very well defined. Also, the peak potential differences between anodic peak and the cathodic peak (ΔE) were obtained. As shown in Fig 37, the linear relationship between Scan Rate and Current show a better result to 0.1 μ M DNA (Higher signal On and OFF). On the other hand, the signal suppression % versus Scan Rate in SL-DNA and dsDNA shows a higher Signal suppression % at the 0.1 μ M immobilized on the gold electrode (Fig. 34b and Fig. 34d) compare with a signal suppression of 1.0 μ M (Fig. 36b and Fig. 36d)

It is clear that suitable amount of SL-DNA immobilized on the electrode surface is an advantage to provide efficient electron transfer between DNA and electrode. The effective surface area of the electrode decides the limited amount of SL-DNA and dsDNA for electrooxidation. According to the modified electrode prepared with 15 μ l SL-DNA of 0.1 μ M exhibiting the strongest electrochemical response was used for the VPD experiments.

Figure 35 MeB Signal On (SL-DNA-Before Hybridized) and MeB signal OFF (dsDNA-Hybridized). Cyclic voltammogram in Immobilization Buffer of 1 μM SL-DNA and dsDNA at Gold electrode at different Scan rates a) 1V/s b) 10V/s c) 100V/s

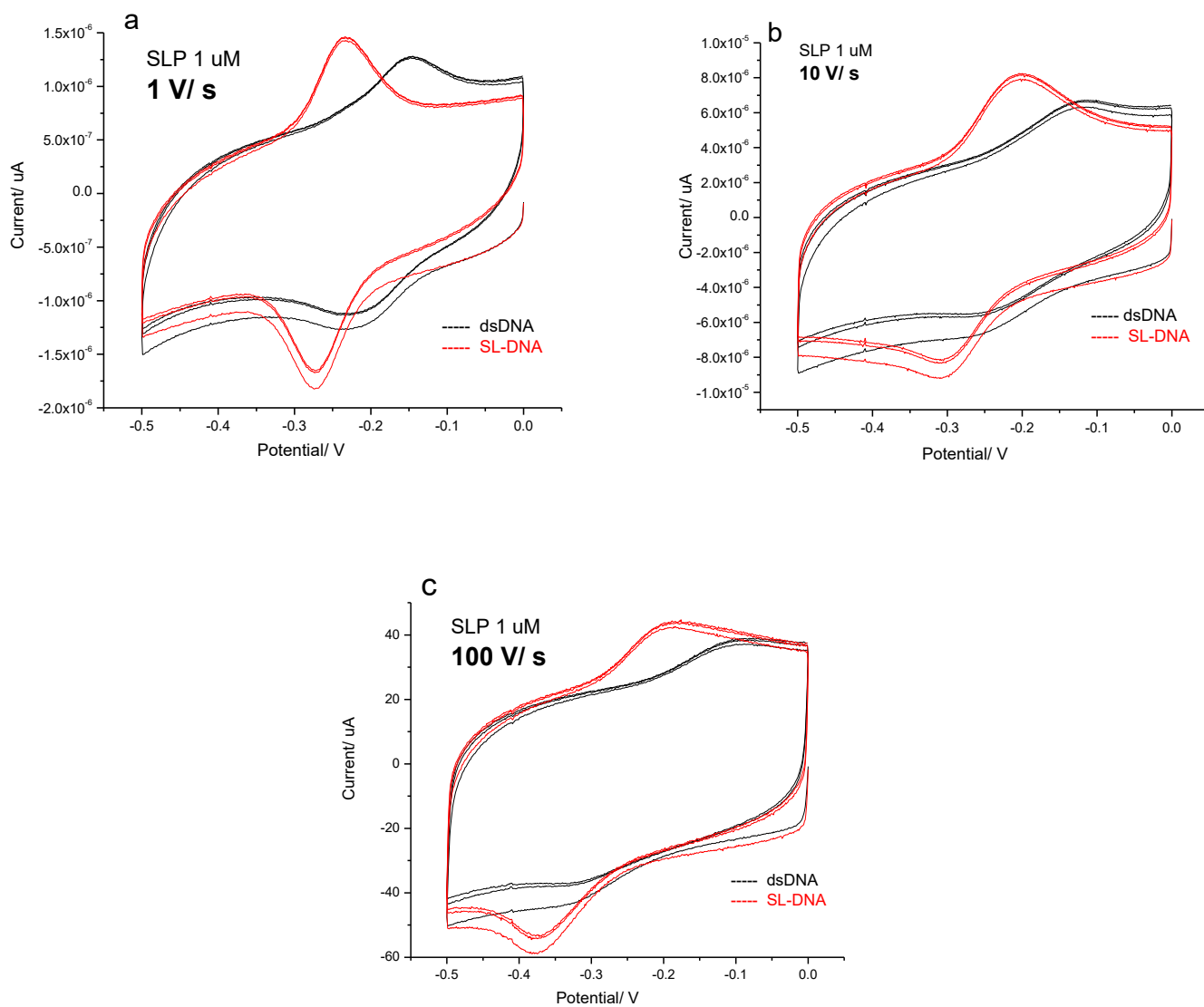
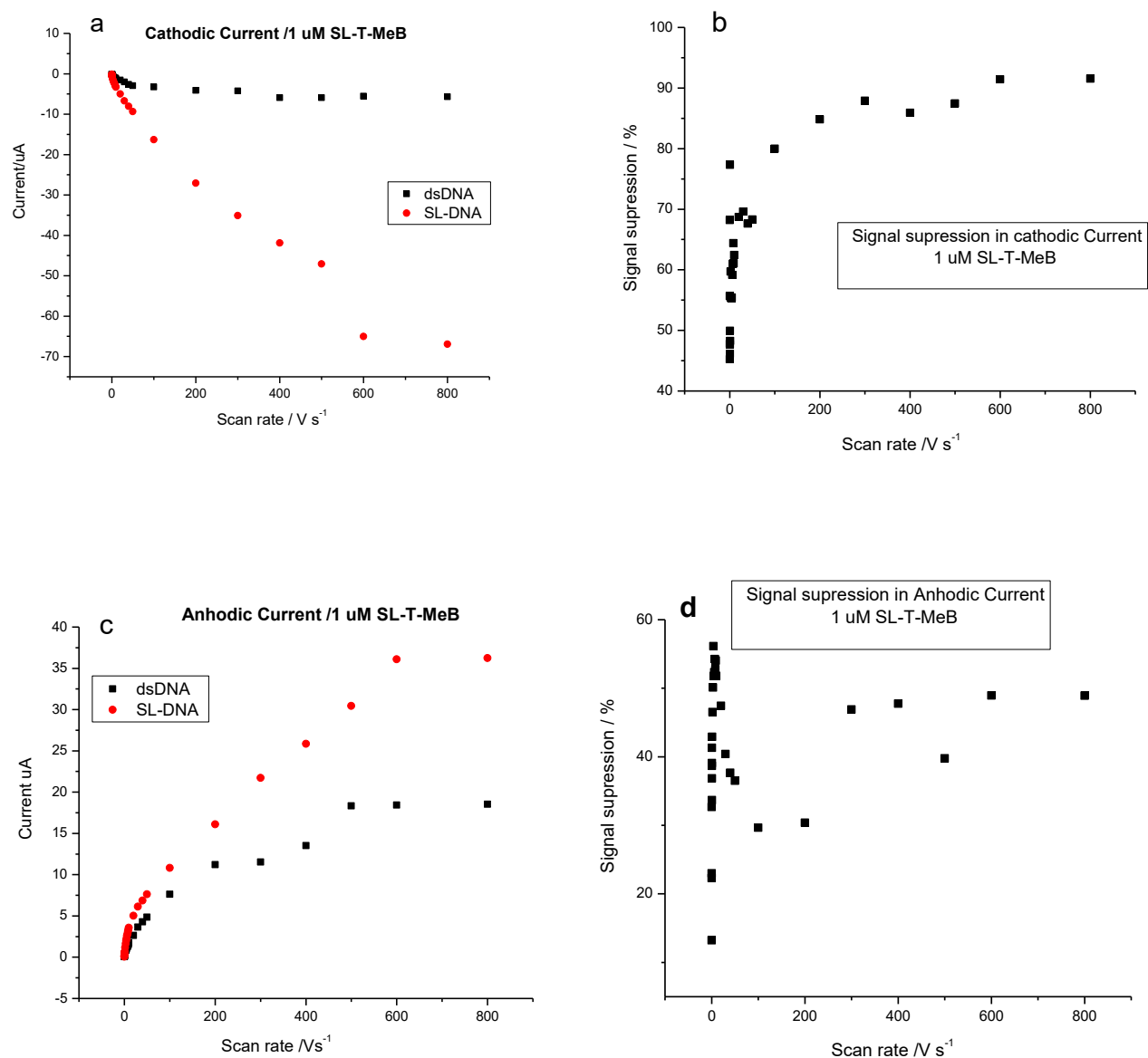


Table 18 Electrochemical parameters obtained from a CV of 1 μ M SL-DNA and dsDNA immobilized for different Scan rates.

Scan rate V/s	I μ A(cathodic)			AFTER HYB	I μ A(anodic)	
	After Hybridization	Before HYB	Signal supression CC		Before HYB	Signal supression CC
0.1	-0.04527	-0.1021	0.556611166	0.05068	0.06523	0.223056876
0.2	-0.07807	-0.1426	0.452524544	0.1068	0.1231	0.132412673
0.3	-0.1006	-0.1926	0.477673936	0.1149	0.1492	0.229892761
0.4	-0.1153	-0.3627	0.682106424	0.1977	0.2936	0.326634877
0.5	-0.2285	-0.4367	0.476757499	0.2341	0.353	0.336827195
0.6	-0.1158	-0.5101	0.772985689	0.2704	0.4282	0.368519383
0.7	-0.2559	-0.5772	0.556652807	0.2951	0.4844	0.390792733
0.8	-0.3201	-0.6396	0.499530957	0.3332	0.5432	0.386597938
0.9	-0.3747	-0.6958	0.461483185	0.3501	0.5966	0.413174656
1	-0.3917	-0.7572	0.482699419	0.3713	0.6504	0.429120541
2	-0.51	-1.266	0.597156398	0.6186	1.157	0.4653414
3	-0.7216	-1.616	0.553465347	0.8102	1.624	0.501108374
4	-0.8578	-1.919	0.552996352	0.8657	1.974	0.561448835
5	-0.9503	-2.131	0.554059127	1.077	2.235	0.518120805
6	-0.948	-2.32	0.59137931	1.23	2.581	0.523440527
7	-1.011	-2.592	0.609953704	1.297	2.836	0.542665726
8	-1.057	-2.969	0.643987875	1.463	3.096	0.52745478
9	-1.179	-3.027	0.610505451	1.526	3.319	0.540222959
10	-1.248	-3.322	0.624322697	1.725	3.578	0.517887088
20	-1.565	-5.001	0.687062587	2.637	5.018	0.474491829
30	-2.031	-6.68	0.695958084	3.658	6.138	0.404040404
40	-2.604	-8.041	0.676159682	4.275	6.86	0.376822157
50	-2.965	-9.355	0.683057189	4.842	7.625	0.364983607
100	-3.266	-16.31	0.799754752	7.618	10.83	0.296583564
200	-4.107	-27.05	0.848170055	11.21	16.1	0.303726708
300	-4.248	-35.1	0.878974359	11.54	21.73	0.468936954
400	-5.896	-41.87	0.859183186	13.51	25.86	0.477571539
500	-5.899	-47.05	0.874622742	18.33	30.44	0.3978318
600	-5.56	-65.03	0.914501	18.43	36.1	0.489473684
800	-5.67	-66.93	0.915284626	18.52	36.25	0.489103448

Figure 36 Cathodic(a,b) and Anodic Current(c,d) versus Scan rate of the 1 μ M SL-DNA and dsDNA . Data took from the Cyclic voltammogram in Immobilization Buffer of 1 μ M SL-DNA and dsDNA at Gold electrode at different Scan rates



2.4.2.2 Interaction of SL-DNA with 7ESTAC01

Cyclic voltammetry investigated the electrochemical responses on SL-DNA/GE to different concentrations of 7ESTAC01. CVs of 1.0 μM SL-DNA in Immobilization Buffer were investigated at 0.1V/s. After the addition of 7ESTAC01, the demonstrated bonding interaction between 7ESTAC01 and SL-DNA occurred (Fig.38), showing signal apparently OFF due to the interaction of 7ESTAC01 with the SL-DNA. The apparently signal Off is explained due the 7ESTAC01 doesn't hybridize the SL-DNA how clearly was demonstrated with the DNA complementary. The interaction between dsDNA and 7ESTAC01 was investigated by Molecular modeling, and UV-Vis absorption spectrometry showed intercalation of 7ESTAC01 with the minor groove DNA. Predominant hydrophobic interaction and hydrogen bonding between the adenine (A6) and Esther carbonyl of the 7ESTAC01 structure (Fig.20 and Fig.21) .

The UV-Vis absorption spectrometry, showed a Binding constant of $K_b = 6,57 \times 10^4 \text{ L mol}^{-1}$ (Table 15, Fig. 16b) . An isosbestic point has been observed at 297 nm. Such spectral behavior is associated with the intercalation as a dominant binding mode. This dominant binding possible for the hydrogen binding show us a strong interaction of 7ESTAC01 with the DNA. As shown in Fig. 38, after the addition of 7ESTAC01, the strong bonding between 7ESTAC01 and SL-DNA/GE was demonstrated, which changed the electroactivity of SL-DNA, slightly decreased the CV peak current and a notable potential shift.

Figure 37 A) ΔE separation of oxidation and reduction peaks before and after hybridization / SL-T-P =0.1 μM B) ΔE separation of oxidation and reduction peaks before and after hybridization / SL-T-P =1 μM

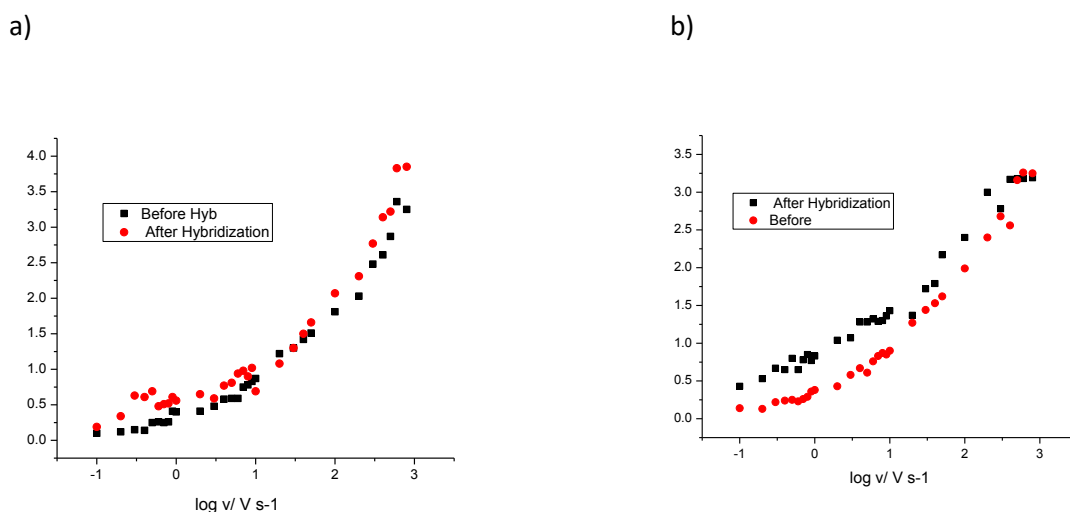
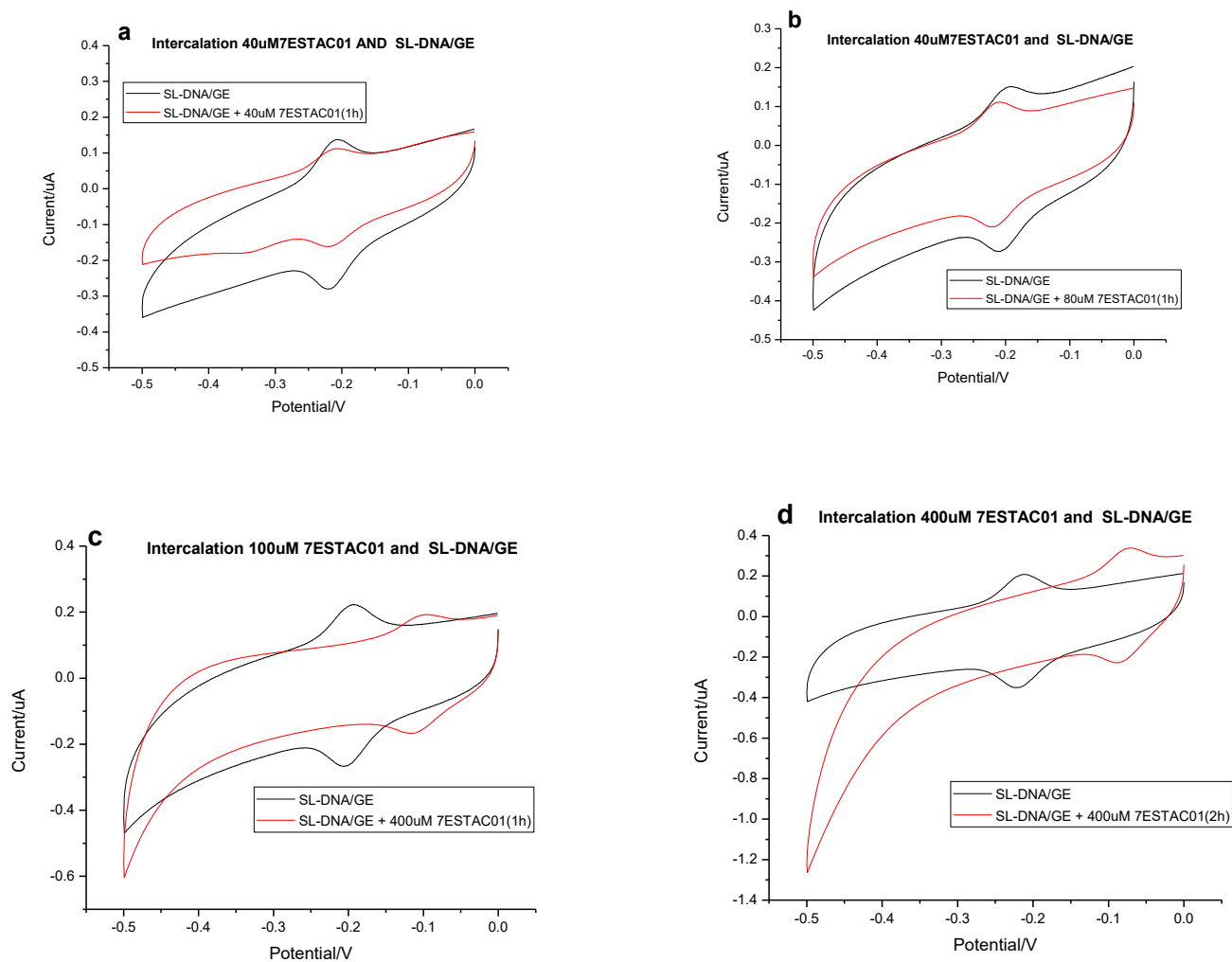


Figure 38 Interaction of 7ESTAC01 with SL-DNA immobilized on the Gold Electrode. Cyclic voltammogram in Immobilization Buffer of 1 μ M SL-DNA and 7ESTAC01 at different concentrations



2.4.2.3 Detection of DNA damage evaluated by oxidation.

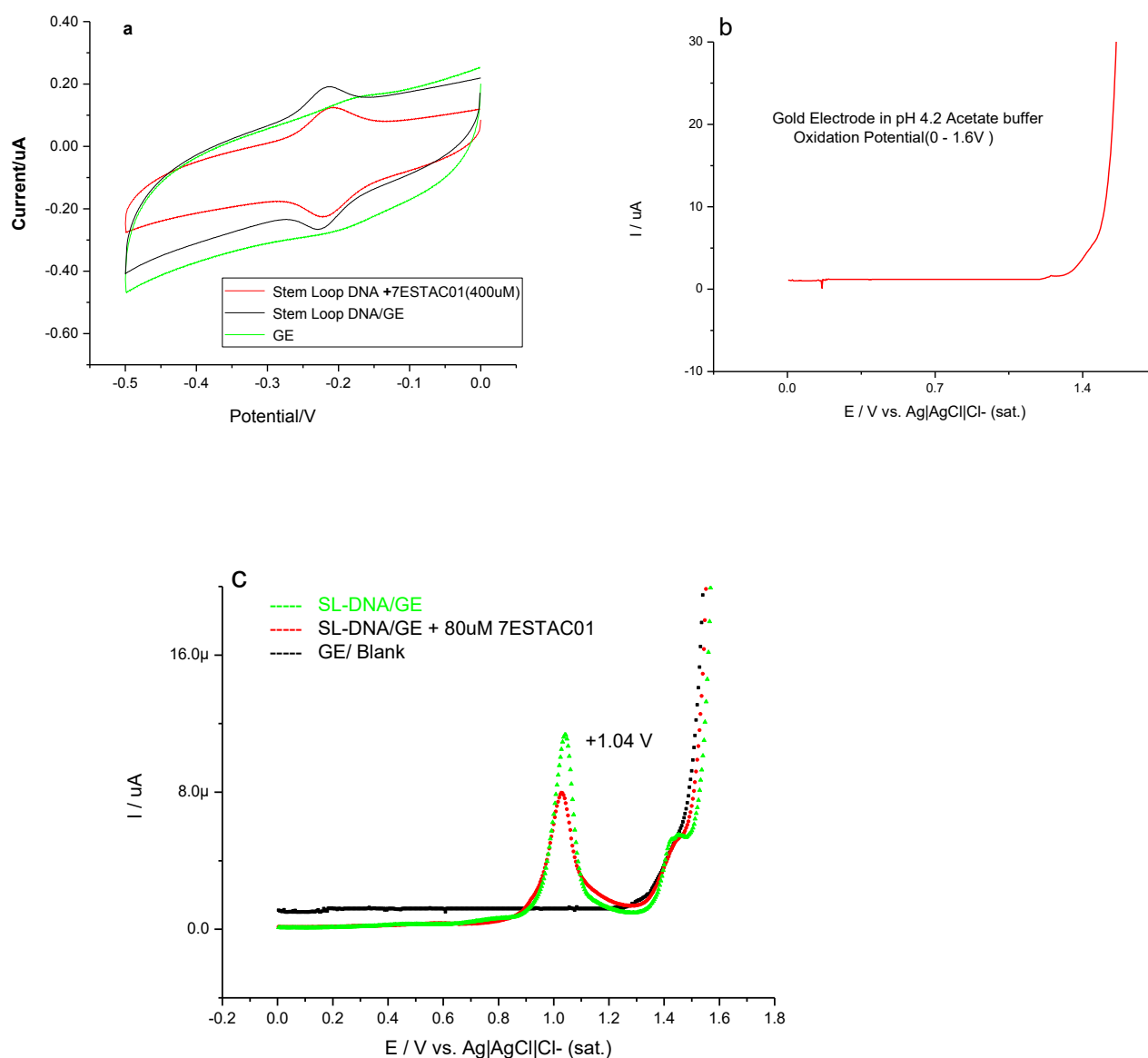
The DPV peak potentials of Guanine on SL-DNA/GE and dsDNA/GE were further evaluated. As indicated in fig. 39c and Fig. 44, SL-DNA/GE exhibit much higher DPV peak current than dsDNA/GE suggested that SL-DNA possessed better electron transfer property. These results imply that the presence of double strand on the stem and a single strand on the loop of the SL-DNA biosensor help to facilitate the electron transfer.

The DPV signal of these modified GE was mainly ascribed to the electrochemical oxidation of guanine bases, then apparently a better proximity of guanines on the SL-DNA than the guanines on the dsDNA affected the electron transfer efficiency. Similar results were corroborated by a work of Shang Huang et. al. They tested four types of single-stranded DNA(ssDNA) modified gold electrode. The ssDNA/GE showed the highest DPV oxidation peak was the biosensor with a shorter distance between guanine base and the electrode surface.

To evaluate the Guanine Oxidation on the SL-DNA and dsDNA, we tested the influence of scan number on the oxidation reaction. As evidence in the Fig. 44c and Fig. 44 d, as the number of scans increase the DPV peak current increase. Compared with SL-DNA/GE and dsDNA/GE, SL-DNA/GE exhibited much higher DPV peak current conforming the number of scan increase (Fig 44c). These results validated the importance role of the electroactive oxidation of the guanine bases immobilized on the gold electrode. Also, showed that differences in the electrochemical responses of DNA depend on the DNA structure. Then the sensitivity of an electrochemical signal to changes in DNA conformation is determined by changes in accessibility and proximity of the Guanine positions.

Finally, for our SL-DNA biosensor, it is expected, as the oxidative damage of the guanine increases the DPV peak current increases.

Figure 39 Stem-Loop DNA on the gold electrode and Intercalation of 7ESTAC01 a) Cyclic Voltammetry in immobilization Buffer b) VPD in Acetate Buffer pH. 4.2 with different concentration of 7ESTAC01



2.4.3 Interaction of SL-DNA/dsDNA with 7ESTAC01 inducing oxidative DNA damage.

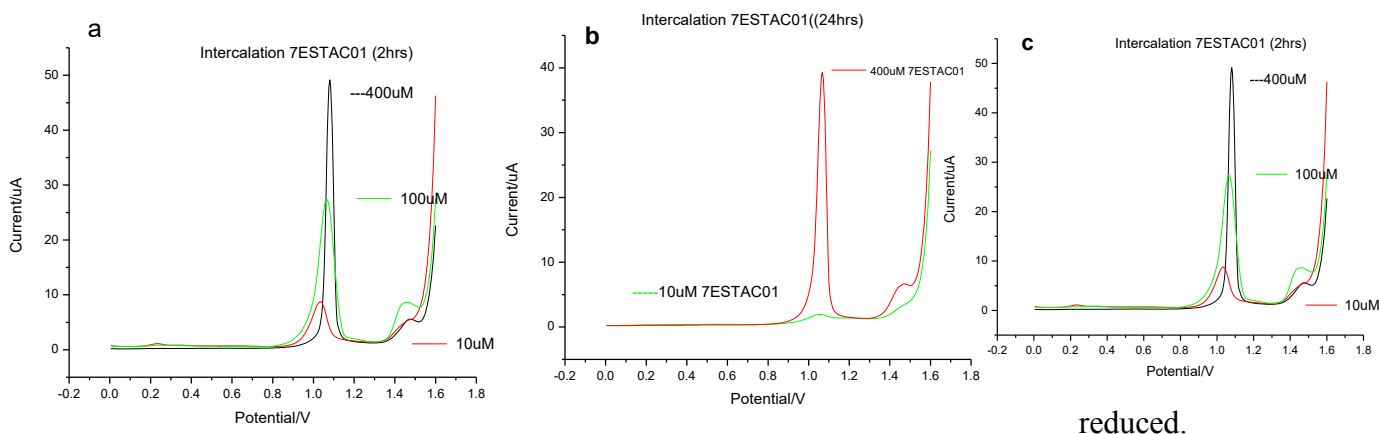
The DPV peak current differences between SL-DNA and their corresponding DNA/GE-7ESTAC01 system were further investigated in Acetate buffer (pH 4.2). As illustrated in Fig. 41, Fig. 42 and Fig. 43 the DPV peak potentials of Guanine on GE were in agreement with the values reported in the previous literature (Guanine Potential: +1.02 V). Gold electrode showed a tiny DPV oxidation peak current of 1.48 μA at peak potential of +1.348 V (Fig. 39b). According to the Fig. 41 to evaluate the timing of interaction of 7ESTAC01 and SL-

DNA/GE, different timing of interaction was tested taking the range from 1h, 2 hours and 24 hours. In general, when 7ESTAC01 was present the oxidation peak current increased, which indicated the formation of 7ESTAC01-SL-DNA/GE and the increased of electron transfer ability of SL-DNA on the surface of GE. It is important mentioned that this interaction was measured with a non-reduced 7ESTAC01. Then the oxidation of 7ESTAC01 is facilitating the electron transfer between this acridine-thiophene with the SL-DNA.

As shown in Fig 12b, the interaction of 7ESTAC01 and reduced 7ESTAC01 and dsDNA calf thymus was investigated using a ssDNA in glassy carbon. It showed that the reduced form of 7ESTAC01 exhibited Guanine oxidation signal of 37.41 %. Compare with the 7ESTAC01 non-reduced exhibited a guanine oxidation signal of 14.69% (Fig.12 and Table 11). To evaluated the difference and the behavior between reduced and non-reduced form 7ESTAC01, DPV of SL-DNA/GE and dsDNA/GE were investigated. As shown in fig.42a and Fig42b, the reduced form of 7ESTAC01 showed DPV peak current higher than the non-

Figure 41

Figure 40 SL-DNA and different concentration of 7ESTAC01 .Compound immobilized on the surface of the electrode for a) 1 h b)2 hours c) 24 hours SL-DNA and different concentration of 7ESTAC01 .Compound immobilized on the surface of the electrode for a) 1 h b)2 hours c) 24 hours

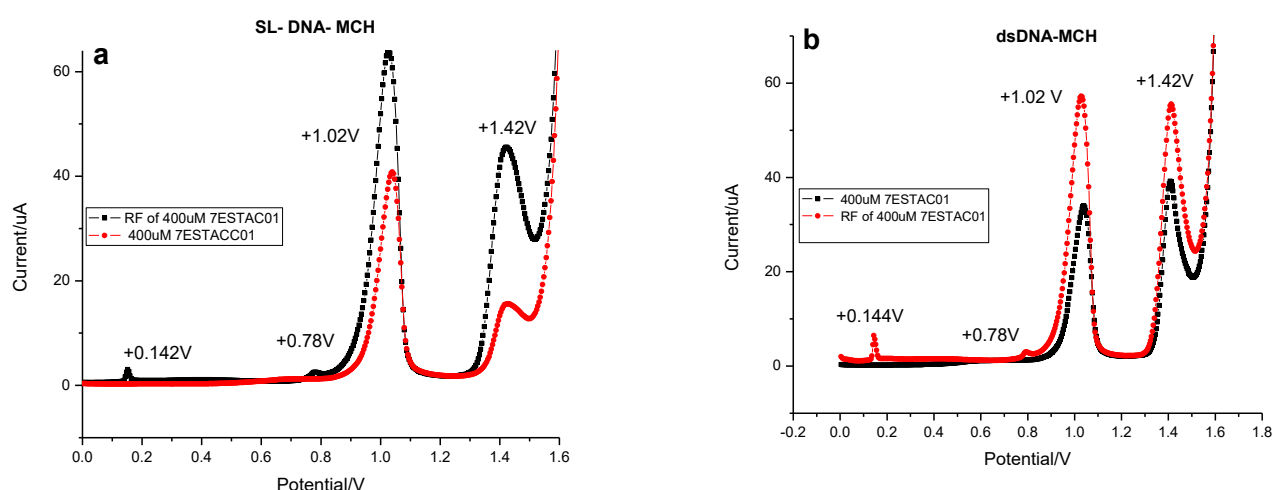


To obtain the maximum sensitivity for measure the interaction of 7ESTAC01 with SL-DNA/GE and dsDNA/GE and after the optimization of time of interaction and reduced form of 7ESTAC01 how the best condition to evaluated the interaction; 2 hours and reduced 7ESTAC01, respectively were chosen. Finally as illustrated in Fig.43 After the addition of 7ESTAC01, the strong bonding interaction between 7ESTAC01 and guanine base of SL-DNA and dsDNA was occurred, which increased the DPV peak current of SL-DNA and dsDNA conforming increased the concentration of 7ESTAC01. Also either to SL-DNA and

dsDNA, when 7ESTAC01 was present, the oxidation peak potential was observed in the less positive side (i.e. 1.02- 0.92V). Finally and not less important the presence of the 8-oxoG after the addition of reduced 7ESTAC01 demonstrates the possible DNA lesion of the dsDNA(GE) biosensor after the addition of reduced 7ESTAC01 in solution. These results not only validated the strong interaction between 7ESATC01 and guanine bases of dsDNA and SL-DNA but also emphasized the apparently more damage in dsDNA than SL-DNA.(Fig.43 c)

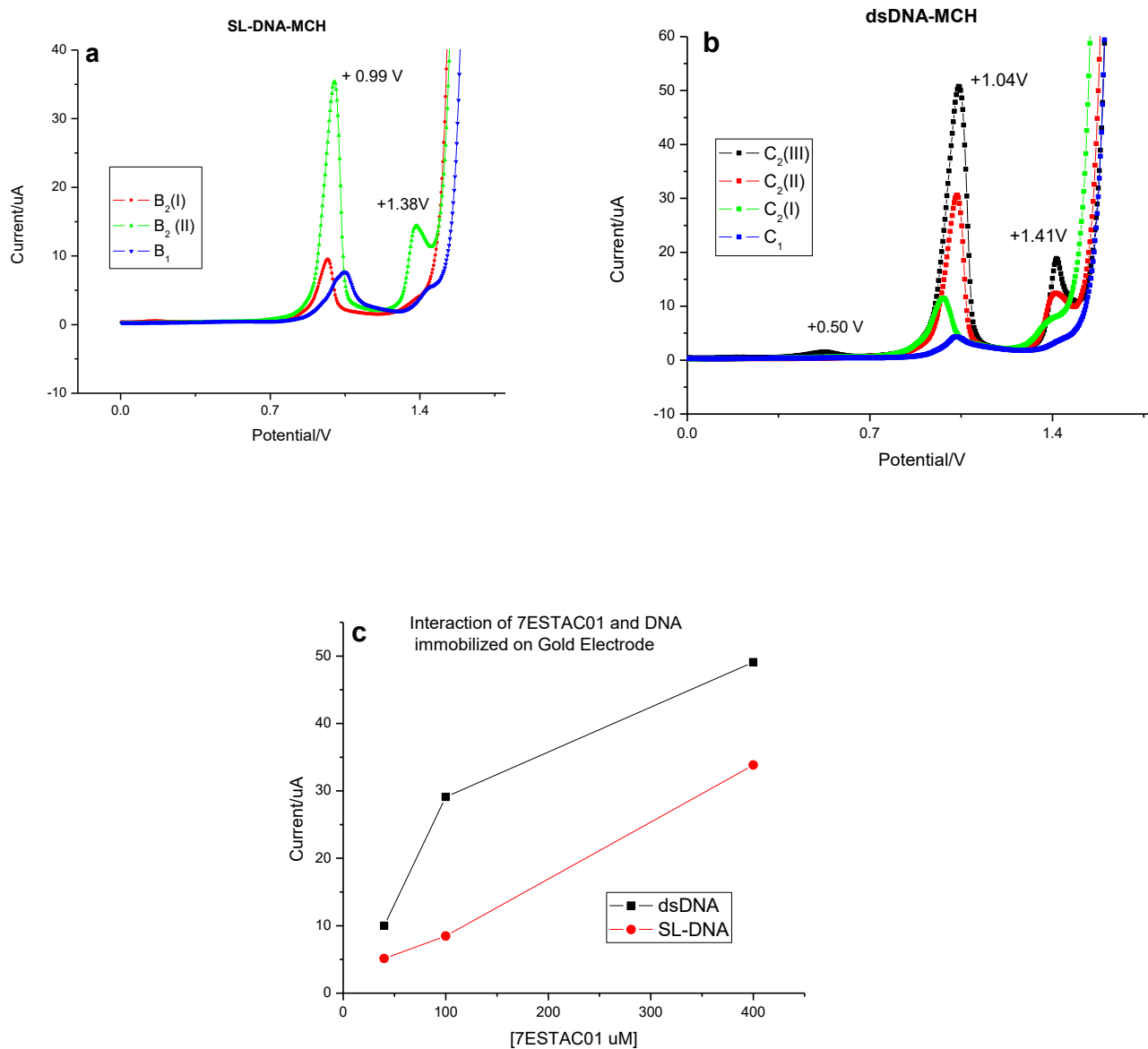
2.4.3.1 7estac01 in solution and reduced form of 7ESTAC01

Figure 42 VPD of SL-DNA/GE and dsDNA/GE in Ph. 4.2 acetate buffer a) 400 uM 7estac01 in solution, acetate buffer with 1 hour of interaction: vpd oxidation applying -0.122 v of reduction potential of 7ESATC01 during 300 sec in stem-loop biosensor b) vpd oxidation applying -0.122 v of reduction potential of 7estac01 during 300 sec in 2wj biosensor for 10 um 7estac01 in solution, acetate buffer with 1 hour of interaction .



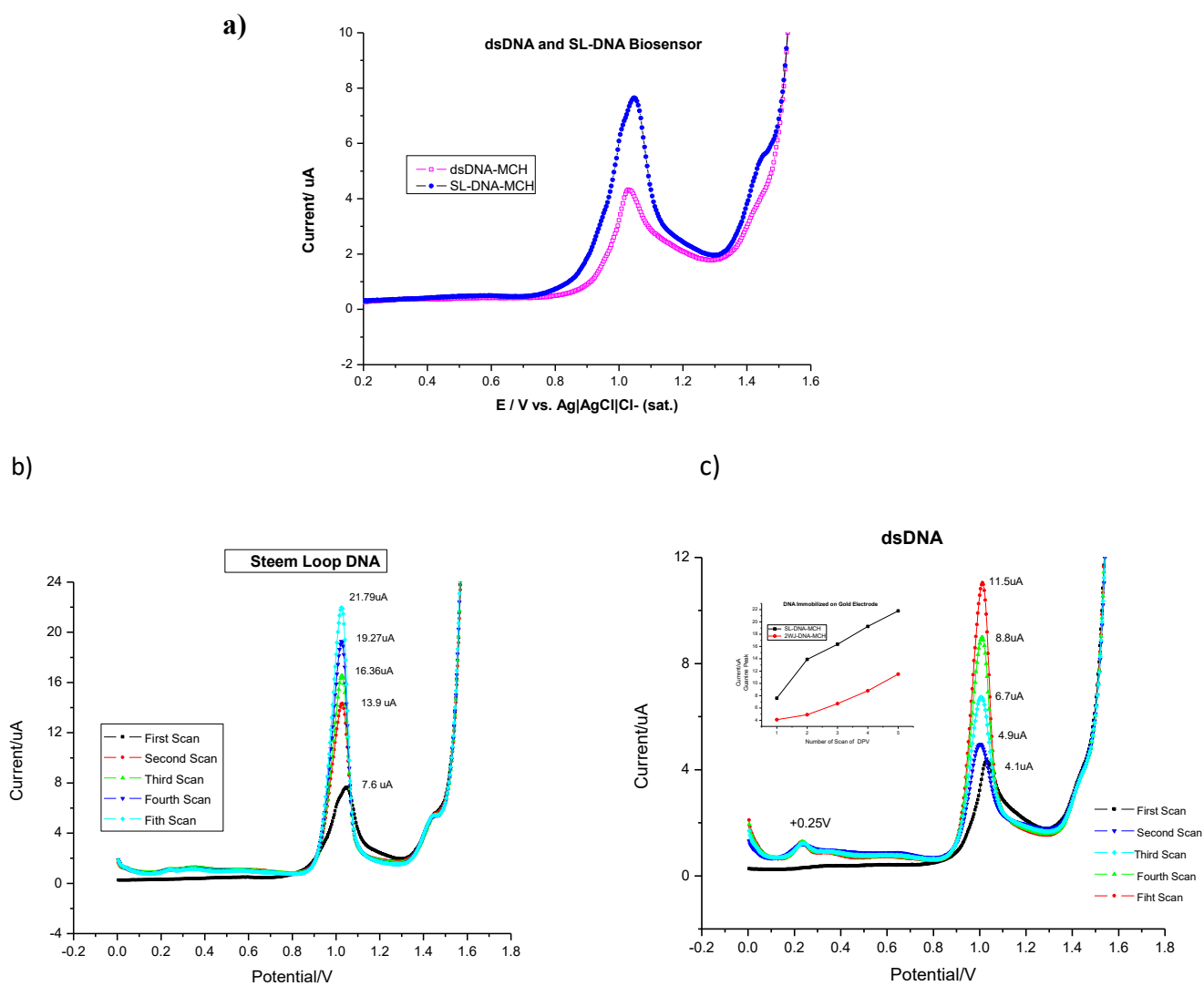
2.4.3.2 Reduced form of 7ESTAC01 against Blanks

Figure 43 . a) I(100 uM 7ESTAC01),II (400uM 7ESTAC01). 7ESTAC01 in solution using Acetate buffer with 2 hour of interaction: VPD oxidation .Reduce form of 7estac01 was obtained applying -0.122 v of reduction potential during 300 sec in Stem-loop biosensor after the hour of interaction between 7esatc01 and SL-DNA



2.4.3.2.1 DNA immobilized on the surface of the Gold Electrode (Blanks)

Figure 44 . DNA immobilized on the surface of the Gold Electrode. VPD in Acetate Buffer pH. 4.2



2.5. CONCLUSION

Chapter 2

- The Stem-Loop DNA immobilization was standardized to get a maximum conductivity to detect DNA-drug interaction.
- The novelty of the SL-DNA/GE biosensor is that i) enables VPD oxidation signal to detect DNA interaction; ii) it is highly sensitive to detect minimal damage because of the homogenous and covalent immobilization of the DNA on the surface of the Gold electrode.
- The SL-DNA biosensor, demonstrated, as the oxidative damage of the guanine increases the DPV peak current increases.
- We validated the strong interaction between 7ESATC01 and Guanine bases of dsDNA and SL-DNA but also emphasized the apparently more damage in dsDNA than SL-DNA.
- dsDNA/GE-7ESTAC01 system exhibit much higher DPV peak current than SL-DNA/GE-7ESTAC01, suggested that reduced 7ESTAC01 is possibly breaking the hydrogen bond force or producing a strong damage on the double strand during the oxidation.
- The SL-DNA/GE validated the importance role of the electroactive oxidation of the guanine bases immobilized on the gold electrode.
- The sensitivity of an electrochemical signal to changes in DNA conformation determined by changes in accessibility and proximity of the Guanine positions to the Electrode

REFERENCES

- ABREU, F. C.; GOULART, M. O. F.; OLIVEIRA BRETT, A. M. Detection of the damage caused to DNA by niclosamide using an electrochemical DNA-biosensor. **Biosensors and Bioelectronics**, v. 17, n. 11–12, p. 913-919, 12// 2002. ISSN 0956-5663. Disponível em: < <http://www.sciencedirect.com/science/article/pii/S0956566302000829> >.
- ADAMS, A. et al. Crystal structure of 9-amino-N-[2-(4-morpholinyl)ethyl]-4-acridinecarboxamide bound to d(CGTCACG)(2): implications for structure–activity relationships of acridinecarboxamide topoisomerase poisons. **Nucleic Acids Research**, Oxford, UK, v. 30, n. 3, p. 719-725, 09/25/received 11/27/revised/11/27/accepted 2002. ISSN 0305-1048 1362-4962. Disponível em: < <http://www.ncbi.nlm.nih.gov/pmc/articles/PMC100304/> >.
- AYDOĞDU, G. et al. A novel electrochemical DNA biosensor based on poly-(5-amino-2-mercapto-1,3,4-thiadiazole) modified glassy carbon electrode for the determination of nitrofurantoin. **Sensors and Actuators B: Chemical**, v. 197, p. 211-219, 7/5/ 2014. ISSN 0925-4005. Disponível em: < <http://www.sciencedirect.com/science/article/pii/S0925400514002433> >.
- BAGULEY, B. C. et al. Mechanisms of action of DNA intercalating acridine-based drugs: how important are contributions from electron transfer and oxidative stress? **Current medicinal chemistry**, v. 10, n. 24, p. 2643-2649, 2003. ISSN 0929-8673.
- BENVIDI, A. et al. A highly sensitive and selective electrochemical DNA biosensor to diagnose breast cancer. **Journal of Electroanalytical Chemistry**, v. 750, p. 57-64, 8/1/ 2015. ISSN 1572-6657. Disponível em: < <http://www.sciencedirect.com/science/article/pii/S1572665715002234> >.
- BOAL, A. K.; BARTON, J. K. Electrochemical detection of lesions in DNA. **Bioconjugate chemistry**, v. 16, n. 2, p. 312-321, 2005. ISSN 1043-1802.
- BOON, E. M. et al. Intercalative stacking: a critical feature of DNA charge-transport electrochemistry. **The Journal of Physical Chemistry B**, v. 107, n. 42, p. 11805-11812, 2003. ISSN 1520-6106.
- BOUFFIER, L. et al. Electrochemistry and bioactivity relationship of 6-substituted-4H-pyrido[4,3,2-kl]acridin-4-one antitumor drug candidates. n. 1878-562X (Electronic), 20120926 DCOM- 20130213
- BOUMENDJEL, A. et al. Acridone derivatives: Design, synthesis, and inhibition of breast cancer resistance protein ABCG2. **Bioorganic & Medicinal Chemistry**, v. 15, n. 8, p. 2892-2897, 4/15/ 2007. ISSN 0968-0896. Disponível em: < <http://www.sciencedirect.com/science/article/pii/S0968089607001186> >.
- BRETT, A. M. O. et al. Detection of the damage caused to DNA by a thiophene-S-oxide using an electrochemical DNA-biosensor. **Journal of Electroanalytical Chemistry**, v. 549, p. 91-99, 6/5/ 2003. ISSN 1572-6657. Disponível em: < <http://www.sciencedirect.com/science/article/pii/S0022072803002456> >.

CHOLEWINSKI, G.; DZIERZBICKA K FAU - KOŁODZIEJCZYK, A. M.;
KOŁODZIEJCZYK, A. M. Natural and synthetic acridines/acridones as antitumor agents:
their biological activities and methods of synthesis. n. 1734-1140 (Print), 20110523 DCOM-
20110916

DENG, Z.; HU, J.; LIU, S. Reactive Oxygen, Nitrogen, and Sulfur Species (RONSS)-
Responsive Polymersomes for Triggered Drug Release. LID - 10.1002/marc.201600685 [doi].
n. 1521-3927 (Electronic), 20170227

DOGAN-TOPAL, B. et al. Investigation of anticancer drug lapatinib and its interaction with
dsDNA by electrochemical and spectroscopic techniques. **Sensors and Actuators B:
Chemical**, v. 194, p. 185-194, 4// 2014. ISSN 0925-4005. Disponível em: <
<http://www.sciencedirect.com/science/article/pii/S0925400513015694> >.

ELIAS, B.; SHAO, F.; BARTON, J. K. Charge migration along the DNA duplex: hole versus
electron transport. **Journal of the American Chemical Society**, v. 130, n. 4, p. 1152-1153,.

FERAPONTOVA, E. E. Electrochemistry of guanine and 8-oxoguanine at gold electrodes.
Electrochimica acta, v. 49, n. 11, p. 1751-1759, 2004. ISSN 0013-4686.

FERREYRA, N. F.; RIVAS, G. A. Self-Assembled Multilayers of Polyethylenimine and
DNA: Spectrophotometric and Electrochemical Characterization and Application for the
Determination of Acridine Orange Interaction. **Electroanalysis**, v. 21, n. 15, p. 1665-1671,
2009. ISSN 1521-4109. Disponível em: < <http://dx.doi.org/10.1002/elan.200904593> >.

FOJTA, M.; PALEČEK, E. Supercoiled DNA-modified mercury electrode: A highly sensitive
tool for the detection of DNA damage. **Analytica chimica acta**, v. 342, n. 1, p. 1-12, 1997.
ISSN 0003-2670.

GOODELL, J. R. et al. Synthesis and evaluation of acridine- and acridone-based anti-herpes
agents with topoisomerase activity. **Bioorganic & Medicinal Chemistry**, v. 14, n. 16, p.
5467-5480, 8/15/ 2006. ISSN 0968-0896. Disponível em: <
<http://www.sciencedirect.com/science/article/pii/S0968089606003440> >.

GORODETSKY, A. A. et al. Coupling into the base pair stack is necessary for DNA-
mediated electrochemistry. **Bioconjugate chemistry**, v. 18, n. 5, p. 1434-1441, 2007. ISSN
1043-1802.

HUANG, S. et al. An electrochemical biosensor based on single-stranded DNA modified
gold electrode for acrylamide determination. **Sensors and Actuators B: Chemical**, v. 224, p.
22-30, 3/1/ 2016. ISSN 0925-4005. Disponível em: <
<http://www.sciencedirect.com/science/article/pii/S0925400515304755> >.

IBÁÑEZ, D. et al. Study of Adenine and Guanine Oxidation Mechanism by Surface-
Enhanced Raman Spectroelectrochemistry. **Journal of Physical chemistry C**. 2015, V. 119,
n. 15, p. 8191-8198, 2015a. ISSN 1932-7447.

JELEN, F.; FOJTA, M.; PALEČEK, E. Voltammetry of native double-stranded, denatured
and degraded DNAs. **Journal of Electroanalytical Chemistry**, v. 427, n. 1, p. 49-56,

1997/04/30 1997. ISSN 1572-6657. Disponível em: <
<http://www.sciencedirect.com/science/article/pii/S0022072896050309>>.

KALANUR, S. S.; KATRAHALLI, U.; SEETHARAMAPPA, J. Electrochemical studies and spectroscopic investigations on the interaction of an anticancer drug with DNA and their analytical applications. **Journal of Electroanalytical Chemistry**, v. 636, n. 1–2, p. 93-100, 11/15/ 2009. ISSN 1572-6657. Disponível em: <
<http://www.sciencedirect.com/science/article/pii/S0022072809003362>>.

KARADENIZ, H. et al. Disposable electrochemical biosensor for the detection of the interaction between DNA and lycorine based on guanine and adenine signals. **Journal of pharmaceutical and biomedical analysis**, v. 33, n. 2, p. 295-302, 2003. ISSN 0731-7085.

KOVACIC, P.; WAKELIN, L. P. Review. DNA molecular electrostatic potential: novel perspectives for the mechanism of action of anticancer drugs involving electron transfer and oxidative stress. **Anti-cancer drug design**, v. 16, n. 4, p. 175-184, 2001. ISSN 0266-9536.

LABUDA, J.; OVÁDEKOVÁ, R.; GALANDOVÁ, J. DNA-based biosensor for the detection of strong damage to DNA by the quinazoline derivative as a potential anticancer agent. **Microchimica Acta**, v. 164, n. 3-4, p. 371-377, 2009. ISSN 0026-3672.

LI, Q.; BATCHELOR-MCAULEY, C.; COMPTON, R. G. Electrochemical oxidation of guanine: Electrode reaction mechanism and tailoring carbon electrode surfaces to switch between adsorptive and diffusional responses. **The Journal of Physical Chemistry B**, v. 114, n. 21, p. 7423-7428, 2010. ISSN 1520-6106.

LIU, T.; BARTON, J. K. DNA electrochemistry through the base pairs not the sugar–phosphate backbone. **Journal of the American Chemical Society**, v. 127, n. 29, p. 10160-10161, 2005a. ISSN 0002-7863.

LUCARELLI, F. et al. Carbon and gold electrodes as electrochemical transducers for DNA hybridisation sensors. **Biosensors and Bioelectronics**, v. 19, n. 6, p. 515-530, 2004. ISSN 0956-5663.

MCEWEN, G. D.; CHEN, F.; ZHOU, A. Immobilization, hybridization, and oxidation of synthetic DNA on gold surface: electron transfer investigated by electrochemistry and scanning tunneling microscopy. **Analytica Chimica Acta**, v. 643, n. 1-2, p. 26–37, 2009. Disponível em: < <http://doi.org/10.1016/j.aca.2009.03.050>>.

MERIC, B. et al. Electrochemical biosensor for the interaction of DNA with the alkylating agent 4, 4'-dihydroxy chalcone based on guanine and adenine signals. **Journal of pharmaceutical and biomedical analysis**, v. 30, n. 4, p. 1339-1346, 2002a. ISSN 0731-7085.

MILLS, D. M. et al. A Single Electrochemical Probe Used for Analysis of Multiple Nucleic Acid Sequences. **Electroanalysis**, v. 29, n. 3, p. 873-879, 2017. ISSN 1521-4109. Disponível em: < <http://dx.doi.org/10.1002/elan.201600548>>.

NEPALI, K. et al. Rational approaches, design strategies, structure activity relationship and mechanistic insights for anticancer hybrids. **European journal of medicinal chemistry**, v.

77, p. 422-487, 2014. ISSN 0223-5234.

NISHIMORI, Y. et al. Synthesis of Molecular Wires of Linear and Branched Bis (terpyridine)-Complex Oligomers and Electrochemical Observation of Through-Bond Redox Conduction. **Chemistry–An Asian Journal**, v. 2, n. 3, p. 367-376, 2007. ISSN 1861-471X.

NOH, J. et al. Amplification of oxidative stress by a dual stimuli-responsive hybrid drug enhances cancer cell death. n. 2041-1723 (Electronic), 20150420 DCOM- 20160229

OLIVEIRA, C. B.; MARIA OLIVEIRA-BRETT, A. DNA-electrochemical biosensors: AFM surface characterisation and application to detection of in situ oxidative damage to DNA. **Combinatorial chemistry & high throughput screening**, v. 13, n. 7, p. 628-640, 2010. ISSN 1386-2073.

OLIVEIRA-BRETT, A.; DICULESCU, V.; PIEDADE, J. Electrochemical oxidation mechanism of guanine and adenine using a glassy carbon microelectrode. **Bioelectrochemistry**, v. 55, n. 1, p. 61-62, 2002. ISSN 1567-5394.

OLIVEIRA-BRETT, A. M.; SILVA, L. A. D.; BRETT, C. Adsorption of guanine, guanosine, and adenine at electrodes studied by differential pulse voltammetry and electrochemical impedance. 2002a. ISSN 0743-7463.

OUBERAI, M. et al. 3,4-Dihydro-1H-[1,3]oxazino[4,5-c]acridines as a new family of cytotoxic drugs. **Bioorganic & Medicinal Chemistry Letters**, v. 16, n. 17, p. 4641-4643, 9/1/ 2006. ISSN 0960-894X. Disponível em: < <http://www.sciencedirect.com/science/article/pii/S0960894X0600655X> >.

PALEČEK, E. et al. Electrochemical biosensors for DNA hybridization and DNA damage. **Biosensors and Bioelectronics**, v. 13, n. 6, p. 621-628, 1998. ISSN 0956-5663.

PAN, H.-Z. et al. Electrochemical DNA biosensor based on a glassy carbon electrode modified with gold nanoparticles and graphene for sensitive determination of *Klebsiella pneumoniae* carbapenemase. **Journal of Biotechnology**, v. 214, p. 133-138, 11/20/ 2015. ISSN 0168-1656. Disponível em: < <http://www.sciencedirect.com/science/article/pii/S0168165615301218> >.

PONTINHA, A. D. R. et al. Triazole-acridine conjugates: redox mechanisms and in situ electrochemical evaluation of interaction with double-stranded DNA. **Bioelectrochemistry (Amsterdam, Netherlands)**, v. 89, p. 50-56, 2013/02// 2013. ISSN 1567-5394. Disponível em: < <http://europepmc.org/abstract/MED/23059201> >. Disponível em: < <https://doi.org/10.1016/j.bioelechem.2012.08.005> >.

PUTIC, A. et al. Structure–activity relationship studies of acridones as potential antiproliferative agents. 1. Synthesis and antiproliferative activity of simple N-unsubstituted 10H-acridin-9-ones against human keratinocyte growth. **European Journal of Medicinal Chemistry**, v. 45, n. 8, p. 3299-3310, 8// 2010. ISSN 0223-5234. Disponível em: < <http://www.sciencedirect.com/science/article/pii/S0223523410002953> >.

RADI, A.-E.; EISSA, A.; NASSEF, H. M. Voltammetric and spectroscopic studies on the binding of the antitumor drug dacarbazine with DNA. **Journal of Electroanalytical**

Chemistry, v. 717–718, p. 24-28, 3/15/ 2014. ISSN 1572-6657. Disponível em: <
<http://www.sciencedirect.com/science/article/pii/S1572665714000149> >.

RAFIQUE, B. et al. Interaction of anticancer drug methotrexate with DNA analyzed by electrochemical and spectroscopic methods. **Biosensors and Bioelectronics**, v. 44, p. 21-26, 6/15/ 2013. ISSN 0956-5663. Disponível em: <
<http://www.sciencedirect.com/science/article/pii/S0956566312008846> >.

RAUF, S. et al. Electrochemical approach of anticancer drugs–DNA interaction. **Journal of Pharmaceutical and Biomedical Analysis**, v. 37, n. 2, p. 205-217, 2/23/ 2005. ISSN 0731-7085. Disponível em: <
<http://www.sciencedirect.com/science/article/pii/S0731708504005631> >.

SARAVANAKUMAR, G.; KIM, J.; KIM, W. J. Reactive-Oxygen-Species-Responsive Drug Delivery Systems: Promises and Challenges. n. 2198-3844 (Linking), 20170120

SAZHNIKOV, V. A. et al. Synthesis, structure and spectral properties of 9-diaryl-amino-substituted acridines. **Journal of Molecular Structure**, v. 1053, p. 79-88, 12/5/ 2013. ISSN 0022-2860. Disponível em: <
<http://www.sciencedirect.com/science/article/pii/S0022286013007655> >.

SIRAJUDDIN, M.; ALI S FAU - BADSHAH, A.; BADSHAH, A. Drug-DNA interactions and their study by UV-Visible, fluorescence spectroscopies and cyclic voltametry. n. 1873-2682 (Electronic), 20130530 DCOM- 20140106

VISPÉ, S. et al. Novel tetra-acridine derivatives as dual inhibitors of topoisomerase II and the human proteasome. **Biochemical Pharmacology**, v. 73, n. 12, p. 1863-1872, 6/15/ 2007. ISSN 0006-2952. Disponível em: <
<http://www.sciencedirect.com/science/article/pii/S0006295207001347> >.

VYSKOČIL, V.; LABUDA, J.; BAREK, J. Voltammetric detection of damage to DNA caused by nitro derivatives of fluorene using an electrochemical DNA biosensor. **Analytical and bioanalytical chemistry**, v. 397, n. 1, p. 233-241, 2010. ISSN 1618-2642.

WONG, E. L.; GOODING, J. J. Charge transfer through DNA: a selective electrochemical DNA biosensor. **Analytical chemistry**, v. 78, n. 7, p. 2138-2144, 2006. ISSN 0003-2700.

YUN XIA, H.; YA HU, X. Determination of isoniazid using a gold electrode by differential pulse voltammetry. **Analytical letters**, v. 38, n. 9, p. 1405-1414, 2005. ISSN 0003-2719.